eman ta zabal zazu

Universidad    Euskal Herriko
del País Vasco    Unibertsitatea

# Shortcuts to adiabaticity in trapped ions

# Mikel Palmero

*Supervisor:*

**Prof. J. Gonzalo Muga**

Departamento de Química-Física

Facultad de Ciencia y Tecnología

Universidad del País Vasco/Euskal Herriko Unibertsitatea

(UPV/EHU)

Leioa, January 2017

*"If I had asked my customers what they wanted, they would have said a faster horse."*

Henry Ford

# *Acknowledgements*

First and foremost, I should thank my thesis supervisor, Prof. Gonzalo Muga, who embraced me in the group, put all of this project into motion and has directly supervised it from start to end. The rest of the group has also been an important part of this work. I specially thank all my office mates for being alongside me; the new ones, those who are already gone, and those (the one) that have been all the way down.

Outside the group, we have also had many collaborators, from whom I was lucky to learn and profit. Special mention to those who hosted me in my trips to Shanghai, Mainz, Zurich, Toulouse, Boulder, Granada and Jerusalem.

I also wanted to express my gratitude to my family and friends, who, although not scientifically, have definitely contributed to this thesis by supporting me, like that time when my parents took me out for dinner to celebrate my first paper.

# Contents

# List of Figures

# List of Tables

# List of publications

I) **The results of this Thesis are based on the following articles**

## Published Articles

1. M. Palmero, E. Torrontegui, D. Guéry-Odelin, and J. G. Muga
   *Fast transport of two ions in an anharmonic trap*
   Phys. Rev. A **88**, 053423 (2013).

2. M. Palmero, R. Bowler, J. P. Gaebler, D. Leibfried, and J. G. Muga
   *Fast transport of mixed-species ion chains within a Paul trap*
   Phys. Rev. A **90**, 053408 (2014).

3. M. Palmero, S. Martínez-Garaot, J. Alonso, J. P. Home, and J. G. Muga
   *Fast expansion and compression of trapped ion-chains*
   Phys. Rev. A **91**, 053411 (2015).

4. M. Palmero, S. Martínez-Garaot, U. G. Poschinger, A. Ruschhaupt, and J. G. Muga
   *Fast separation of two trapped ions*
   New J. Phys. **17**, 093031 (2015).

5. M. Palmero, Shuo Wang, D. Gury-Odelin, Jr-Shin Li, and J. G. Muga
   *Shortcuts to adiabaticity for an ion in a rotating radially-tight trap*
   New J. Phys. **18**, 043014 (2016).

## Pre-Print Articles

6. M. Palmero, S. Martínez-Garaot, D. Leibfried, D. J. Wineland, and J. G. Muga
   *Fast phase gates with trapped ions*
   arXiv:1609.01892.

II) **Other articles produced during the Thesis period**

## Published Articles not included in this Thesis

7. M. Palmero, E. Torrontegui, J. G. Muga, and M. Modugno
   *Detecting quantum backflow by the density of a Bose-Einstein condensate*
   Phys. Rev. A **87**, 053618 (2013).

8. Sh. Mardonov, M. Palmero, M. Modugno, E. Ya. Sherman, and J. G. Muga
   *Interference of spin-orbit-coupled Bose-Einstein condensates*
   EPL **106**, 60004 (2014).

9. Xiao-Jing Lu, Mikel Palmero, Andreas Ruschhaupt, Xi Chen, and Juan Gonzalo Muga
   *Optimal transport of two ions under slow spring-constant drifts*
   Phys. Scr. **90**, 074038 (2015).

10. S. Martínez-Garaot, M. Palmero, D. Gury-Odelin, and J. G. Muga
    *Fast bias inversion of a double well without residual particle excitation*
    Phys. Rev. A **92**, 053406 (2015).

## Pre-Print Articles not included in this Thesis

11. S. Martínez-Garaot, M. Palmero, J. G. Muga, and D. Guéry-Odelin
    *Fast driving between arbitrary states of a quantum particle by trap deformation*
    arXiv:1609.01887.

12. I. Lizuain, M. Palmero, and J. G. Muga
    *Dynamical normal modes for time-dependent Hamiltonians in two dimensions*
    arXiv:1611.05229.

# Introduction

During the last 30 years, the fields of atomic physics and quantum optics have experienced a huge development. The variety of fields and applications, such as metrology, spectroscopy, communications, quantum information processing, new quantum based technologies and so on makes of quantum optics an attractive topic. The evolution of the techniques has allowed us to reach a point where manipulations of single atoms are very precise, and allows for the development of these quantum based applications. The importance and reach of this progress is recognized and made visible through multiple Nobel Prize awards. In 1989, my birth year, Norman Ramsey for his work with atomic clocks [1] and Hans Dehmelt and Wolfgang Paul for developing the ion trapping technique [2, 3] shared the Nobel Prize in physics. 8 years later, in 1997, the same award was shared by Steven Chu [4], Claude Cohen-Tannoudji [5] and William Phillips [6] for developing atom cooling techniques. Another Nobel prize was shared in 2001 by Wolfgang Ketterle [7], and by Carl Wieman and Eric Cornell [8] for diluting the long before predicted Bose-Einstein Condensates. In 2005, the honorees were Roy Glauber for his contribution to the theory of optical coherence [9], and John Hall [10] and Theodor Hänsch [11] for developing precision spectroscopy techniques. Lastly, the 2012 Nobel Prize in physics was also for contributions in the field of quantum optics, as Serge Haroche [12] and David Wineland [13] won it after their development of techniques that allow for the precise measurement and control of individual quantum systems. These 5 awards in the last 30 years show clearly the weight of the field, not only in the physics community, but also in society.

One of the hottest topics in quantum optics is the so called quantum computer,

which is a proposed device that uses quantum phenomena to process information based on quantum states (qubits) rather than in classical states (bits), which should make it much more powerful for certain tasks. A universal quantum computer, equivalent to the classical Turing machine, was theoretically described by David Deutsch already in year 1985 [14], but it was not until 1995 when Ignacio Cirac and Peter Zoller proposed a physical scheme where a quantum computer could actually be built by using trapped ions technology [15]. The basic idea was to trap ions using electromagnetic fields (Paul traps), and implement the qubits making use of the internal levels of each ion. These ions interact with each other through the electric Coulomb force, so the quantum information can be transferred from one to another. Using lasers, one could induce coupling or entanglement between ions, what is necessary for logic gate operations. Since then, it has been proven how such a scheme allows for all basic building blocks of a quantum based computer architecture, namely, initialization, readout, individual ion manipulation and entanglement. Moreover, in recent years the fidelity achieved has been high enough [16–18] making trapped ions a good candidate to get a fault-tolerant quantum computer. The ability to control trapped ions with high precision and to perform a number of coherent operations with them, places this proposal as a leading quantum information-processing architecture [19–21].

However, soon after Cirac and Zoller published their letter [15], it became clear that, although trapped ions were a suitable platform to perform basic operations, managing a large number of ions within a single trap was to turn into a problematic task. For that reason, Wineland and coworkers [22, 23] proposed an alternative scheme, where ions were to be manipulated individually or in small groups in an interaction region to perform the necessary logic operations and then carried to a different zone to do the readout. In this scheme, one should have many interaction regions where operations are happening simultaneously for a large number of ions. This scheme avoids the need of manipulating many ions within a single trap, but requires a synchronization between different regions and the ability to control ion dynamics, without heating or excitation that would cause the loss of the information the qubit is carrying. Since then, many works have proposed similar schemes

or further developed the original one [21, 24–29]. A proof of principle of such scheme was done in NIST in 2009 [30]. However, it was obvious after this work, that slow adiabatic processes that would keep the qubit unaffected throughout the whole process were indeed too slow, as small imperfections in the design of the trap produce heating and decoherence for processes longer than around 100 $\mu$s. On the other side, fast uncontrolled processes produce diabatic excitations, which are not desirable either.

A way out is to design the required dynamical processes using the so called shortcuts-to-adiabaticity [31]. These are processes that drive the system to the same quantum state that would result from an adiabatic process in times much shorter than the usually required in adiabatic processes. A bunch of different techniques exist to design such processes. Some are based in optimizing adiabatic protocols, so that they find the quickest possible adiabatic route, or they accelerate a given adiabatic process by manipulating control parameters. Others, transiently excite the system, but are designed to recover the same initial eigenstate at final time. Not following the constraints given by the adiabatic theorem allows for very quick (sometimes arbitrarily quick) drivings, but the proper design of the Hamiltonian makes possible to get to the same final state.

One of the most used techniques is the "Invariant based inverse engineering" [32]. This technique relies on first designing the evolution of the quantum system such that it will reach the final state we are interested in by obliging the invariant and the Hamiltonian to commute at initial and final time. Then, we inversely obtain the control parameters that will drive the Hamiltonian according to that design. This protocol is limited in a sense, because we need an exact dynamical invariant related to the type of Hamiltonian we want to design. However, if it is possible to get this invariant, the design of the shortcut protocol is usually simple, and most importantly, we get analytical results that are straightforward to adapt when varying the values of the parameters, or when trying to adapt the protocol to work in the lab. A number of simple dynamical processes for a single atom were designed using this technique, including atom expansion [32] and transport [33]. When considering Coulomb interactions between the ions in a chain, it is not

possible to find an exact invariant, because having a term inverse to the position makes impossible to find a closed algebra [34]. However, in this Thesis I apply the invariant-based technique in the regime of small oscillations so that simple formulae apply. Ways to go beyond that approximation will be also implemented.

In Chapters 1 and 2 I design shortcut protocols to transport ion chains, first considering equal mass ions and then different mass ions. Ion shuttling is probably the most sensitive dynamical process in trapped ion architectures, as its adiabatic process implies the longest final times for the usual parameters involved. In Chapter 3, I design quick phase gates. Quantum logic gates are the core of any quantum processor device. Here I accelerate a scheme that has already been tested in the laboratory adiabaticaly. It is based on creating a phase by moving the ions with nearly homogeneous forces that depend on the internal state of each ion. The protocol is somewhat similar to the pure transport scenario but with enough peculiarities and added complexities to deserve a separate treatment and chapter. Chapter 4 addresses the ion chain expansion/compression problem, and Chapter 5 the ion chain separation/merging. These two problems are similar under the normal mode approximation, although the inversion to the lab Hamiltonian is very different for both cases. Chapters 6 and 7 are devoted to the ion rotation. In Chapter 6, the rotation for a single ion is designed, a problem that had not been addressed yet. In Chapter 7, this analysis is extended to 2-ion chains, both for equal and different masses. Finally, a short chapter extracts conclusions and gives a collective view of the thesis.

The thesis is rather long and the mathematics it contains are extensive. For that reason, I wrote it in such a manner that each chapter is self contained. Although all of them are related, it is not necessary reading the whole thesis to understand one particular chapter, so they can be read individually. The notation is consistent within each chapter, but not necessarily from one chapter to another.

# Chapter 1

# Fast transport of two ions in an anharmonic trap

> *"I didn't fail the test, I just found 100 ways to do it wrong."*
>
> Benjamin Franklin

I design fast trajectories of a trap to transport two ions using a shortcut-to-adiabaticity technique based on invariants. The effects of anharmonicity are analyzed first perturbatively, with an approximate, single relative-motion mode description. Then I use classical calculations and full quantum calculations. This allows to identify discrete transport times that minimize excitation in the presence of anharmonicity. An even better strategy to suppress the effects of anharmonicity in a continuous range of transport times is to modify the trajectory using an effective trap frequency shifted with respect to the actual frequency by the coupling between relative and center of mass motions.

## 1.1 Introduction

Quantum information processing based on trapped ions may be applied to a large number of qubits (and become scalable) by moving the ions between fixed zones where logic operations are performed [23, 26, 27, 35]. The transport should be fast, but excitations should also be avoided at the destination site. Different approaches have been proposed to implement faster-than-adiabatic transport of cold atoms [33, 36–41]. Diabatic transport of cold neutral atoms was demonstrated by Guéry-Odelin and coworkers [37] and, recently, fast transport of single or two trapped ions was also realized by two groups [28, 42, 43]. One of the proposed approaches makes use of invariants to design trap trajectories without final excitation [31, 33, 40, 41]. It is very flexible and provides by construction, under specific conditions, a motionally unexcited final transported state. It also allows for further trajectory optimization taking into account different experimental constraints, and robustness versus noise [44]. The invariant-based inverse engineering method had been applied so far to model the fast transport of a single particle [33, 40] and Bose-Einstein condensates [41]. In this chapter, I extend the theoretical analysis in [33] to two Coulomb-interacting particles within a single trap, focusing on the effects of a mild anharmonicity which is present in any experimental setting [36, 45]. In Sec. 1.2, I study the transport of two ions first in a harmonic trap and then in an anharmonic trap with an added time-dependent linear potential to compensate the inertial force. The applicability of this compensating method may be limited so other options are explored. In particular, I consider in Sec. 1.3 the effect of anharmonicity when the trap trajectories are designed for an unperturbed (harmonic) trap. This is done using an approximate one-dimensional (1D) theory combined with perturbation theory. In Sec. 1.4, I study numerically the full two-dimensional (2D) problem. The chapter ends with a discussion in Sec. 1.5 and the Appendix A on the extension of some of the results to the transport of $N$ ions.

## 1.2 Two-ion transport

### 1.2.1 Harmonic Trap

Let me examine first the transport of two single-charge ions of mass $m$ in an effectively 1D harmonic trap that moves from 0 to $d$ in a time $t_f$. Let $\mathsf{q_1}$ and $\mathsf{q_2}$ be the coordinates of the two ions with momenta $\mathsf{p_1}$ and $\mathsf{p_2}$ and $Q_0(t)$ the trajectory of the trap minimum. The Hamiltonian includes a kinetic term, a harmonic potential, and an interaction potential due to the Coulomb force,

$$
\begin{aligned}
H \;=\; & \frac{\mathsf{p_1}^2}{2m} + \frac{1}{2}m\omega^2(\mathsf{q_1} - Q_0)^2 \\
+ \; & \frac{\mathsf{p_2}^2}{2m} + \frac{1}{2}m\omega^2(\mathsf{q_2} - Q_0)^2 \\
+ \; & \frac{C_c}{\mathsf{q_1} - \mathsf{q_2}}.
\end{aligned}
\tag{1.1}
$$

$\omega/(2\pi)$ is the trap frequency and $C_c = \frac{e^2}{4\pi\epsilon_0}$, where $e$ is the electron charge and $\epsilon_0$ the vacuum permittivity. Here and in the following, the time argument of the trap position will be frequently omitted, i.e., $Q_0 = Q_0(t)$. I set $\mathsf{q_1} > \mathsf{q_2}$ because of the strong Coulomb repulsion. The wave functions of the ions never superpose, so we may effectively treat the particles as distinguishable and the symmetrization of the wave function is not necessary as it will not provide any new physical effect. This assumption is largely accepted when interpreting current experiments.

Let me now introduce coordinates and momenta, as well as corresponding operators, for center of mass (CM) and relative motion,

$$
\begin{aligned}
Q &= \frac{1}{2}(\mathsf{q_1} + \mathsf{q_2}); \quad P = \mathsf{p_1} + \mathsf{p_2}, \\
r &= \frac{1}{2}(\mathsf{q_1} - \mathsf{q_2}); \quad p = \mathsf{p_1} - \mathsf{p_2}.
\end{aligned}
\tag{1.2}
$$

This gives equal effective masses for relative and CM motions. The generalization for $N$ ions, see the Appendix A, also holds this property. Substituting the new

coordinates in Eq. (1.1), the Hamiltonian takes the form

$$
\begin{aligned}
H(Q, P, r, p) &= \frac{P^2}{2M} + \frac{1}{2}M\omega^2(Q - Q_0)^2 \\
&+ \frac{p^2}{2M} + \frac{1}{2}M\omega^2 r^2 + \frac{C_c}{2r},
\end{aligned}
\tag{1.3}
$$

where $M = 2m$ is the total mass. The Hamiltonian is the sum of two terms, $H = H_{cm} + H_r$, where each term depends only on one of the pairs' coordinate-momentum. We may thus "separate variables" and find time-dependent solutions of the Schrödinger equation.

The relative part of the Hamiltonian $H_r$ does not depend on $Q_0(t)$ so the relative motion is not affected by the transport and will remain unexcited. Thus, we only need to design a trajectory for which the CM is unexcited at final time. This may be achieved adiabatically or via shortcuts-to-adiabaticity. The CM Hamiltonian, $H_{cm}$, has the form of a particle of mass $M$ in a harmonic trap, so any of the shortcut-to-adiabaticy techniques known (using Fast-Forward, optimal control, invariants, or their combination [33, 36, 38, 39]) may be applied to find a suitable $Q_0(t)$.

To inverse engineer the trap trajectory making use of invariants, the invariant is designed first, consistent with a predetermined structure of the Hamiltonian [33]. The invariant is parametrized by the classical trajectory $Q_c(t)$ that satisfies the classical equation of motion $\ddot{Q}_c + \omega^2(Q_c - Q_0) = 0$ and boundary conditions $Q_c(0) = \dot{Q}_c(0) = \ddot{Q}_c(0) = Q_0(0) = 0$; $Q_c(t_f) = Q_0(t_f) = d$; $\dot{Q}_c(t_f) = \ddot{Q}_c(t_f) = 0$. They imply the initial and final commutativity between the invariant and the Hamiltonian, and the stability of the solution when the Hamiltonian remains constant beyond the boundary times. A simple polynomial interpolation gives [33]

$$
\begin{aligned}
Q_c &= d\left(10s^3 - 15s^4 + 6s^5\right), \\
Q_0 &= \frac{d}{\omega^2 t_f^2}\left(60s - 180s^2 + 120s^3\right) \\
&+ d\left(10s^3 - 15s^4 + 6s^5\right),
\end{aligned}
\tag{1.4}
$$

where $s = t/t_f$. Each initial eigenstate of $H_{cm}(0)$ would evolve exactly according to the "transport mode"

$$\Psi_n(Q,t) = e^{-\frac{i}{\hbar}[E_n t + \int_0^t \frac{M\dot{Q}_c^2}{2} dt']} e^{iM\dot{Q}_c Q/\hbar} \Phi_n(Q - Q_c), \tag{1.5}$$

where $\Phi_n(x)$ are the eigenfunctions of the harmonic oscillator and $E_n$ the corresponding energies. At $t_f$ the modes become again eigenstates of the Hamiltonian $H(t_f)$, but at intermediate times they are in general a superposition of several eigenstates of $H(t)$. Note that, apart from transport between stationary states, it is also possible to design launching protocols, in which the system begins at rest and ends up with a given center-of-mass velocity, and, similarly, stopping protocols [33].

The separability between CM and relative motions is still valid for two ions of different masses if they oscillate with the same trapping frequency, but it breaks down if the frequency depends on position $Q_0$, if the two ions experience different trapping frequencies, or in presence of anharmonicity. We shall concentrate on this latter case, as it occurs in all traps and affects neutral atoms as well.

## 1.2.2 Anharmonic Trap

We now consider an additional quartic potential in the Hamiltonian

$$
\begin{aligned}
H &= \frac{\mathsf{p}_1^2}{2m} + \frac{1}{2}m\omega^2 \left[ (\mathsf{q}_1 - Q_0)^2 + \beta(\mathsf{q}_1 - Q_0)^4 \right] \\
&+ \frac{\mathsf{p}_2^2}{2m} + \frac{1}{2}m\omega^2 \left[ (\mathsf{q}_2 - Q_0)^2 + \beta(\mathsf{q}_2 - Q_0)^4 \right] \\
&+ \frac{C_c}{\mathsf{q}_1 - \mathsf{q}_2},
\end{aligned} \tag{1.6}
$$

where $\beta$ is a perturbative constant with dimensions $[L]^{-2}$ that sets the "strength" of the anharmonicity. Nonrigid transport with a time-dependent trap frequency or time-dependent anharmonicities due to noise or control limitations is clearly of interest, but I shall only address here rigid transport as a first simpler step before considering more ambitious goals.

In terms of CM and relative coordinates we have

$$
\begin{aligned}
H &= \frac{P^2}{2M} + \frac{1}{2}M\omega^2[(Q - Q_0)^2 + \beta(Q - Q_0)^4] \\
&+ \frac{p^2}{2M} + \frac{1}{2}M\omega^2(r^2 + \beta r^4) + \frac{C_c}{2r} \\
&+ 3M\omega^2\beta(Q - Q_0)^2 r^2 \\
&= H_{cm} + H_r + H_c.
\end{aligned} \tag{1.7}
$$

The first two lines of Eq. (1.7) may be identified as (perturbed) CM and relative Hamiltonians, $H_{cm}$ and $H_r$. Unlike the harmonic trap, there is now a coupling term $H_c$ (third line) that depends both on $Q$ and $r$ so the variables cannot be separated. No nontrivial invariants are known for this Hamiltonian [46, 47], so in principle we cannot inverse-engineer the trap trajectory exactly using invariants. One approximate option is to design it for the unperturbed harmonic oscillator. An exact alternative is to apply a linear potential to compensate the inertial force as in [33, 48, 49].

### 1.2.3 Compensating Force Approach

In this subsection I introduce an additional time-dependent linear term in the Hamiltonian to compensate for the effect of the trap motion in the trap frame and avoid final excitations. This generalizes for two ions the results in [33]. The extension of the compensating force approach to $N$ ions was discussed by Masuda in [48] using the Fast-Forward approach, and may also be carried out following the Appendix A.

Let me first define a unitary transformation [33, 50] that shifts the momentum and position of the center-of-mass coordinate

$$
\mathcal{U} = e^{iPQ_0(t)/\hbar}e^{-iM\dot{Q}_0(t)Q/\hbar}. \tag{1.8}
$$

This amounts to changing the reference system from a laboratory frame to the rest frame of the trap.[1]

We first rewrite the Hamiltonian in the lab frame as

$$H(Q - Q_0, r, P, p) = \frac{P^2}{2M} + \frac{p^2}{2M} + U(Q - Q_0, r), \qquad (1.9)$$

where $U(Q - Q_0, r)$ can be any arbitrary potential. The equation for the transformed (trap frame) wave function $|\Phi\rangle = \mathcal{U}|\Psi\rangle$ takes the form[2]

$$
\begin{aligned}
i\hbar\partial_t|\Phi\rangle &= H_{trap}|\Phi\rangle \\
&= \left[ H(Q, r, P, p) + M(Q + Q_0)\ddot{Q}_0 + \frac{1}{2}M\dot{Q}_0^2 \right]|\Phi\rangle, \qquad (1.10)
\end{aligned}
$$

where $H_{trap} = \mathcal{U}H\mathcal{U}^\dagger + i\hbar(\partial_t\mathcal{U})\mathcal{U}^\dagger$. To compensate the inertial term $M(Q + Q_0)\ddot{Q}_0$ in the trap frame we may apply, in the laboratory frame, the term

$$ - MQ\ddot{Q}_0, \qquad (1.11)$$

or, equivalently, a force $m\ddot{Q}_0$ on each particle. To make the term $\frac{1}{2}M\dot{Q}_0^2$ disappear, we may perform a further transformation $|\Phi'(t)\rangle = \mathcal{U}'(t)|\Phi(t)\rangle$, with $\mathcal{U}'(t) = e^{\frac{i}{\hbar}\int_0^t \frac{1}{2}M\dot{Q}_0^2 dt'}$. This is independent of all operators, so that $\mathcal{U}'H_{trap}\mathcal{U}'^\dagger$ does not modify the Hamiltonian, but $i\hbar(\partial_t\mathcal{U}')\mathcal{U}'^\dagger = -M\dot{Q}_0^2/2$. We finally get

$$i\hbar\partial_t|\Phi'\rangle = \left[ \frac{P^2}{2M} + \frac{p^2}{2M} + U(Q, r) \right]|\Phi'\rangle. \qquad (1.12)$$

The resulting potential does not depend anymore on time, and any stationary state in the rest frame of the trap will remain so during transport. This holds for arbitrary potentials, even if $Q$ and $r$ are coupled, as in Eq. (1.7).

A lower bound for the maximum acceleration of the compensating force is $2d/t_f^2$ [33]. Since the forces that can be applied are typically limited by experimental constraints, the compensation is not always easy to implement in practice, if at

---

[1] Since $P$ and $Q$ do not commute, alternative orderings are possible but they only change the Hamiltonian by purely time-dependent terms without physical effect.

[2] Use $e^{-iM\dot{Q}_0 Q/\hbar}Pe^{iM\dot{Q}_0 Q/\hbar} = P + M\dot{Q}_0$ and $e^{iQ_0 P/\hbar}Qe^{-iQ_0 P/\hbar} = Q + Q_0$.

all. For this reason, I study in the following alternative strategies. First, I shall design the trap motion for an unperturbed harmonic potential and analyze the effect of anharmonicity.

## 1.3   1D approximation

In this section, I discuss a simple approximation that provides valuable hints, even in analytical form, on the transport behavior of two ions in presence of anharmonicities. The idea is to freeze the relative motion coordinate at $r = r_e$, the minimum of the potential part that depends on $r$ only. Equivalently, we may consider a single-mode approximation in which relative-motion excitations are neglected. Neglecting constant terms, the resulting Hamiltonian has the same form as the one for the frozen relative coordinate, substituting $r_e$ and $r_e^2$ by the average values $\langle r \rangle$ and $\langle r^2 \rangle$ in the ground relative-motion mode. With my parameters, the average and minimum values of $r$ are equal up to the third significant number, so the difference is negligible and I use for simplicity the frozen values.

With this assumption, and adding a constant term without physical effect, the Hamiltonian (1.7) becomes

$$H = \frac{P^2}{2M} + \frac{1}{2}M\omega^2[(6\beta r_e^2 + 1)(Q - Q_0)^2 + \beta(Q - Q_0)^4], \qquad (1.13)$$

which we may also write as $H = H_0 + \beta H_1$, where $H_1$ is a perturbation of the harmonic Hamiltonian $H_0$:

$$H_1 = \frac{1}{2}M\omega^2[6r_e^2(Q - Q_0)^2 + (Q - Q_0)^4]. \qquad (1.14)$$

Let the initial state be $|\Psi_n(0)\rangle$. Using time-dependent perturbation theory, the final wave vector $|\Psi(t_f)\rangle$ is given by [33, 44, 51]

$$
\begin{aligned}
|\Psi(t_f)\rangle \;=\; & U_0(t_f, 0)|\Psi_n(0)\rangle \\
& - \frac{i\beta}{\hbar} \int_0^{t_f} dt \, U_0(t_f, t) H_1(t)|\Psi_n(t)\rangle \\
& - \frac{\beta^2}{\hbar^2} \int_0^{t_f} dt \int_0^t dt' \, U_0(t_f, t) H_1(t) U_0(t, t') H_1(t')|\Psi_n(t')\rangle \\
& + \mathcal{O}(\beta^3),
\end{aligned}
\tag{1.15}
$$

where $U_0$ is the unperturbed propagator for $H_0$. In terms of the complete set of transport modes [see Eq. (1.5)] it takes the form

$$
U_0(t, t') = \sum_j |\Psi_j(t)\rangle\langle\Psi_j(t')|.
\tag{1.16}
$$

To calculate the fidelity $F := |\langle\Psi_n(t_f)|\Psi(t_f)\rangle|$ up to second-order it is useful to separate the sum into $j = n$ and $j \neq n$ terms in the second order contribution of Eq. (1.15). When computing $|\langle\Psi_n(t_f)|\Psi(t_f)\rangle|^2$, the square of first-order terms is canceled by the second-order term with $j = n$. Thus, the fidelity, up to second order, may finally be written as

$$
F = \left(1 - \sum_{j \neq n} |f_{j,n}^{(1)}|^2\right)^{1/2},
\tag{1.17}
$$

where $f_{j,n}^{(1)} = \frac{-i\beta}{\hbar} \int_0^{t_f} dt \, \langle\Psi_j(t)|H_1(t)|\Psi_n(t)\rangle$.[3] Due to the orthogonality properties of the Hermite polynomials, transitions induced by the quadratic perturbation will only be nonzero for one- and two-level jumps. Instead, the quartic part of the perturbation will lead to jumps from one to four levels. The $f_{j,n}^{(1)}$ transition amplitudes can be explicitly calculated so that the second-order fidelity is known analytically, although the form is too lengthy to be displayed here. Simplified expressions will be provided later. We compare the fidelity in second order with the exact, numerical one (using the Split-Operator method) in Fig. 1.1, starting

---

[3]Similarly, the final average phonon number is $\langle j \rangle = n + \sum_{j \neq n} (j - n)|f_{j,n}^{(1)}|^2$.
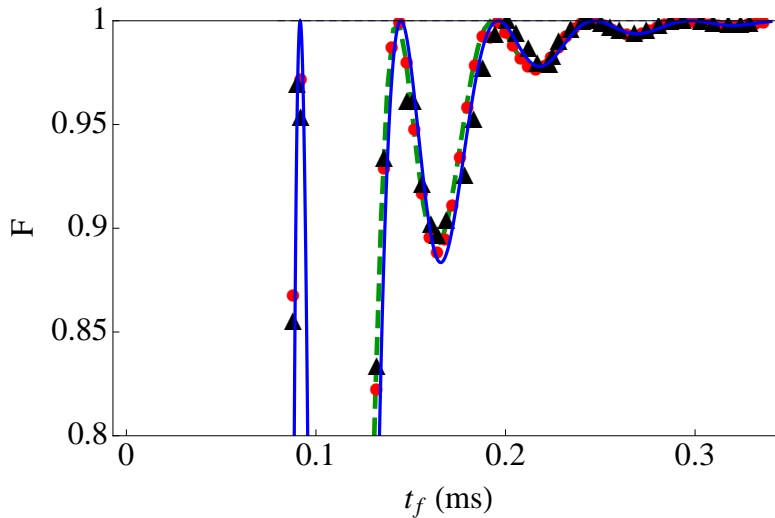
FIGURE 1.1:    Fidelity of the anharmonic system vs final time $t_f$ following the inverse engineering trajectory using second-order perturbation theory (blue thick line), 1D dynamics for the initial ground state of the harmonic oscillator (red dotted line); 1D dynamics for the initial ground state of the perturbed 1D Hamiltonian (green dashed line); 2D dynamics for the initial ground state of the 2D Hamiltonian (filled triangles). $M = 2m = 29.93 \times 10^{-27}$ kg corresponding to $^9$Be$^+$ ions, $\omega/(2\pi) = 20$ kHz, $d = 370$ $\mu$m, $r_e = 62$ $\mu$m and $\beta = 10^6$ m$^{-2}$.

both with the ground state of the harmonic trap $\Phi_0(0)$ and the exact ground state of the anharmonic trap. The results are hardly distinguishable. In the numerical examples I use the parameters in [42] except for a lower trap frequency to enhance anharmonic effects. The trap trajectory $Q_0(t)$ is chosen as in Eq. (1.4), using invariant-based engineering for the unperturbed system with a polynomial ansatz for $Q_c$. The fidelity oscillates, reaching the maximum value of one at discrete values of $t_f$. The occurrence of maxima is a generic feature that does not depend on the specific value of $\beta$ chosen. In the following, I work out a theory to explain and predict them.

I shall now study the effect of each perturbation separately. The quadratic perturbation amounts to having designed the trap trajectory with the "wrong" trap frequency and, as we will see, is the dominant perturbation except for very short times. The influence of the quartic perturbation was analyzed in [33] but only with a much less accurate first-order approach. The effect of the two perturbations is quite different as seen in Fig. 1.2. The quadratic perturbation provides a fidelity almost identical to that of the total perturbation, reproducing its oscillations and
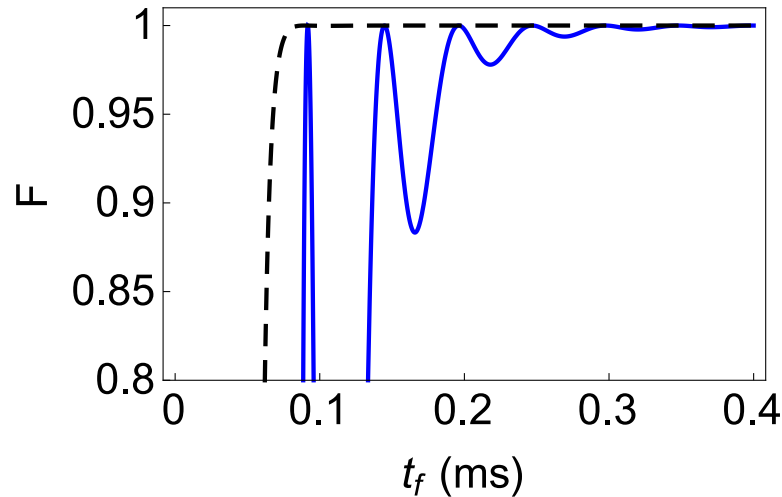
FIGURE 1.2: Fidelity vs final time ($t_f$) for the second-order perturbation theory, indistinguishable from an exact 1D quantum dynamical calculation (the initial state is the ground state of the perturbed harmonic oscillator) for the quadratic perturbation (blue thick line) in Eq. (1.14), and the quartic perturbation (black dashed line) in Eq. (1.14). Same parameters as in Fig. 1.1.

peak times. The quartic perturbation alone leads to a sudden growth in the fidelity around a critical time $t_f^{cr}$, followed by fidelity 1 for longer final times. To estimate the behavior of $t_f^{cr}$ with respect to transport and potential parameters we note that the maximum of $|Q_c(t) - Q_0(t)|$ is $10d/(\omega^2 t_f^2 3^{1/2})$. Comparing the quadratic and quartic contributions to the potential there, we get

$$t_f^{cr} = \alpha \frac{\beta^{1/4}d^{1/2}}{\omega}, \qquad (1.18)$$

where $\alpha \approx 16.5$ is adjusted numerically. For the parameters of Fig. 1.2 this occurs for shorter times than the one corresponding to the first peak of the quadratic perturbation so the effect of the quartic perturbation is negligible.

Let me now analyze in more detail the quadratic perturbation alone. It implies one and two vibrational quanta as mentioned before. If we consider only $n \to n\pm1$ the results are already very similar to the fidelity in Fig. 1.2. Since one-level transitions are dominant we can write down an explicit approximate form for the
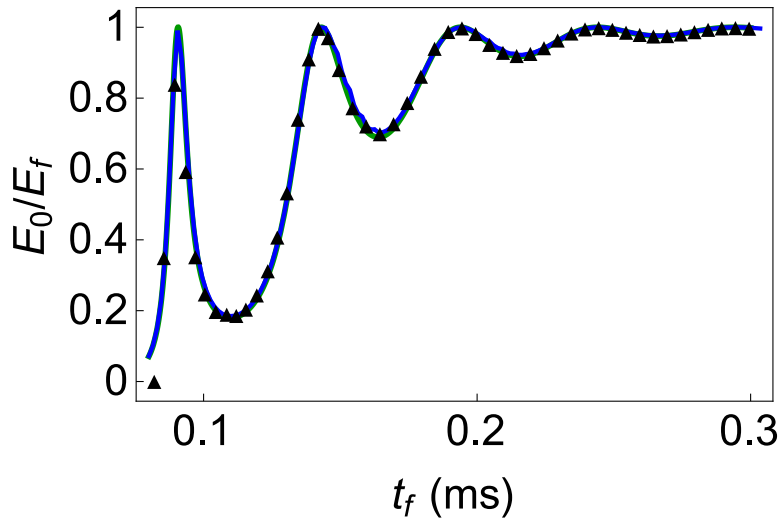
FIGURE 1.3: I plot $E_0/(E_0+E_{ex})$, where $E_0$ is the ground-state energy for the 1D Hamiltonian and $E_{ex}$ is the excitation energy after the transport, for the 1D quantum evolution (blue solid line), 2D quantum evolution (black triangles), and a single classical trajectory (green dashed line). Same parameters as in Fig. 1.1.

fidelity based on them:

$$
\begin{aligned}
f_{n\pm1,n}^{(1)} &= \frac{\pm360id\beta r_e^2 e^{\mp\frac{1}{2}it_f\omega}\sqrt{2(1+n)M\hbar}}{t_f^5\omega^{9/2}} \\
&\times \left[6t_f\omega\cos\left(\frac{t_f\omega}{2}\right) + (t_f^2\omega^2 - 12)\sin\left(\frac{t_f\omega}{2}\right)\right],
\end{aligned}
\tag{1.19}
$$

(note the square root scaling with the mass). This amplitude is zero, and the fidelity one, when

$$
6t_f\omega\cos\left(\frac{t_f\omega}{2}\right) + (t_f^2\omega^2 - 12)\sin\left(\frac{t_f\omega}{2}\right) = 0.
\tag{1.20}
$$

There is a $\beta$-independent solution for, approximately, every oscillation period. This result also follows from a simple classical argument: Consider a classical trajectory $\widetilde{Q}_c(t)$ satisfying

$$
\frac{\ddot{\widetilde{Q}}_c}{\widetilde{\omega}^2} + \widetilde{Q}_c - Q_0(\omega) = 0,
\tag{1.21}
$$

where $Q_0(\omega) = Q_0(t;\omega)$ is the trap trajectory calculated as before with $\omega$, Eq. (1.4), and $\tilde{\omega} = \omega\sqrt{1+6\beta r_e^2}$ is an effective trap frequency, shifted with respect to

$\omega$ because of the relative-CM coupling [see Eq. (1.13)]. Its energy for $\widetilde{Q}_c(0) = \dot{\widetilde{Q}}_c(0) = 0$ is given by

$$E_{ex}(t) = \frac{1}{2}M\dot{\widetilde{Q}}_c^2(t) + \frac{1}{2}M\widetilde{\omega}^2\left[\widetilde{Q}_c(t) - Q_0(t)\right]^2. \tag{1.22}$$

At time $t_f$ we have

$$\begin{aligned} E_{ex}(t_f) &= \frac{7200d^2M(\omega^2 - \tilde{\omega}^2)^2}{t_f^{10}\omega^4\tilde{\omega}^8} \\ &\times \left[6t_f\tilde{\omega}\cos\left(\frac{t_f\tilde{\omega}}{2}\right) + (t_f^2\tilde{\omega}^2 - 12)\sin\left(\frac{t_f\tilde{\omega}}{2}\right)\right]^2. \end{aligned} \tag{1.23}$$

The condition for a zero is the same as Eq. (1.20) substituting $\omega \to \tilde{\omega}$. This leads to a very small displacement (and dependence on $\beta$) of the zeros for our parameters. In Fig. 1.3 I represent $E_0/(E_0 + E_{ex}(t_f))$ which is indistinguishable from the curve where the excitation energy is calculated with quantum dynamics. We may conclude unambiguously that the oscillations are not quantum in nature.

Rather than adjusting the transport time to the discrete set of zeros, a better, more robust strategy that allows for a continuous set of final times is to design the trap trajectory taking into account the frequency shift. Changing $\omega \to \tilde{\omega}$ in Eq. (1.4) we get an adjusted trajectory $Q_0(t; \tilde{\omega})$ for which $E_{ex}(t_f) = 0$ by construction for any $t_f$. Similarly, $Q_0(t; \tilde{\omega})$ gives fidelity one for all $t_f$ in the 1D model, if only the quadratic perturbation is considered. In the protocol based on $Q_0(t; \tilde{\omega})$, the only disturbance comes from the quartic term that sets the speed limitation given by Eq. (1.18). Figure 1.4 shows the impressive results of this simple approach. In practice, $\tilde{\omega}/(2\pi)$ may be measured as the effective CM-mode frequency.

Higher, more realistic trap frequencies lead to similar results but for a larger $\beta$. Simple estimates of the fidelity or excitation may be drawn from Eqs. (1.19) or (1.22). Figure 1.5 depicts the classical excitation energy of Eq. (1.22) for a realistic trap frequency and different values of $\beta$ using the (unshifted) $\omega$ in $Q_0(t)$. Notice that for these large-$\beta$ values the times of minimum excitation do change with $\beta$, and that, for the adjusted trajectory $Q_0(t; \tilde{\omega})$, $E_{ex}(t_f) = 0$ as before.
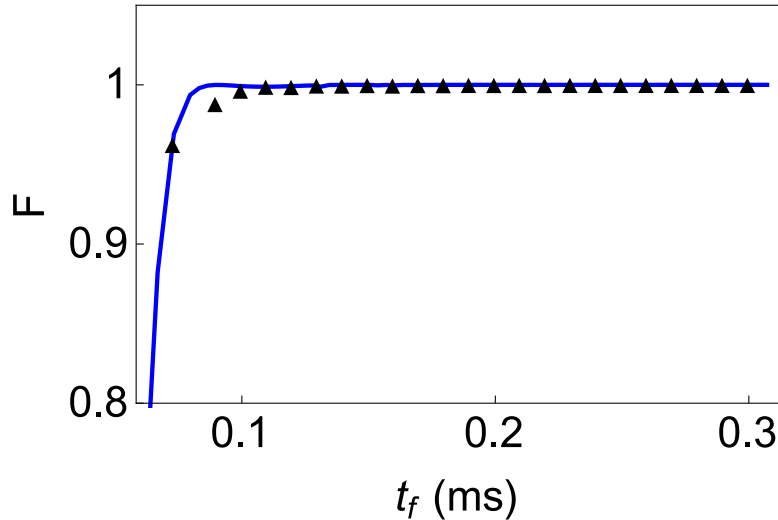
FIGURE 1.4: Fidelity vs final time $t_f$ for adjusted trap trajectories $Q_0(t; \tilde{\omega})$. The initial condition is the ground state. 1D: blue solid line; 2D: filled triangles. Same parameters as in Fig. 1.1.

## 1.4 Full 2D analysis

We have also examined the evolution of the state according to the full two-dimensional Hamiltonian (1.7), without freezing the relative motion, using a 2D split-operator method to simulate quantum dynamics. The computation is performed in the trap frame to reduce the numerical grid size. Figure 1.1 shows that the quantum fidelities of the 1D model are in very good agreement with the fidelities calculated for 2D dynamics. Figure 1.3 shows energy ratios for 1D and 2D calculations. To compare them on equal footing in 2D, the minima of the potential and the ground-state relative energy are subtracted. Again, the 1D and 2D quantum calculations are remarkably close to each other. 2D calculations may also be found in Fig. 1.4 for the transport designed using a shifted frequency. They confirm the excellent performance of this strategy with respect to the anharmonic perturbation.
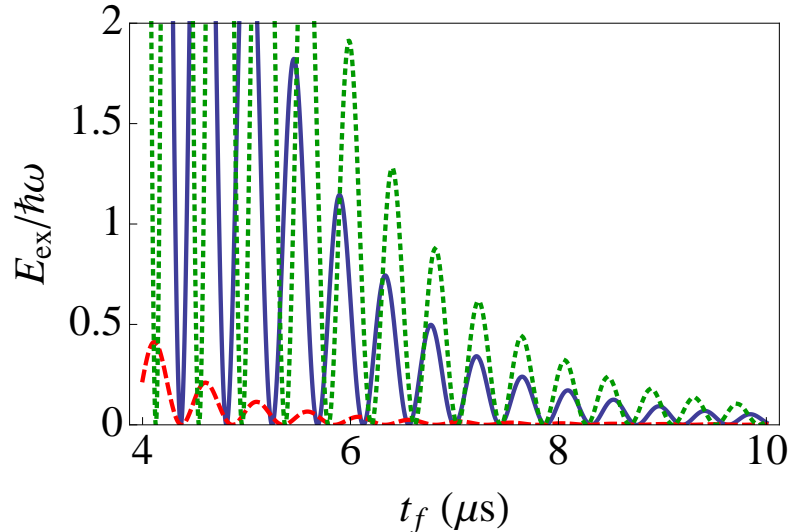
FIGURE 1.5: Motional excitation vs final time. $M = 2m = 29.93 \times 10^{-27}$ kg, $\omega/(2\pi) = 2$ MHz, $d = 370$ $\mu$m for the three cases and $\beta = 6.4 \times 10^9$ m$^{-2}$, $r_e = 2.807\mu$m (solid blue line), $\beta = 10^9$ m$^{-2}$, $r_e = 2.883$ $\mu$m (red dashed line), and $\beta = 10^{10}$ m$^{-2}$, $r_e = 2.764$ $\mu$m (green dotted line). The middle value of $\beta$ $(6.4 \times 10^9)$ is chosen so that at $t_f = 8$ $\mu$s the excitation is similar to the one seen experimentally in [42]. The trap trajectory is given by Eq. (1.4). If instead the adjusted trajectory $Q_0(t; \tilde{\omega})$ is used, then $E_{ex}(t_f) = 0$.

## 1.5 Discussion

For two ions in a harmonic trap, the relative motion is uncoupled to the CM motion. They may be transported faster than adiabatically treating the center of mass as a single particle and applying different shortcuts to adiabaticity. For anharmonic traps, CM and relative motion are coupled. A 1D model for the CM has been first worked out based on a single relative-motion mode, or, equivalently, freezing the relative coordinate. The full 2D quantum calculations show excellent agreement with this model in the parameter range studied. It is possible to achieve fast and faithful transport for an arbitrary trap shape by compensating for the inertial force in the trap frame with a linear potential. That may be difficult in practice so other strategies to get high fidelities have been explored. For a quartic anharmonicity the effective 1D potential includes a quartic and a quadratic perturbation. The latter is usually dominant except for very short transport times. If the trap trajectory is the one designed for the unperturbed (harmonic) trap, the quartic perturbation alone implies a sharp increase to one of the fidelity, while

the quadratic perturbation induces (classical) fidelity oscillations with respect to the final time $t_f$. Taking into account the shift in the effective trap frequency due to the coupling, the trap trajectory is much more robust and the effect of the quadratic perturbation is canceled.

The extension to transport of different-mass ion chains will be studied in Chapter 2. The results of this chapter and its extension in Appendix A were published in [52], and later used by Pedregosa-Gutiérrez and others in [53] to perform fast transport of large ion clouds.

# Chapter 2

# Fast transport of mixed-species ion chains within a Paul trap

*"The key is failing fast and failing cheap."*

Geoff Deane

I investigate the dynamics of mixed-species ion crystals during transport between spatially distinct locations in a linear Paul trap in the diabatic regime. In a general mixed-species crystal, all degrees of freedom along the direction of transport are excited by an accelerating well, so unlike the case of same-species ions, where only the center-of-mass mode is excited, several degrees of freedom have to be simultaneously controlled by the transport protocol. I design protocols that lead to low final excitations in the diabatic regime using invariant-based inverse engineering for two different-species ions and also show how to extend this approach to longer mixed-species ion strings. Fast transport of mixed-species ion strings can significantly reduce the operation time in certain architectures for scalable quantum-information processing with trapped ions.

## 2.1    Introduction

As was mentioned in the previous chapter, a possible scalable architecture for a quantum processor based on trapped ions implies shuttling of individual or small groups of ions. In principle, it is permissible to excite the motion of the ions during transport, as long as all excitations are removed at the end of the transport [31]. As I will show below, this general approach may lead to transport durations that are much shorter than what would be possible in an adiabatic approach. Previous work concentrated on transport of one particle, cold neutral atom clouds, two ions, or ion clouds [31, 33, 36–43, 52–56]. Here, I extend the study in Chapter 1 by studying the transport of mixed-species ion chains with initial and final excitations of the motion close to the ground state. The use of two different ion species allows for sympathetic cooling of the ion motion of one species without disturbing the quantum information held by the other species [30]. Another building block utilized in [30, 57] required transport of a four-ion crystal, where two ions carry the qubit information and the other two are used to cool the coupled motion of the crystal. I first study the transport of two different-mass ions, and design protocols to transport them over a distance of $370 \, \mu$m in durations significantly smaller than $100 \, \mu$s leaving them in a low-energy state of motion. My approach employs invariant based inverse engineering of shortcuts to adiabaticity [33, 52]. I then extend these techniques to longer ion chains, and specifically a four-ion chain. I limit the study to two- and four-ion chains since they are enough to perform one- and two-qubit gates and therefore to build a universal set of gates while avoiding the problems inherent to longer chains.

## 2.2    Invariant-based inverse engineering

The invariant-based inverse-engineering method has proved useful for single-particle transport [33, 40, 55], and for several equal mass ions [52]. For one particle of mass $m$ in 1D the Hamiltonians that belong to the "Lewis-Leach family" [58]

may be written in terms of a potential $U$ that moves along $\alpha(t)$, and a force $F$ as

$$H = \frac{p^2}{2m} - F(t)q + \frac{1}{2}m\omega^2(t)q^2 + \frac{1}{\rho^2(t)}U\left[\frac{q - \alpha(t)}{\rho(t)}\right], \tag{2.1}$$

where $p$ is the momentum, $\rho$ is a scaling length parameter, and $\omega$ an angular frequency. This $H$ has the following dynamical invariant:

$$\begin{aligned} I &= \frac{1}{2}m[\rho(p - m\dot{\alpha}) - m\dot{\rho}(q - \alpha)]^2 \\ &+ \frac{1}{2}m\omega_0^2\left(\frac{q - \alpha}{\rho}\right)^2 + U\left(\frac{q - \alpha}{\rho}\right), \end{aligned} \tag{2.2}$$

provided the functions $\rho$, $\alpha$, $F$ and $\omega$ satisfy the auxiliary equations

$$\ddot{\rho} + \omega^2(t)\rho = \frac{\omega_0^2}{\rho^3}, \tag{2.3}$$

$$\ddot{\alpha} + \omega^2(t)\alpha = \frac{F(t)}{m}. \tag{2.4}$$

For the simple case in which the potential is purely harmonic with constant angular frequency $\omega(t) = \omega_0$, we have $U = 0$, $F(t) = m\omega_0^2 Q_0(t)$, where $Q_0(t)$ is the trap trajectory; $\alpha(t)$ becomes a classical trajectory satisfying a Newton's equation for the moving trap, and the scaling length parameter is $\rho = 1$; therefore, the auxiliary equation (2.3) is trivially satisfied. The inverse-engineering strategy imposes boundary conditions for $\alpha$ at the boundary times $t_b = \{0, t_f\}$, where the transport starts at $t = 0$ and ends at $t = t_f$. With $\alpha(0) = \dot{\alpha}(t_b) = 0$, and $\alpha(t_f) = d$, the static asymptotic Hamiltonians [$H(t \leq 0)$ and $H(t \geq t_f)$] and the invariant commute at the initial and final times. In this manner, the eigenstates of the initial trap are transported (mapped) via the dynamical modes of the invariant up to the eigenstates of the final trap. In addition, $\ddot{\alpha}(t_b) = 0$ is usually imposed to provide a continuous trap trajectory at the boundary times. Then $\alpha(t)$ is interpolated and, by substituting $\alpha(t)$ into Eq. (2.4), we may solve for the trap trajectory $Q_0(t)$. In general, the evolution is diabatic, with transient excitations but no final excitation by construction.

## 2.3   Dynamical normal-mode coordinates

The goal is to transport a chain of ions with different mass between two sites separated by a distance $d$ in a time $t_f$ without final motional excitation. I assume tight radial confinement so that the transport dynamics of each ion is effectively one-dimensional, and also that the external trap potential is harmonic. I label the ions as $i = 1, 2, ..., N$. They have position coordinates $q_1, q_2, ..., q_N$ and masses $m_1, m_2, ...m_N$. With the position of the minimum of the external potential $Q_0 = Q_0(t)$, the Hamiltonian is

$$H = \sum_{i=1}^{N} \frac{p_i^2}{2m_i} + \sum_{i=1}^{N} \frac{1}{2} u_0(q_i - Q_0)^2 + \sum_{i=1}^{N-1} \sum_{j=i+1}^{N} \frac{C_c}{q_i - q_j}, \qquad (2.5)$$

where $u_0$ is the spring constant of the external trap, and $C_c = \frac{e^2}{4\pi\epsilon_0}$, with $\epsilon_0$ the vacuum permittivity and $e$ the electric charge of an electron. For later use let us also define the potential $V \equiv H - \sum_{i=1}^{N} \frac{p_i^2}{2m_i}$. I assume that all ions have the same charge $e$, and that their locations obey $q_1 > q_2 > \cdots > q_N$, with negligible overlap of probability densities due to the strong Coulomb repulsion. For equal masses [52], the dynamics for the center of mass and relative motion are uncoupled. The motion of the trap only affects the center of mass, whose dynamics is governed by a Lewis-Leach Hamiltonian (2.1), so that transport without final excitation may be designed as described for a single particle. However, for ions with different masses, center of mass and relative motions are coupled. To cope with this coupling I apply a dynamical normal mode approach that approximately separates the Hamiltonian into a sum of independent harmonic oscillators. The equilibrium positions $\{q_i^{(0)}\}$, are found by solving the system $\{\partial V/\partial q_i = 0\}$ for all ions. For $N = 2$ the equilibrium positions are

$$\begin{aligned} q_1^{(0)} &= Q_0 + x_0/2, \\ q_2^{(0)} &= Q_0 - x_0/2, \end{aligned} \qquad (2.6)$$

where

$$x_0 = 2 \left( \frac{C_c}{4u_0} \right)^{1/3}. \tag{2.7}$$

Diagonalizing $V_{ij} = \frac{1}{\sqrt{m_i m_j}} \frac{\partial^2 V}{\partial q_i \partial q_j} \big|_{\{q_i, q_j\} = \{q_i^{(0)}, q_j^{(0)}\}}$, we get the eigenvalues

$$\lambda_\pm = \omega_1^2 \left[ 1 + \frac{1}{\mu} \pm \sqrt{1 - \frac{1}{\mu} + \frac{1}{\mu^2}} \right], \tag{2.8}$$

where $\omega_1 = (u_0/m_1)^{1/2}$, and $\mu = m_2/m_1$, with $\mu \geq 1$. These eigenvalues are related to the normal-mode angular frequencies by

$$\Omega_\pm = \sqrt{\lambda_\pm}. \tag{2.9}$$

The eigenvectors are $v_\pm = \begin{pmatrix} a_\pm \\ b_\pm \end{pmatrix}$, where

$$
\begin{aligned}
a_+ &= \left( \frac{1}{1 + \left( 1 - \frac{1}{\mu} - \sqrt{1 - \frac{1}{\mu} + \frac{1}{\mu^2}} \right)^2 \mu} \right)^{1/2}, \\
b_+ &= \left( 1 - \frac{1}{\mu} - \sqrt{1 - \frac{1}{\mu} + \frac{1}{\mu^2}} \right) \sqrt{\mu} a_+, \\
a_- &= \left( \frac{1}{1 + \left( 1 - \frac{1}{\mu} + \sqrt{1 - \frac{1}{\mu} + \frac{1}{\mu^2}} \right)^2 \mu} \right)^{1/2}, \\
b_- &= \left( 1 - \frac{1}{\mu} + \sqrt{1 - \frac{1}{\mu} + \frac{1}{\mu^2}} \right) \sqrt{\mu} a_-. 
\end{aligned}
\tag{2.10}
$$

Thus, the mass-weighted, dynamical, normal-mode coordinates are

$$
\begin{aligned}
\mathsf{q}_+ &= a_+ \sqrt{m_1} \left( q_1 - Q_0 - \frac{x_0}{2} \right) + b_+ \sqrt{\mu m_1} \left( q_2 - Q_0 + \frac{x_0}{2} \right), \\
\mathsf{q}_- &= a_- \sqrt{m_1} \left( q_1 - Q_0 - \frac{x_0}{2} \right) + b_- \sqrt{\mu m_1} \left( q_2 - Q_0 + \frac{x_0}{2} \right),
\end{aligned}
$$

$$\tag{2.11}$$

and the inverse transformations are

$$q_1 = \frac{1}{\sqrt{m_1}} (b_- \mathsf{q}_+ - b_+ \mathsf{q}_-) + Q_0 + \frac{x_0}{2},$$

$$q_2 = \frac{1}{\sqrt{\mu m_1}} (-a_- \mathsf{q}_+ + a_+ \mathsf{q}_-) + Q_0 - \frac{x_0}{2}. \tag{2.12}$$

Unlike the usual treatments for static traps [59], one has to consider explicitly the time dependence of the parameter $Q_0(t)$ when writing down the Hamiltonian in the new coordinates. I apply the change-of-variables unitary operator

$$U = \int d\mathsf{q}_+ d\mathsf{q}_- dq_1 dq_2 |\mathsf{q}_+, \mathsf{q}_-\rangle \langle \mathsf{q}_+, \mathsf{q}_- | q_1, q_2 \rangle \langle q_1, q_2 |, \tag{2.13}$$

where the transformation matrix is

$$\langle \mathsf{q}_+, \mathsf{q}_- | q_1, q_2 \rangle = \delta[q_1 - q_1(\mathsf{q}_+, \mathsf{q}_-)] \delta[q_2 - q_2(\mathsf{q}_+, \mathsf{q}_-)].$$

The Hamiltonian in the new frame is $H' = UHU^\dagger - i\hbar U(\partial_t U^\dagger)$, and the wavefunction $|\psi'\rangle = U|\psi\rangle$. For the part $UHU^\dagger$, I substitute the definitions (2.12) in the Hamiltonian (2.5) for $N = 2$. For the noninertial term, $-i\hbar U(\partial_t U^\dagger)$, I apply the chain rule in Eq. (2.12) and Eq. (2.11). Keeping only terms up to the harmonic approximation,

$$UHU^\dagger = \frac{\mathsf{p}_+^2}{2} + \frac{1}{2}\Omega_+^2 \mathsf{q}_+^2 + \frac{\mathsf{p}_-^2}{2} + \frac{1}{2}\Omega_-^2 \mathsf{q}_-^2,$$

$$-i\hbar U(\partial_t U^\dagger) = -P_{0+}\mathsf{p}_+ - P_{0-}\mathsf{p}_-, \tag{2.14}$$

where $\mathsf{p}_\pm$ are momenta conjugate to $\mathsf{q}_\pm$, and

$$P_{0\pm} = \dot{Q}_0(\sqrt{m_1}a_\pm + \sqrt{\mu m_1}b_\pm). \tag{2.15}$$

The linear-in-momentum terms are cumbersome for a numerical or analytical treatment, so I apply a further transformation to the frame moving with the center of the trap and remove them formally [60]. The wave function is transformed as $|\psi''\rangle = \mathcal{U}|\psi'\rangle$, whereas the corresponding Hamiltonian takes the form $H'' = \mathcal{U}H'\mathcal{U}^\dagger + i\hbar(\partial_t \mathcal{U})\mathcal{U}^\dagger$. I choose $\mathcal{U} = e^{-i(P_{0+}\mathsf{q}_+ + P_{0-}\mathsf{q}_-)/\hbar}$ to shift the momenta,

so that each mode Hamiltonian in

$$
\begin{aligned}
H'' &= \frac{\mathsf{p}_+^2}{2} + \frac{1}{2}\Omega_+^2 \left( \mathsf{q}_+ + \frac{\dot{P}_{0+}}{\Omega_+^2} \right)^2 \\
&+ \frac{\mathsf{p}_-^2}{2} + \frac{1}{2}\Omega_-^2 \left( \mathsf{q}_- + \frac{\dot{P}_{0-}}{\Omega_-^2} \right)^2
\end{aligned}
\tag{2.16}
$$

belongs to the Lewis-Leach family.

## 2.4   Inverse engineering for two modes

The invariants corresponding to the Hamiltonians in Eq. (2.16) are known and the trajectory can be designed to avoid excitations. I also impose $\dot{Q}_0(t_b)(0) = 0$ so that $|\psi''(0)\rangle = |\psi'(0)\rangle$ and $|\psi''(t_f)\rangle = |\psi'(t_f)\rangle$. Primed and double-primed wave functions are related to each other by the unitary transformation in such a way that their initial and final states coincide. The auxiliary equations analogous to Eq. (2.4) for the modes in Eq. (2.16) are

$$
\ddot{\alpha}_\pm + \Omega_\pm^2 \alpha_\pm = -\dot{P}_{0\pm},
\tag{2.17}
$$

where the $\alpha_\pm$ are the centers of invariant-mode wave functions in the doubly-primed space [33]. Now, one can design these $\alpha_\pm$ functions to get unexcited modes after the transport, and from them inverse engineer $\dot{P}_{0\pm}$. I set the boundary conditions

$$
\alpha_\pm(t_b) = \dot{\alpha}_\pm(t_b) = \ddot{\alpha}_\pm(t_b) = 0.
\tag{2.18}
$$

Substituting these conditions into Eq. (2.17), we find $\dddot{Q}_0(t_b) = 0$ for both modes. To satisfy all the conditions in Eq. (2.17), I tried a polynomial ansatz $Q_0(t; \{a_n\}) = \sum_{n=0}^{9} a_n t^n$. I fixed $a_{0-5}$ as functions of $a_{6-9}$ so that $Q_0(0) = 0$, $Q_0(t_f) = d$, $\dot{Q}_0(t_b) = \ddot{Q}_0(t_b) = 0$. I then select the solutions $\alpha_\pm$ in Eq. (2.17) that satisfy $\alpha_\pm(t_b) = 0$, which implies $\ddot{\alpha}_\pm(t_b) = 0$, since $\dot{P}_{0,\pm}(t_b) = 0$ in Eq. (2.17). The four parameters $a_{6-9}$ are calculated numerically for each $t_f$ by solving the system of four equations $\dot{\alpha}_\pm(t_b) = 0$. Figure 2.1 shows that, for the approximate Hamiltonian
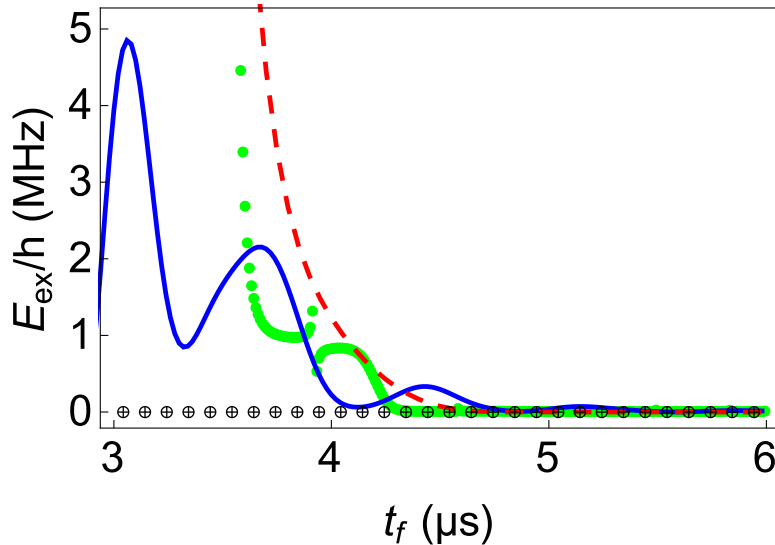
FIGURE 2.1:  Motional excitation quanta vs. transport duration $t_f$ for the two ions, transported over $d = 370$ $\mu$m using the exact Hamiltonian. The external potential minimum moves according to the nonic polynomial $Q_0(t; \{a_n\})$ set to satisfy Eq. (2.17) (green dots); the polynomial ansatz trajectory $Q_0(t; \{b_n\})$, Eq. (2.20), (solid blue line); and the cosine ansatz trajectory $Q_0(t; \{c_n\})$, Eq. (2.21), (dashed red line). The excitation for the nonic polynomial trajectory $Q_0(t; \{a_n\})$ using the uncoupled Hamiltonian (2.16) is also shown (black symbols). The parameters used are $\omega_1/(2\pi) = 2$ MHz, masses of $^9$Be$^+$ for the first ion and $^{24}$Mg$^+$ for the second. Both ions are initially in the motional ground state.

with two uncoupled modes, the final excitation vanishes (see the black symbols horizontal line). However, the higher-order terms in the actual Hamiltonian modify and couple the modes, exciting the system at short transport times (green dots in Fig. 2.1).

The approach I have just described requires a numerical evaluation of the coefficients to find $Q_0(t; \{a_n(t_f)\})$ for each $t_f$. Therefore, I considered a different approximation that yields an analytical solution $Q_0(t)$ with $Q_0(0) = 0$, $Q_0(t_f) = d$, and $\dot{Q}_0(t_b) = \ddot{Q}_0(t_b) = 0$. The resulting $Q_0(t)$ leads to a similar level of final excitation when inserted into the full Hamiltonian as the more accurate approach. I first rewrite the Hamiltonian (2.5) in the center of mass, $Q = (m_1/M)q_1 + (m_2/M)q_2$,

and relative, $r = q_1 - q_2$, coordinates, with $M = m_1 + m_2$,

$$
\begin{aligned}
H &= \frac{P^2}{2M} + \frac{1}{2}M\omega^2(Q - Q_0)^2 \\
&+ \frac{p^2}{2m_r} + \frac{1}{2}m_r\omega_r^2 r^2 + \frac{C_c}{r} \\
&+ \frac{m_2 - m_1}{2}\omega^2(Q - Q_0)r,
\end{aligned}
\tag{2.19}
$$

where $m_r = m_1 m_2/M$, $\omega^2 = 2u_0/M$, $\omega_r^2 = (m_1^2 + m_2^2)/(2m_1m_2)\omega^2$, and $P$ is the total momentum. Neglecting the coupling term in (2.19), one can construct trap trajectories that leave the center of mass unexcited. Rewriting $\alpha = Q_c$, I first design $Q_c$ and then obtain $Q_0$ from Eq. (2.4). The four boundary conditions $\dot{Q}_0(t_b) = \ddot{Q}_0(t_b) = 0$ are consistent with $Q_c^{(3)}(t_b) = Q_c^{(4)}(t_b) = 0$ along with the conditions $Q_c(0) = 0$, $Q_c(t_f) = d$, $\dot{Q}_c(t_b) = \ddot{Q}_c(t_b) = 0$. I assume a polynomial ansatz $Q_c(t) = d\sum_{n=0}^{9} b_n s^n$ that satisfies all conditions and obtain $Q_0(t)$ from Eq. (2.4),

$$
Q_0(t) = \frac{d}{t_f^2\omega^2}\sum_{n=0}^{9} b_n n(n-1)s^{n-2} + d\sum_{n=0}^{9} b_n s^n,
\tag{2.20}
$$

where $s = t/t_f$ and $\{b_0, ..., b_9\} = \{0, 0, 0, 0, 0, 126, -420, 540, -315, 70\}$ for all values of $t_f$. An alternative ansatz with a sum of Fourier cosines also leads to analytical expressions:

$$
\begin{aligned}
Q_c(t) &= \frac{d}{256}\left\{c_0 + \sum_{n=1}^{3} c_n \cos\left[\frac{(2n-1)\pi t}{t_f}\right]\right\}, \\
Q_0(t) &= \frac{d\pi^2}{256\omega^2 t_f^2}\sum_{i=1}^{3} -c_n(2n-1)^2 \cos\left[\frac{(2n-1)\pi t}{t_f}\right] \\
&+ \frac{d}{256}\left\{c_0 + \sum_{n=1}^{3} c_n \cos\left[\frac{(2n-1)\pi t}{t_f}\right]\right\},
\end{aligned}
\tag{2.21}
$$

where $\{c_0, ..., c_3\} = \{128, -150, 25, -3\}$. The resulting trap trajectories (2.20), (2.21) are simple and explicit and lead to small excitations in a similar range of parameters as the approach based on normal modes. Some example trajectories for different transport durations are shown in Fig. 2.2.
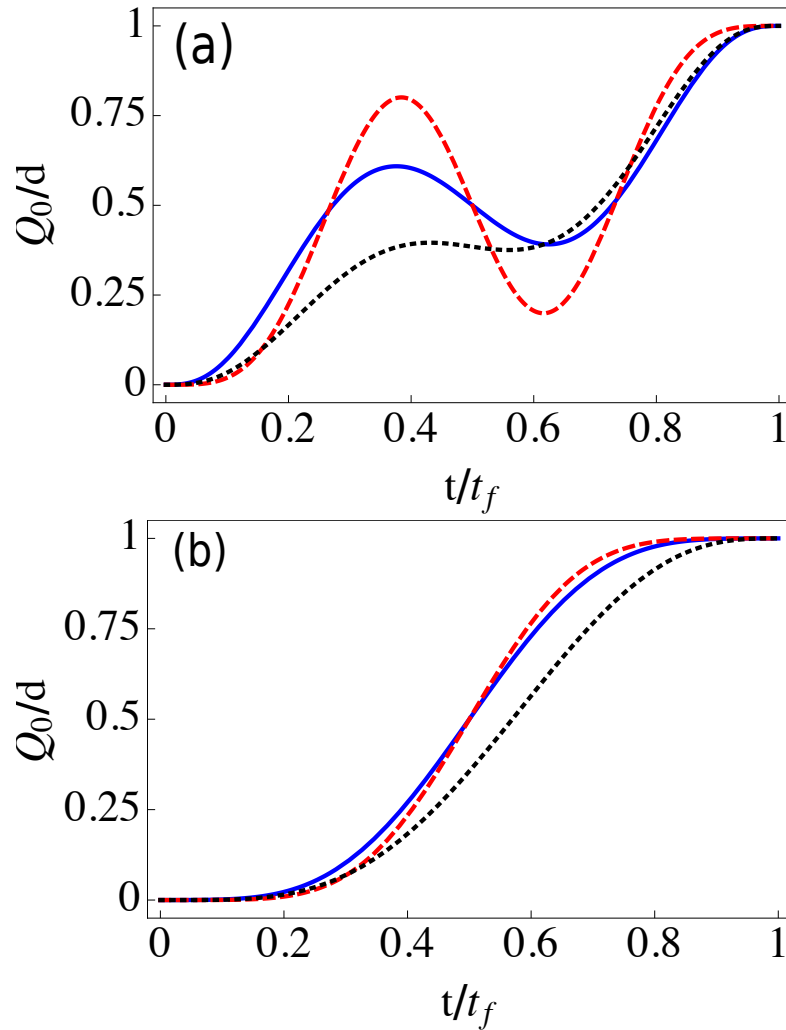
FIGURE 2.2:   Trap trajectories given by $Q_0(t; \{a_n\})$ (dashed black line), Eq. (2.20) (solid blue line), and Eq. (2.21) (dotted red line) for different final times: (a) $t_f = 2\pi/\omega_1$, (b) $t_f = 10 \times 2\pi/\omega_1$; $\omega_1/(2\pi) = 2$ MHz, masses of $^9\text{Be}^+$ for the first ion and $^{24}\text{Mg}^+$ for the second, $d = 370$ $\mu$m.

## 2.5   Four and $N$ ions

I extend now the normal-mode approach to $N$-ion chains, with dynamical normal mode coordinates

$$\mathsf{q}_\nu = \sum_{j=1}^{N} a_{\nu j} \sqrt{m_j}(q_j - \delta_j^{(0)} - Q_0), \tag{2.22}$$

and corresponding momenta $p_\nu$, where the equilibrium points with respect to the trap center, $\delta_j^{(0)}$, are in general found numerically. Generalizing Eq. (2.16) to $N$

ions one finds the uncoupled normal-mode Hamiltonian

$$H'' = \sum_{\nu=1}^{N} \frac{\mathsf{p}_\nu^2}{2} + \sum_{\nu=1}^{N} \frac{1}{2} \Omega_\nu^2 \left( \mathsf{q}_\nu + \frac{\dot{P}_{0\nu}}{\Omega_\nu^2} \right)^2, \tag{2.23}$$

where $P_{0\nu} = \dot{Q}_0 \sum_j a_{\nu j} m_j^{1/2}$, and $\Omega_\nu$ is the angular frequency of the $\nu$th normal mode. The auxiliary equations that have to be satisfied for all $\nu$ simultaneously are

$$\ddot{\alpha}_\nu + \Omega_\nu^2 \alpha_\nu = -\dot{P}_{0\nu}. \tag{2.24}$$

Further imposing, in analogy to Eq. (2.17), $\alpha_\nu(t_b) = \dot{\alpha}_\nu(t_b) = \ddot{\alpha}_\nu(t_b) = 0$ implies $\dot{Q}_0(t_b) = \ddot{Q}_0(t_b) = 0$, exactly as for $N = 2$. Thus, one may construct approximate trap trajectories that are in fact identical in form to the ones for $N = 2$ in Eqs. (2.20) or (2.21), but with $\omega = \sqrt{N u_0 / M}$. I found that the final excitations for a four-ion Be-Mg-Mg-Be chain (see blue solid line in Fig. 2.3), are very similar to those for Be-Mg shown in Fig. 2.1. One can improve the results even further by treating $\omega$ as a variational free parameter. The dashed red line in Fig. 2.3 shows the final excitation for $\omega = 0.983\sqrt{4u_0/M}$. The calculations for the four-ion chain are performed with classical trajectories for the ions, initially at rest in their equilibrium positions. The corresponding quantum calculation is very demanding, but it is not expected to deviate significantly from the classical result [52] in the nearly harmonic regime considered here. For transporting longer ion chains longer final times will be needed, as more nonharmonic terms and coupling term would be neglected in the normal-mode approximation.

## 2.6  Discussion

The approximate approaches I have implemented to transport ions of different mass without final excitation may be compared with other approaches: the "compensating force approach" [33, 39], the transport based on a linear-in-time displacement of the trap, or a more refined error-function trajectory [27].
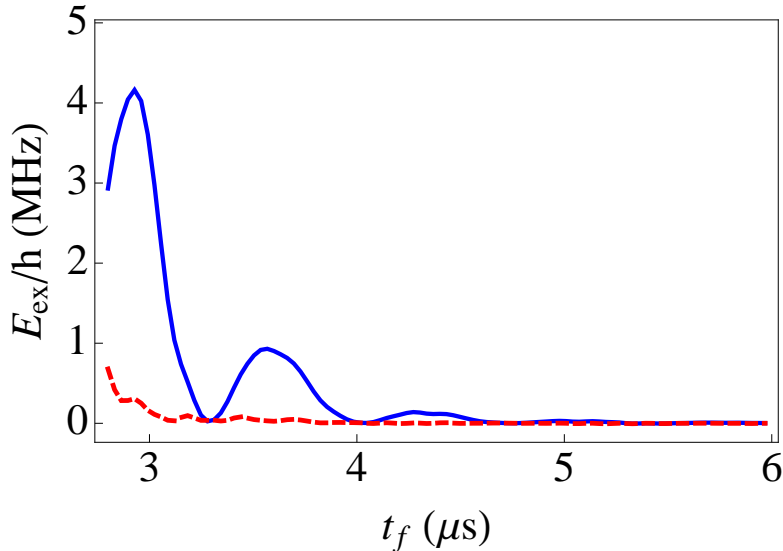
FIGURE 2.3:    Final excitation energy for a Be-Mg-Mg-Be chain transported over $d = 370$ $\mu$m using the external potential minimum trajectory in Eq. (16) with $\omega = \sqrt{4u_0/M}$(blue solid line) and with $\omega = 0.983\sqrt{4u_0/M}$ (dashed red line). The calculation is based on classical equations of motion with the ions at rest in their equilibrium positions at $t = 0$.

Let us first discuss the "compensating force approach" [33, 39]. The idea behind is that the acceleration of the trap induces in the trap frame a noninertial Hamiltonian term $MQ\ddot{Q}_0(t)$, $M$ being the total mass of the ion chain and $Q$ the center-of-mass coordinate, that may be exactly compensated by applying a time-dependent term $H_{\text{com}} = -MQ\ddot{Q}_0(t)$. This has been discussed for $N$ equal masses [48, 52, 61] but the result holds for an arbitrary collection of masses in an arbitrary external potential under rigid transport by noticing that the total potential must be of the form $V(Q-Q_0; \{r_j\})$, where $\{r_j\}$ represents a set of relative coordinates. The decomposition of $H_{\text{com}}$ into terms for each ion, $H_{\text{com}} = -\sum_i m_i q_i \ddot{Q}_0$, implies that ions of different mass should be subjected to different forces. However, the available technology in linear Paul traps provides forces proportional to the charge (equal for all equally-charged ions), so the compensation is a formal result without a feasible experimental counterpart.

As for the linear displacement of the trap, $Q_0(t) = td/t_f$ in $[0, t]$, and at rest otherwise, we have performed numerical calculations of the final excitation energy for different values of $t_f$ and the two ions considered in Sec. 2.3. The excitation oscillates rapidly, see Fig. 2.4 (a), and the upper envelope reaches 0.1 vibrational
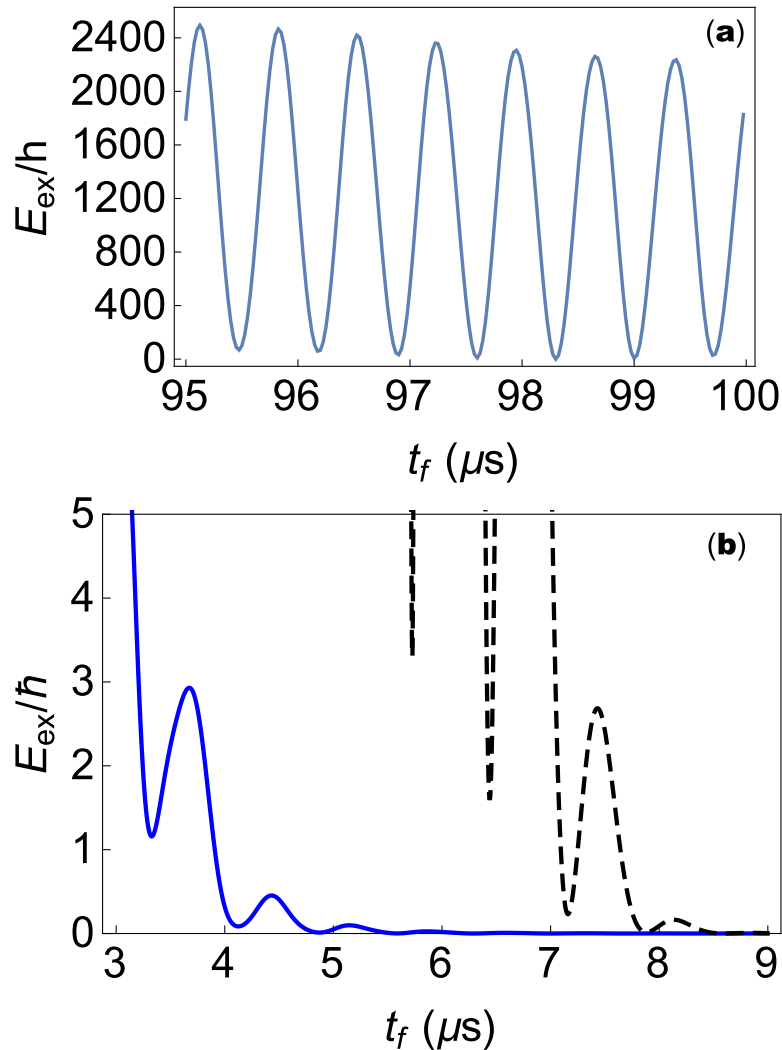
FIGURE 2.4:  Excitation energy vs. final time for (a) a linear-in-time transport of two ions, $Q_0(t) = td/t_f$ and (b) the trap trajectory designed in Eq. (2.20), (blue-solid line) and an "error function" trap trajectory, Eq. (2.25) (black-dashed). We find optimal results for $\sigma = 10^{-6}s$. Other parameters as in Fig. 1.

quanta of ion 1 for times as large as 9.5 ms. The first excitation minimum with significant excitation reduction is around 99 $\mu$s, see Fig. 2.4 (a). Excitation minima occur for each mode $\nu$ as zeroes of the Fourier transform of $\dot{Q}_0$ at $\Omega_\nu$ [27, 37, 42]. For a linear-in-time trap displacement this occurs every mode period. 99 $\mu$s is a time when the transform of both modes vanishes. This excitation minimum, however, is very unstable with respect to small timing errors. In any case, it is about twenty times larger than the times achieved in Sec. 2.3.

Finally, I compare the performance of my protocol in Eq. (2.20) with an error-function trajectory [27]. Imposing a Gaussian form on the velocity $\dot{Q}_0$ gives

$$Q_0(t) = -\frac{d}{2}\frac{\operatorname{erf}\left(\frac{-2t+t_f}{2\sqrt{2}\sigma}\right)}{\operatorname{erf}\left(\frac{t_f}{2\sqrt{2}\sigma}\right)} + \frac{d}{2}, \tag{2.25}$$

where $\sigma$ is the width of the Gaussian. In Fig. 2.4 (b) I optimize $\sigma$ and compare the excitation for this trajectory with the one in Eq. (2.20). The error-function trajectory is clearly a good design, but still, the protocol developed in this chapter outperforms it by a factor of 2.

In summary, I have described protocols for diabatic transport of mixed-species chains of ions that displace the minimum of a harmonic external potential along prescribed trajectories. My protocols should allow for diabatic transport over distances and durations that are relevant for quantum information processing with minimal final excitation of the ion crystals. In past experiments on scalable quantum information processing, adiabatic transport of mixed-species ion chains has been one of the most time-consuming processes [30]; therefore, the approaches described might lead to considerable practical improvements. This work may be extended in several directions, e.g., to include noise, parameter drifts (as was done in [62]) and anharmonicities [36, 40, 52], or to optimize the trap trajectories according to different criteria [40]. The results of this chapter were published in [63]. Later, in [62], the two ion transport was designed when considering errors in the frequency or trap position.

# Chapter 3

# Fast phase gates with trapped ions

> *"I think that's the single best piece of advice: constantly think about how you could be doing things better and questioning yourself."*
>
> Elon Musk

I implement faster-than-adiabatic two-qubit phase gates using smooth state-dependent forces. The forces are designed to leave no final motional excitation, independently of the initial motional state in the harmonic, small-oscillations limit. They are simple, explicit functions of time and the desired logical phase of the gate, and are based on quadratic invariants of motion and Lewis-Riesenfeld phases of the normal modes.

## 3.1  Introduction

Realizing the full potential of quantum information processing requires a sustained effort to achieve scalability, and to make basic dynamical or logical operations faster, more accurate and reliable under perturbations. Two-qubit gates are crucial building blocks in any scheme of universal quantum computing and have received much attention. An important step forward was the theoretical proposal of geometric gates with reduced sensitivity to the vibrational quantum numbers [64–67], with the first experimental realization in [68]. Soon after, Leibfried et al. [69] demonstrated a phase gate of the form

$$|\uparrow\uparrow\rangle \to |\uparrow\uparrow\rangle, \ |\downarrow\downarrow\rangle \to |\downarrow\downarrow\rangle,$$
$$|\uparrow\downarrow\rangle \to i|\uparrow\downarrow\rangle, \ |\downarrow\uparrow\rangle \to i|\downarrow\uparrow\rangle, \tag{3.1}$$

with two trapped ions of the same species subjected to state-dependent forces, where each spin-up/down arrow represents an eigenstate of the $\sigma_z$-operator for one of the ion qubits. Generalizations of this gate with the potential of reduced gate times were discussed by García-Ripoll et al. [70, 71], and in [72]. The gate mechanism satisfies a number of desirable properties: it is insensitive to the initial motional state of the ions, at least in the small-oscillations regime, where the motion is inside the Lamb-Dicke regime and the nonlinearities of the Coulomb coupling are negligible; it depends on "geometric" properties of the dynamics (phase-space areas), which makes it resistant to certain errors; it allows for close distances, and thus strong interactions among the ions; and, finally, it may in principle be driven in short, faster-than-adiabatic times. The forces designed to make the ions return to their initial motional state in a rotating frame of phase-space coordinates [66, 67], are different for different qubit state configurations, leading to qubit-state dependent motional trajectories that produce a differential phase. Pulsed forces with abrupt kicks were designed [72–75], and also smooth force evolutions that vanish but have nonvanishing derivatives at boundary times [71], but in practice no force patterns with infinite derivatives are possible and smooth envelopes are desirable to minimize experimental errors.

In this chapter, I revisit the phase gates and tackle the design of smooth forces as an inverse problem, via Lewis-Riesenfeld invariants [76]. This provides a more general time dependence than previous proposals to achieve faster than adiabatic operations. Hereafter, forces are assumed to be induced by off-resonant lasers that do not change the internal states. However, the basic ideas should be applicable to Mølmer and Sørensen type gates that flip the qubit spins during gates as well[1] [77]. Specifically, I design forces to implement the operation

$$| \uparrow\uparrow \rangle \to e^{i\phi(\uparrow\uparrow)} | \uparrow\uparrow \rangle, \ | \downarrow\downarrow \rangle \to e^{i\phi(\downarrow\downarrow)} | \downarrow\downarrow \rangle,$$
$$| \uparrow\downarrow \rangle \to e^{i\phi(\uparrow\downarrow)} | \uparrow\downarrow \rangle, \ | \downarrow\uparrow \rangle \to e^{i\phi(\downarrow\uparrow)} | \downarrow\uparrow \rangle, \tag{3.2}$$

such that $\Delta\phi \equiv \phi(\uparrow\downarrow) + \phi(\downarrow\uparrow) - \phi(\uparrow\uparrow) - \phi(\downarrow\downarrow) = \pm\pi$, where the qubits could be realized with two different species, which may have practical importance to scale up quantum information processing with trapped ions [78]. Gates of the form (3.2) are computationally equivalent, up to single-qubit $z-$rotations to the standard phase gate diag$[1, 1, 1, -1]$ written in the basis $\{| \uparrow\uparrow \rangle, | \uparrow\downarrow \rangle, | \downarrow\uparrow \rangle, | \downarrow\downarrow \rangle\}$ [79].

My analysis demonstrates that invariant-based inverse Hamiltonian design is not limited to population control, and may be adjusted for phase control as well[2]. It was known that the phase of a given mode of the invariant (a time-dependent eigenstate of the invariant which is also a solution of the time-dependent Schrödinger equation) could be controlled [32], but the fact that "global phases", for a given internal state configuration, of arbitrary motional states can be controlled as well in a simple way had been overlooked. This is interesting for applying shortcuts to adiabaticity [31] in quantum information processing. In particular, I will derive ready-to-use, explicit expressions for the state-dependent forces, and may benefit from the design freedom offered by the invariant-based method to satisfy further optimization criteria.

---

[1]The Mølmer & Sørensen gate [64, 67] can be mathematically described in the same language, replacing the eigenvectors of $\sigma_z$, $| \uparrow \rangle$ and $| \downarrow \rangle$, by the eigenvectors of $\sigma_x$, $|+\rangle$ and $|-\rangle$. This allows for an interchange of methods among the gate (3.2) and the Mølmer & Sørensen gate.

[2]In all other chapters of this Thesis, I am only worried about conserving populations of each eigenstate at the end of the studied process, only in this chapter will the phases be controlled to get a predetermined value at the end of the process.

To evaluate the actual performance of the phase gate at short times I have to compute fidelities, excitation energies, and/or their scaling behavior, according to the dynamics implied by the Hamiltonian including the anharmonicity of the Coulomb repulsion. This is important, as inversion protocols that work near perfectly in the small-oscillations regime, fail for the large amplitudes of ion motion that occur in fast gates, and only a rough estimate of the domain of validity could be found in [71]. Here, I have numerically checked the validity of the phase gate up to gate times less than one oscillation period without assuming the approximations used in the small-amplitude regime. An additional perturbing effect with respect to an idealized limit of homogeneous spin-dependent forces is the position dependence of the forces induced by optical beams. This may be serious at the large motional amplitudes required for short gate times, when the ion motion amplitude becomes comparable to the optical wavelength as I illustrate with numerical examples.

The analytical theory for small oscillations is worked out in Secs. 3.2, 3.3 and 3.4. Then, I consider in Sec. 3.5 two ions of the same species, which implies some simplifications, and a physical constraint, namely, equal forces on both ions if they are in the same internal state, and make the additional assumption that the force is equal and opposite in the other state (more general forces are treated in Appendix B). I also consider a more complete Hamiltonian including the anharmonicity of the Coulomb force and the spatial dependence of the light fields to find numerically the deviations with respect to ideal results within the small oscillations approximation. Finally, in Sec. 3.6, I consider phase gates between ions of different species. The appendices present: generalizations of the results for arbitrary proportionalities between the state-dependent forces (Appendix B), alternative useful expressions for the phases (Appendix C), an analysis to determine the worst possible fidelities (Appendix D), the calculation of the width of the position of one ion in the two-ion ground state (Appendix E), and alternative inversion protocols (Appendix F).

## 3.2 The model

Consider two ions of charge $e$, masses $m_1$, $m_2$, and coordinates $x_1$, $x_2$, trapped within the same, radially-tight, effectively one-dimensional (1D) trap. I assume the position $x_1$ of "ion 1" to fulfill $x_1 < x_2$ at all times due to Coulomb repulsion, with $x_2$ the position of "ion 2". Qubits may be encoded for each ion in two internal levels corresponding to "spin up" ($|\uparrow\rangle$) eigenstate of $\sigma_z$, with eigenvalue $\sigma_i^z = 1$, and "spin down" eigenstate ($|\downarrow\rangle$), with eigenvalue $\sigma_i^z = -1$, $i = 1, 2$. Off-resonant lasers induce state-dependent forces that are assumed first to be homogeneous over the extent of the motional state (Lamb-Dicke approximation). Later in the chapter, I shall analyze the effect of more realistic position-dependent light fields when the Lamb-Dicke condition is not satisfied. For a given spin configuration, $\uparrow\uparrow$, $\downarrow\downarrow$, $\uparrow\downarrow$, or $\downarrow\uparrow$, the Hamiltonian can be written as

$$
\begin{aligned}
\mathcal{H} &= \frac{p_1^2}{2m_1} + \frac{1}{2}u_0 x_1^2 + F_1(t; \sigma_1^z)x_1 \\
&+ \frac{p_2^2}{2m_2} + \frac{1}{2}u_0 x_2^2 + F_2(t; \sigma_2^z)x_2 \\
&+ \frac{C_c}{x_2 - x_1} - E_0,
\end{aligned}
\tag{3.3}
$$

where $C_c = \frac{e^2}{4\pi\epsilon_0}$, $u_0 = m_1\omega_1^2 = m_2\omega_2^2$, and $\epsilon_0$ is the vacuum permittivity. A constant $E_0$ is added for convenience so that the minimum of

$$
\mathcal{V} = \frac{1}{2}u_0 x_1^2 + \frac{1}{2}u_0 x_2^2 + \frac{C_c}{x_2 - x_1} - E_0
\tag{3.4}
$$

is at zero energy when $x_1$ and $x_2$ assume their equilibrium positions. The laser-induced, state-dependent forces may be independent for different ions as they may be implemented by different lasers on different transitions. For equal-mass ions, the same lasers, and equal and opposite forces on the qubit eigenstates, they may simplify to $F_i = \sigma_i^z F(t)$. In principle, the proportionality between the force for the up and the down state could be different, but, as shown in the Appendix B, the forces for a general proportionality can be related by a simple scaling to the ones found for the symmetric case $F_i = \sigma_i^z F(t)$.

One can determine normal modes for the zeroth order Hamiltonian

$$\mathcal{H}_0 = \frac{p_1^2}{2m_1} + \frac{p_2^2}{2m_2} + \mathcal{V}. \tag{3.5}$$

The equilibrium positions of both ions under the potential $\mathcal{V}$ are

$$x_1^{(0)} = -\sqrt[3]{\frac{C_c}{4u_0}}, \quad x_2^{(0)} = \sqrt[3]{\frac{C_c}{4u_0}}, \tag{3.6}$$

with equilibrium distance $x_0 = x_2^{(0)} - x_1^{(0)}$, which yields $E_0 = 3u_0x_0^2/4$.

Diagonalizing the mass-scaled curvature matrix $V_{ij} = \frac{1}{\sqrt{m_i m_j}} \frac{\partial^2 \mathcal{V}}{\partial x_i \partial x_j}\big|_{\{x_i,x_j\}=\{x_i^{(0)},x_j^{(0)}\}}$, that describes the restoring forces for small oscillations around the equilibrium positions, we get the eigenvalues

$$\lambda_\pm = \omega_1^2 \left[ 1 + \frac{1}{\mu} \pm \sqrt{1 - \frac{1}{\mu} + \frac{1}{\mu^2}} \right], \tag{3.7}$$

where $\omega_1 = (u_0/m_1)^{1/2}$ and $\mu = m_2/m_1$, with $\mu \geq 1$. The normal-mode angular frequencies are

$$\Omega_\pm = \sqrt{\lambda_\pm}, \tag{3.8}$$

and the orthonormal eigenvectors take the form $v_\pm = \begin{pmatrix} a_\pm \\ b_\pm \end{pmatrix}$, where

$$
\begin{aligned}
a_\pm &= \left[ \frac{1}{1 + \left(1 - \frac{1}{\mu} \mp \sqrt{1 - \frac{1}{\mu} + \frac{1}{\mu^2}}\right)^2 \mu} \right]^{1/2}, \\
b_\pm &= \left(1 - \frac{1}{\mu} \mp \sqrt{1 - \frac{1}{\mu} + \frac{1}{\mu^2}}\right) \sqrt{\mu} a_\pm,
\end{aligned}
\tag{3.9}
$$

fulfill

$$
\begin{aligned}
a_\pm^2 + b_\pm^2 &= 1, \\
a_+ a_- + b_+ b_- &= 0, \\
a_+ b_- - a_- b_+ &= 1.
\end{aligned}
\tag{3.10}
$$

The mass-weighted, normal-mode coordinates are

$$\begin{aligned}
\mathsf{x}_+ &= a_+\sqrt{m_1}(x_1 - x_1^{(0)}) + b_+\sqrt{\mu m_1}(x_2 - x_2^{(0)}), \\
\mathsf{x}_- &= a_-\sqrt{m_1}(x_1 - x_1^{(0)}) + b_-\sqrt{\mu m_1}(x_2 - x_2^{(0)}),
\end{aligned} \tag{3.11}$$

and the inverse transformation to the original position coordinates is

$$\begin{aligned}
x_1 &= \frac{1}{\sqrt{m_1}}(b_-\mathsf{x}_+ - b_+\mathsf{x}_-) - \frac{x_0}{2}, \\
x_2 &= \frac{1}{\sqrt{\mu m_1}}(-a_-\mathsf{x}_+ + a_+\mathsf{x}_-) + \frac{x_0}{2}.
\end{aligned} \tag{3.12}$$

Finally, the Hamiltonian (3.3), neglecting higher-order anharmonic terms, and using conjugate "momenta" $\mathsf{p}_\pm = -i\hbar\partial/\partial\mathsf{x}_\pm$,[3] takes the form

$$\mathcal{H} = H_{NM} + \tilde{f}(t), \tag{3.13}$$

where

$$\begin{aligned}
H_{NM} &= H_+ + H_-, \\
H_\pm &= \frac{\mathsf{p}_\pm^2}{2} + \frac{1}{2}\Omega_\pm^2\mathsf{x}_\pm^2 - f_\pm\mathsf{x}_\pm, \\
\tilde{f} &= \frac{x_0}{2}(F_2 - F_1), \\
f_\pm(t) &= \mp\frac{F_1 b_\mp}{\sqrt{m_1}} \pm \frac{F_2 a_\mp}{\sqrt{\mu m_1}}.
\end{aligned} \tag{3.14}$$

The function $\tilde{f}$ depends on time and on the internal states that will determine the forces. By restricting the calculation to a given spin configuration, the dynamics may be worked out in terms of $H_{NM}$ alone, $i\hbar\partial\psi_{NM}/\partial t = H_{NM}\psi_{NM}$, and the wave function that evolves with $\mathcal{H}$ in Eq. (3.13) is $e^{(-i/\hbar)\int_0^t dt'\tilde{f}}\psi_{NM}$. Purely time-dependent terms in the Hamiltonian are usually ignored as they imply global phases. In the phase-gate scenario, however, they are not really global, since they depend on the spin configuration. As the spin configuration may be changed after applying the phase gate, e.g. by resonant interactions, they may lead to

---

[3]The dimensions of the mass weighted coordinates are length times square root of mass, $mkg^{1/2}$, while the dimensions of the conjugate momenta are $kg^{1/2}m/s$.

observable interference effects and, in general, cannot be ignored. However, in the particular gate operation studied later, the extra phase vanishes at the final time $t_f$, so I shall focus on the dynamics and phases generated by the Hamiltonian $H_{NM}$, which represents two independent forced harmonic oscillators with constant frequencies. We can now apply Lewis-Riesenfeld theory [76] in an inverse way [31]: The desired dynamics are designed first, and from the corresponding invariant, the time-dependent functions in the Hamiltonian are inferred [33]. Note that in the inverse problem, the oscillators are "coupled", as only one physical set of forces that will act on both normal modes of the uncoupled system must be designed [63].

## 3.3 One mode

In this section I consider just one mode, and drop the subscripts $\pm$ to make the treatment applicable to both modes. The goal is to find expressions for the corresponding invariants, dynamics, and phases. The Hamiltonian describing a harmonic oscillator with mass-weighted position and momentum is written as

$$
\begin{align}
H &= H_0 + V, & (3.15)\\
H_0 &= \frac{p^2}{2} + \frac{1}{2}\Omega^2 x^2, & (3.16)\\
V &= -f(t)x. & (3.17)
\end{align}
$$

It is possible to find a dynamical invariant of $H$ solving the equation

$$
\frac{dI}{dt} \equiv \frac{\partial I}{\partial t} + \frac{1}{i\hbar}[I, H] = 0. \tag{3.18}
$$

For a moving harmonic oscillator, a simple way to find an invariant is to assume a quadratic (in position and momentum) ansatz with parameters that may be determined by inserting the ansatz in Eq. (3.18). This leads to the invariant

$$
I(t) = \frac{1}{2}(p - \dot{y})^2 + \frac{1}{2}\Omega^2(x - y)^2, \tag{3.19}
$$

where the dot means "time derivative", and the function $y(t)$ must satisfy the differential (Newton) equation

$$\ddot{y} + \Omega^2 y = f, \tag{3.20}$$

so it can be interpreted as a "classical trajectory" (with dimensions $kg^{1/2}m$) in the forced harmonic potential [33].

This invariant is Hermitian, and has a complete set of eigenstates. Solving

$$I(t)\psi_n(t) = \lambda_n \psi_n(t), \tag{3.21}$$

we get the time-independent eigenvalues

$$\lambda_n = \hbar\Omega \left( \frac{1}{2} + n \right), \tag{3.22}$$

and the time-dependent eigenvectors

$$\psi_n(x, t) = e^{\frac{i}{\hbar}\dot{y}x} \phi_n \left( x - y \right), \tag{3.23}$$

where $\phi_n(x)$ are the $n$th eigenvectors of the stationary oscillator,

$$\phi_n(x) = \frac{1}{\sqrt{2^n n!}} \left( \frac{\Omega}{\pi\hbar} \right)^{1/4} e^{-\frac{\Omega x^2}{2\hbar}} H_n \left( \sqrt{\frac{\Omega}{\hbar}}x \right), \tag{3.24}$$

and the $H_n$ are Hermite polynomials. The Lewis-Riesenfeld phases $\theta_n$ must satisfy

$$\hbar\frac{d\theta_n}{dt} = \left\langle \psi_n \left| i\hbar\frac{\partial}{\partial t} - H \right| \psi_n \right\rangle, \tag{3.25}$$

so that the wavefunction (3.28) is indeed a solution of the time-dependent Schrödinger equation. Using Eq. (3.23), they are given by

$$\begin{aligned} \theta_n(t) &= -\frac{1}{\hbar} \int_0^t dt'(\lambda_n + \dot{y}^2/2 - \Omega^2 y^2/2) \\ &= -(n + 1/2)\Omega t - G(t), \end{aligned} \tag{3.26}$$

where

$$G(t) = \frac{1}{2\hbar} \int_0^t dt'(\dot{y}^2 - \Omega^2 y^2). \tag{3.27}$$

Finally, the solution of the Schrödinger equation for the Hamiltonian $H$ can be stated in terms of the eigenstate and Lewis-Riesenfeld phases of the invariant as

$$\psi(x, t) = \sum_n c_n e^{i\theta_n(t)} \psi_n(x, t). \tag{3.28}$$

In the following, I consider that $f$ is such that there are particular solutions $y = \alpha$ of Eq. (3.20) that satisfy at the boundary times $t_b = 0, t_f$ the boundary conditions

$$\alpha(t_b) = \dot{\alpha}(t_b) = 0. \tag{3.29}$$

They guarantee that all states $\Psi_n(x, t) = e^{i\alpha_n^{(\pm)}(t)} \psi_n(x, t)$ end up at the original positions and at rest,

$$\Psi_n(x, t_f) = e^{i\alpha_n(t_f)} \phi_n(x). \tag{3.30}$$

In other words, each initial eigenstate of the Hamiltonian is driven along a path that returns to the initial state with an added path-dependent phase. Moreover, I assume that the force vanishes at the boundary times $t_b = 0, t_f$, $f(t_b) = 0$, and, therefore, from Eq. (3.20),

$$\ddot{\alpha}(0) = \ddot{\alpha}(t_f) = 0. \tag{3.31}$$

Integrating by parts and using Eq. (3.20) as well as the boundary conditions $\alpha(t_b) = 0$, the phase factor common to all $n$ takes the form

$$\phi(t_f) = -G(t_f) = \frac{1}{2\hbar} \int_0^{t_f} dt' f\alpha. \tag{3.32}$$

As the phases $\alpha_n(t_f)$ in Eq. (3.26) have an extra $n$-dependent term, an arbitrary motional state $\psi(t)$ that superposes different $n$-components does not generally return to the same initial projective ray. To remedy this, it is useful to consider a rotating frame, i.e., I define $\psi_I(t) = e^{iH_0 t/\hbar} \psi(t)$, so that

$$\psi_I(t_f) = e^{-iG(t_f)} \psi_I(0), \tag{3.33}$$

with total phase $-G(t_f)$ for an arbitrary motional state. To decompose this phase into dynamical and geometric phases, I first note that

$$i\hbar\frac{\partial\psi_I}{\partial t} = V_I\psi_I, \tag{3.34}$$

where $V_I = -fe^{iH_0t/\hbar}xe^{-iH_0t/\hbar}$. The dynamical phase is

$$
\begin{aligned}
\phi_d &= -\frac{1}{\hbar}\int_0^{t_f} dt\langle\psi_I(t)|V_I(t)|\psi_I(t)\rangle \\
&= -\frac{1}{\hbar}\int_0^{t_f} dt\langle\psi(t)|V(t)|\psi(t)\rangle \\
&= \frac{1}{\hbar}\int_0^{t_f} dt f(t)\langle x(t)\rangle.
\end{aligned}
\tag{3.35}
$$

The expectation value of $x$ corresponds to a classical trajectory, i.e., to a solution of Eq. (3.20), but not necessarily the one corresponding to $\alpha$. To describe a general trajectory, it is useful to define dimensionless positions and momenta as

$$Y = \sqrt{\frac{\Omega}{2\hbar}}\,y, \qquad P = \sqrt{\frac{1}{2\hbar\Omega}}\,p, \tag{3.36}$$

(similarly for other coordinates such as $x$ or $\alpha$) as well as complex-plane combinations $z = Y + iP$.

The general solution of the position and momentum of a classical particle, or the corresponding expectation values for any quantum state, is compactly given in complex form as

$$
\begin{aligned}
z_g(t) &= e^{-i\Omega t}\left\{z_g(0) + \frac{i}{\sqrt{2\hbar\Omega}}\int_0^t d\tau e^{i\Omega\tau}f\right\} \\
&= \tilde{z} + z_0,
\end{aligned}
\tag{3.37}
$$

where

$$\tilde{z} \equiv e^{-it\Omega}z_g(0), \tag{3.38}$$

$$z_0 \equiv \sqrt{\frac{\Omega}{2\hbar}}y_0 + i\sqrt{\frac{1}{2\Omega\hbar}}\dot{y}_0, \tag{3.39}$$

and $y_0$ is a particular solution satisfying $y_0(0) = \dot{y}_0(0) = 0$. For an $f$ such that $y_0(t) = \alpha(t)$, and thus $z_0 = z_\alpha$, the boundary conditions at $t_f$ are satisfied as well in the particular solution [see Eq. (3.29)]. By separating into real and imaginary parts, it can be seen that

$$\Re e(\tilde{z}) \frac{1}{\sqrt{2\Omega\hbar}} f = \frac{\partial \Im m(z_\alpha \tilde{z}^*)}{\partial t}, \tag{3.40}$$

so that

$$\int_0^{t_f} dt\, \Re e(\tilde{z}) f = 0, \tag{3.41}$$

since $z_\alpha(t_b) = 0$. With these results, I rewrite Eq. (3.35) as

$$\phi_d = \frac{1}{\hbar} \int_0^{t_f} dt \left[ \alpha + \sqrt{\frac{2\hbar}{\Omega}} \Re e(\tilde{z}) \right] f = \frac{1}{\hbar} \int_0^{t_f} dt\, f\alpha. \tag{3.42}$$

Therefore, the geometric phase $\phi_g$ is minus the total phase,

$$\phi_g = \phi - \phi_d = -\frac{1}{2\hbar} \int_0^{t_f} dt\, f\alpha = -\phi. \tag{3.43}$$

It is interesting to use the phase-space trajectory in the rotating frame $z_r = e^{i\Omega t} z_g = X_r + iP_r$ to write $\frac{f\langle x \rangle}{\hbar} = \sqrt{\frac{2}{\hbar\Omega}} \Re e(z_g) = 2\Im m(\frac{dz_r}{dt} z_r^*) = 4d\mathcal{A}/dt$, where $d\mathcal{A}$ is the differential of area swept in the rotating-phase space, $d\mathcal{A}/dt = \frac{X_r}{2} \frac{dP_r}{dt} - \frac{P_r}{2} \frac{dX_r}{dt}$. Thus, Eq. (3.35) becomes

$$\phi_d = 4\mathcal{A}. \tag{3.44}$$

Consequently, $\phi_g = -2\mathcal{A}$, and $\phi = 2\mathcal{A}$. The area is equal for all trajectories [values of $z_g(0)$] due to Eq. (3.41), so it may be calculated using $z_g(0) = 0$, i.e., the simple particular solution $z_g = z_\alpha$. Equations (3.43) or (3.44) are known results [71], but they are relevant for my work, so I have rederived them without using coherent states or a concatenation of displacement operators [69]. This is convenient when expressing the wave function directly as a superposition in an orthonormal basis.

## 3.4 Invariant-based inverse Hamiltonian design

The results of the previous section may now be combined to inverse engineer the force. The Hamiltonian $H_{NM}$ involves the two modes so that superscripts or subscripts have to be added to the functions of the previous section to denote the mode.

I assume that forces vanish at the boundary times $t_b = 0, t_f$, $F_1(t_b) = F_2(t_b) = 0$, and thus, $f_\pm(t_b) = 0$. In the rotating frame, $\psi_I(t) = e^{iH^0_{NM}t/\hbar}\psi_{NM}(t)$, where

$$
\begin{aligned}
H^0_{NM} &= H^0_+ + H^0_-, \\
H^0_\pm &= \frac{\mathsf{p}^2_\pm}{2} + \frac{1}{2}\Omega^2_\pm\mathsf{x}^2_\pm,
\end{aligned}
\tag{3.45}
$$

so that

$$
\psi_I(t_f) = e^{-i[G_-(t_f)+G_+(t_f)]}\psi_I(0).
\tag{3.46}
$$

Thus, the phase we are interested in for a given configuration is

$$
\begin{aligned}
\phi(t_f) &= -[G_+(t_f) + G_-(t_f)] \\
&= -\frac{1}{2\hbar}\int_0^{t_f}dt'(\dot{\alpha}^2_+ + \dot{\alpha}^2_- - \Omega^2_+\alpha^2_+ - \Omega^2_-\alpha^2_-) \\
&= \frac{1}{2\hbar}\int_0^{t_f}dt'(f_+\alpha_+ + f_-\alpha_-),
\end{aligned}
\tag{3.47}
$$

see an alternative double-integral expression in Appendix C. The inverse strategy is to design the $\alpha_\pm$ consistently with the boundary conditions, leaving free parameters that are fixed to produce the desired phase. The following section shows this in detail for equal masses.

## 3.5 Equal mass ions

For two equal-mass ions, $m = m_1 = m_2$, $\omega = \omega_1 = \omega_2$, $a_+ = -b_+ = a_- = b_- = 1/\sqrt{2}$, $\Omega_- = \omega$ (center-of-mass mode), and $\Omega_+ = \sqrt{3}\omega$ (stretch mode). This

implies [see Eq. (3.14)] that

$$f_{\pm} = \frac{\pm F_2 - F_1}{\sqrt{2m}},$$ (3.48)

and $F_1$ and $F_2$ are defined as $F_i = \sigma_i^z F(t)$ (see the general case in Appendix B), so that the following values are found

$$\begin{aligned}
f_+(P) &= f_-(A) = 0, \\
f_-(\uparrow\uparrow) &= f_+(\uparrow\downarrow) = -2F/\sqrt{2m}, \\
f_-(\downarrow\downarrow) &= f_+(\downarrow\uparrow) = 2F/\sqrt{2m},
\end{aligned}$$ (3.49)

where $P$ stands for parallel spins, and $A$ for antiparallel ones. If both ions have the same spin, then $f_+(P) = 0$ and no stretch is induced, but the center-of-mass $(-)$ mode is transiently excited. In that case, $\alpha_+(P) = 0$ and

$$\alpha_-(\uparrow\uparrow) = -\alpha_-(\downarrow\downarrow),$$ (3.50)

according to Eqs. (3.20) and the established boundary conditions. For opposite spins $\alpha_-(A) = 0$, and only the stretch $(+)$ mode is transiently excited. In that case

$$\alpha_+(\uparrow\downarrow) = -\alpha_+(\downarrow\uparrow).$$ (3.51)

The phase (3.47) takes two possible forms,

$$\begin{aligned}
\phi(P) &= \frac{1}{\hbar} \int_0^{t_f} dt' \frac{-F}{\sqrt{2m}} \alpha_-(\uparrow\uparrow), \\
\phi(A) &= \frac{1}{\hbar} \int_0^{t_f} dt' \frac{-F}{\sqrt{2m}} \alpha_+(\uparrow\downarrow).
\end{aligned}$$ (3.52)

To inverse engineer the phase, I use the ansatz for $\alpha_+(\uparrow\downarrow)$ as a sum of Fourier cosines, with enough parameters to satisfy all boundary conditions,

$$\alpha_+(\uparrow\downarrow; t) = a_0 + \sum_{n=1}^{4} a_i \cos\left[\frac{(2n-1)\pi t}{t_f}\right].$$ (3.53)

This is an odd function of $(t - t_f/2)$, which implies that $\ddot{\alpha}_+(\uparrow\downarrow; t)$, and thus $f_+(\uparrow\downarrow; t)$, are odd functions too with respect to the middle time of the process
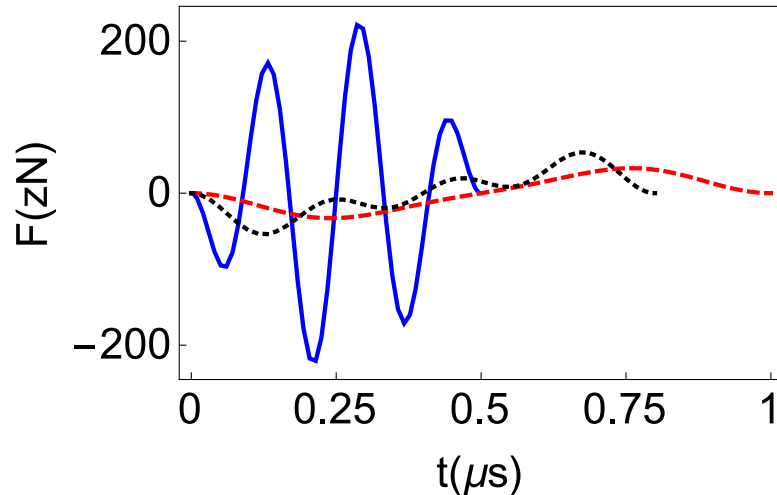
FIGURE 3.1: $F(t)$ for two $^9\text{Be}^+$ ions in a trap with frequency $\omega/2\pi = 2$ MHz. $t_f = 0.5$ $\mu$s (solid blue line), $t_f = 0.8$ $\mu$s (dotted black line), and $t_f = 1$ $\mu$s (dashed red line). The forces on each ion are state dependent, $F_i = \sigma_i^z F(t)$, $i = 1, 2$.

$t_f/2$. The parameters $a_0$, $a_1$, and $a_2$ are fixed to satisfy the corresponding boundary conditions for $\alpha_+(\uparrow\downarrow)$ in Eqs. (3.29) and (3.31),

$$
\begin{aligned}
a_0 &= 0, \\
a_1 &= 2a_3 + 5a_4, \\
a_2 &= -3a_3 - 6a_4.
\end{aligned}
\tag{3.54}
$$

We get $f_+(\uparrow\downarrow; t)$ from Eq. (3.20), $f_+(\uparrow\downarrow; t) = \ddot{\alpha}_+(\uparrow\downarrow; t) + \Omega_+^2 \alpha_+(\uparrow\downarrow; t)$. Due to the boundary conditions, $f_+(0) = f_+(t_f) = 0$. As $f_-(\uparrow\uparrow) = f_+(\uparrow\downarrow)$, we may solve Eq. (3.20) for $\alpha_-(\uparrow\uparrow; t)$ satisfying $\alpha_-(\uparrow\uparrow; t_b) = 0$ [$\ddot{\alpha}_-(\uparrow\uparrow; t_b) = 0$ is automatically satisfied since $f_-(\uparrow\uparrow, t_b) = 0$]. The expression is rather lengthy, but can be considerably simplified by imposing as well $\dot{\alpha}_-(\uparrow\uparrow; t_b) = 0$. This fixes $a_3$ as

$$
a_3 = -\frac{5a_4(25\pi^2 - t_f^2\omega^2)}{49\pi^2 - t_f^2\omega^2}.
\tag{3.55}
$$
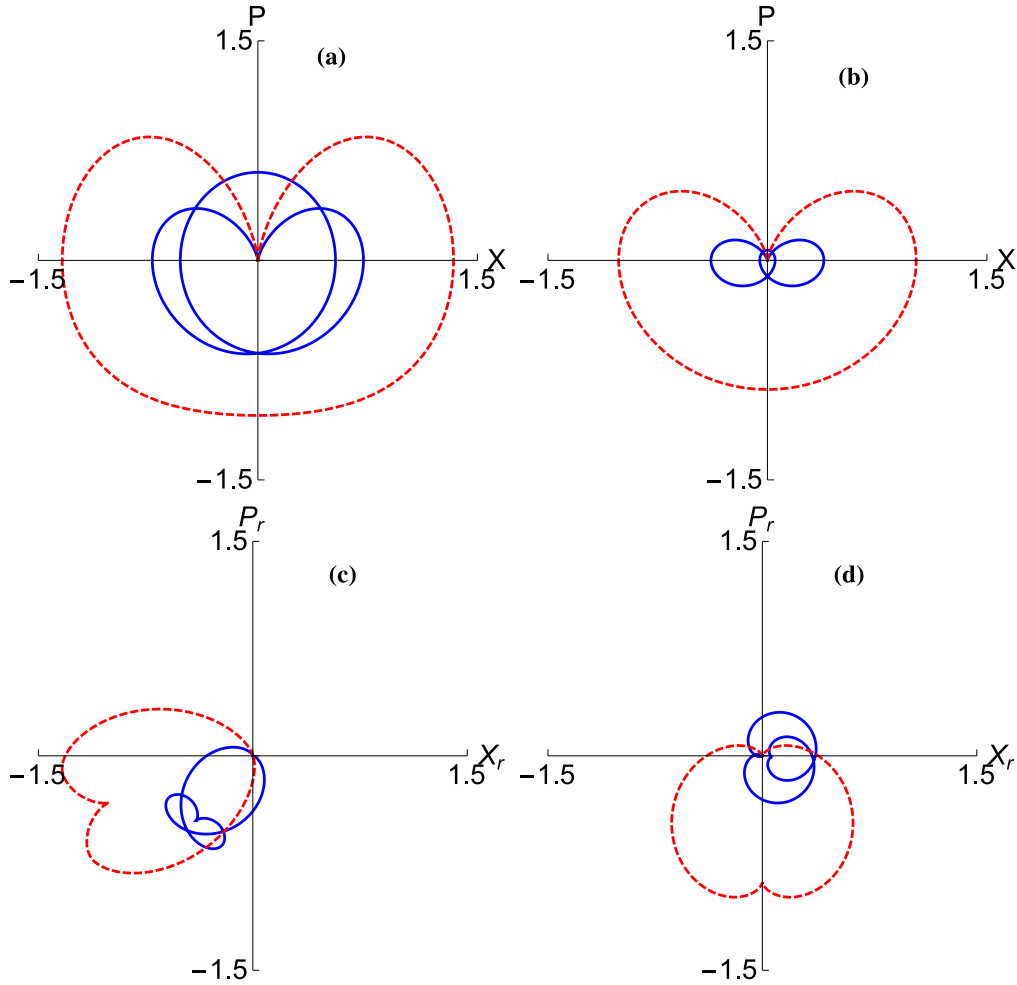
FIGURE 3.2: Parametric plots of the quadratures, $X = \sqrt{\frac{\Omega_\pm}{2\hbar}}\alpha_\pm$ and $P = \sqrt{\frac{1}{2\hbar\Omega_\pm}}\dot{\alpha}_\pm$. The quadratures in the rotating frame are defined as $X_r = \Re(e^{i\Omega_\pm t}Z)$, $P_r = \Im(e^{i\Omega_\pm t}Z)$, where $Z = X + iP$. The solid blue lines represent the stretch $(+)$ mode for antiparallel spins and the dashed red lines the center-of-mass $(-)$ mode for parallel spins. (a) $t_f = 0.8$ $\mu$s, (b) $t_f = 1$ $\mu$s, (c) $t_f = 0.8$ $\mu$s in the rotating frame, and (d) $t_f = 1$ $\mu$s in the rotating frame. The other parameters are chosen as in Fig. 3.1.

At this point, $\alpha_+(\uparrow\downarrow; t)$ and $\alpha_-(\uparrow\uparrow; t)$ are left as functions of the parameter $a_4$,

$$
\begin{aligned}
\alpha_+(\uparrow\downarrow; t) &= 32 a_4 \frac{11\pi^2 + t_f^2\omega^2 + (49\pi^2 - t_f^2\omega^2)\cos\frac{2\pi t}{t_f}}{49\pi^2 - t_f^2\omega^2} \cos\frac{\pi t}{t_f} \sin^4\frac{\pi t}{t_f}, \\
\alpha_-(\uparrow\uparrow; t) &= 32 a_4 \frac{11\pi^2 + 3t_f^2\omega^2 + (49\pi^2 - 3t_f^2\omega^2)\cos\frac{2\pi t}{t_f}}{49\pi^2 - t_f^2\omega^2} \cos\frac{\pi t}{t_f} \sin^4\frac{\pi t}{t_f}.
\end{aligned}
$$

$$(3.56)$$

These are both odd functions with respect to $(t - t_f/2)$ and guarantee a vanishing final excitation in the two modes. They also have vanishing third derivatives at the time boundaries, and thus imply the continuity in the force derivative at time boundaries, i.e., $\dot{F}(t_b) = 0$. Note that $-\frac{1}{\hbar}\int_0^{t_f} dt'[\tilde{f}(A) - \tilde{f}(P)]$ vanishes [see Eq. (3.14)] since $\tilde{f}(P) = 0$ and $\tilde{f}(A)$ is also an odd function of $t - t_f/2$.

The differential phase takes the form [see Eq. (3.47)]

$$
\begin{aligned}
\Delta\phi &\equiv 2[\phi(A) - \phi(P)] \\
&= \frac{2}{\hbar}\int_0^{t_f} dt' \frac{F}{\sqrt{2m}}[\alpha_-(\uparrow\uparrow) - \alpha_+(\uparrow\downarrow)].
\end{aligned}
\tag{3.57}
$$

With the expressions (3.56) for $\alpha_+(\uparrow\downarrow)$ and $\alpha_-(\uparrow\uparrow)$, the integral can be solved to give

$$
\Delta\phi = \frac{12a_4^2 t_f \omega^2(-2051\pi^4 + 476\pi^2 t_f^2\omega^2 - 33t_f^4\omega^4)}{\hbar(-49\pi^2 + t_f^2\omega^2)^2}.
\tag{3.58}
$$

Setting $\Delta\phi = \gamma$, the last free parameter is fixed as

$$
\begin{aligned}
a_4 &= \pm\frac{1}{\omega}(-147\pi^2 + 3t_f^2\omega^2)\sqrt{\frac{\hbar}{6t_f}} \\
&\quad \times \left[\frac{\gamma/2}{-2051\pi^4 + 476\pi^2 t_f^2\omega^2 - 33t_f^4\omega^4}\right]^{1/2}.
\end{aligned}
\tag{3.59}
$$

The polynomial denominator in the last term is negative for all $t_f$ (there are no real roots) so, to get a real $a_4$, $\gamma$ must be chosen as a negative number. I choose $\gamma = -\pi$ to implement the gate (3.2). There are real solutions for $a_4$ for all $t_f$, no matter how small $t_f$ is. In this sense, there is no fundamental lower bound for the method, as long as the small amplitude and Lamb-Dicke approximations are valid. As for the sign alternatives in $a_4$, the different choices imply sign changes for the $\alpha$ and the forces. Hereafter and in all figures, I choose the positive sign.
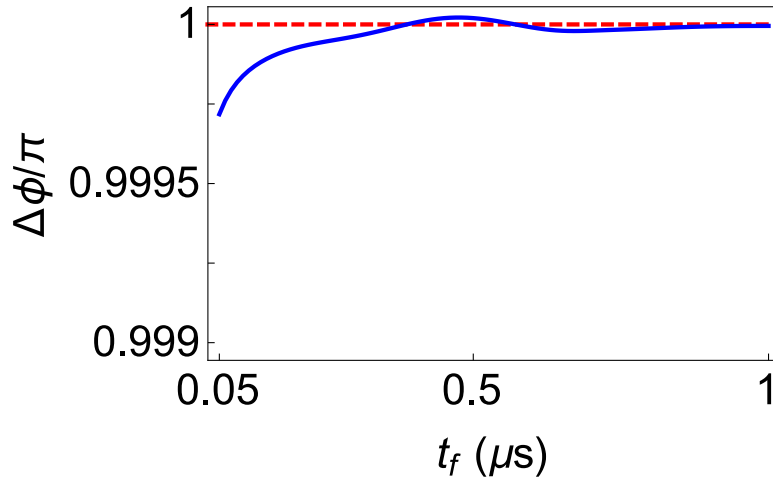
FIGURE 3.3:   $\Delta\phi$ for an exact evolution with the Hamiltonian in Eq. (3.3) (solid blue line), and the target value of this phase (dashed red line). Same parameters as in Fig. 3.1. The initial motional state is the ground state.

The resulting force takes the form

$$
\begin{aligned}
F(t) &= \frac{g_1(t_f) + g_2(t_f)\cos\left(\frac{2\pi t}{t_f}\right) + g_3(t_f)\cos\left(\frac{4\pi t}{t_f}\right)}{t_f^2\sqrt{2051\pi^4 t_f\omega^2 - 476\pi^2 t_f^3\omega^4 + 33t_f^5\omega^6}} \\
&\quad \times\ 2\sqrt{2\pi\hbar m}\cos\left(\frac{\pi t}{t_f}\right)\sin^2\left(\frac{\pi t}{t_f}\right),
\end{aligned}
\tag{3.60}
$$

where

$$
\begin{aligned}
g_1(t_f) &= 3(401\pi^4 - 36\pi^2 t_f^2\omega^2 + 3t_f^4\omega^4), \\
g_2(t_f) &= -4(181\pi^4 - 76\pi^2 t_f^2\omega^2 + 3t_f^4\omega^4), \\
g_3(t_f) &= 2401\pi^4 - 196\pi^2 t_f^2\omega^2 + 3t_f^4\omega^4,
\end{aligned}
\tag{3.61}
$$

which is shown in Fig. 3.1 for different values of $t_f$ (all simulations in this section are for two $^9\text{Be}^+$ ions and a trap frequency $\omega/(2\pi) = 2$ MHz). The results are qualitatively similar to those found in [71] (also the asymptotic behaviour for short operation times, $F \sim t_f^{-5/2}$) with a very different numerical method, but in my case the expression of $F$ is explicit, has a continuous envelope, and the derivatives vanish at the edges, adding stability.

With this force, the trajectories of $\alpha_+(A)$, and $\alpha_-(P)$, see Eqs. (3.50) and
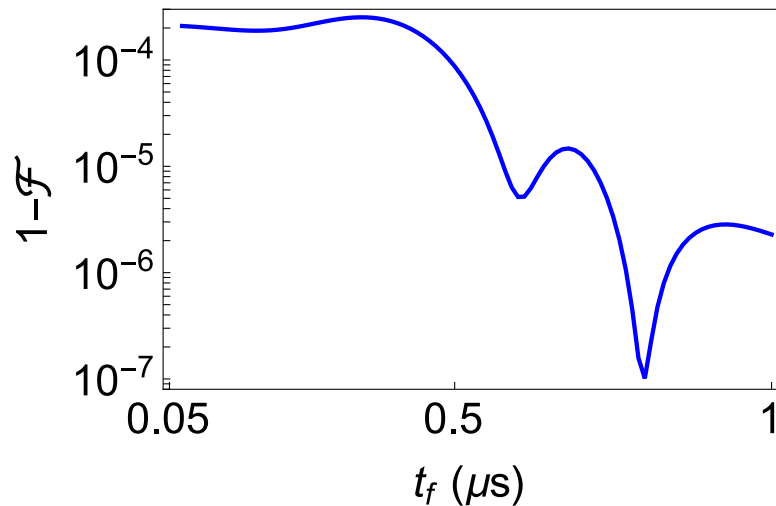
FIGURE 3.4: Worst case infidelity vs final time, which is realized for the initial state $|\uparrow\downarrow\rangle$ [see Eq. (D.8)]. Same parameters as in Fig. 3.1.

(3.51), are given in Fig. 3.2 for two given times $t_f$ in a dimensionless (quadrature) phase space, and in the rotating frame (the phase is twice the area swept in the rotating frame, see Sec. 3.3 [71]). If the initial state is the ground state, they describe, respectively, the dynamics of the stretch mode (for antiparallel spins) and the center-of-mass mode (for parallel spins). Notice that the trajectories lead to larger phase-space amplitudes for shorter times.

The phases within the harmonic (small amplitude) approximation are exact by construction for arbitrarily short times, but we should compare them with the phases when the system is driven by the full Hamiltonian (3.3) that contains the anharmonic Coulomb interaction. To that end, I solve numerically the Schrödinger equation with the Hamiltonian (3.3) by using the "Split-Operator Method" [80]. First, I fix the initial state as the ground state of the system $|\Psi_0\rangle$, which is found by making an initial guess and evolving it in imaginary time [81]. Then, the Split-Operator method is applied in real time to get the evolution of the wave function $|\Psi_t\rangle$. Phases are much more sensitive than populations to numerical errors, so we need a much shorter time step than the one usually required until the results converge. At the final time, the overlap $\mathcal{S} = \langle\Psi_0|\Psi_{t_f}\rangle$, which depends on the spin configuration, is calculated. The phase of the overlap is defined as $\varphi_f = \arg\mathcal{S} \in [0, 2\pi)$. In the quadratic approximation, this includes a global term

$-(\Omega_+ + \Omega_-)t_f/2$ [see Eq. (3.26)] absent in the rotating frame, that is canceled by calculating the phase differential between antiparallel and parallel spins, $2[\varphi_f(\uparrow\downarrow) - \varphi_f(\uparrow\uparrow)]$, displayed in Fig. 3.3. The corresponding infidelities, $1 - |\mathcal{S}|^2$, are shown in Fig. 3.4 for the worst possible case, which is realized for an initial state with antiparallel spins (see Appendix D). The numerical results agree with the ideal result of the quadratic approximation at least up to operation times ten times smaller than an oscillation period $2\pi/\omega$. Shorter times are very demanding computationally.

A different type of stability check is displayed in Fig. 3.5, where a realistic $x$-dependent sinusoidal force on each ion $F_i(t)\sin(\Delta k x + \pi/2)$ is considered instead of the homogeneous one. This force comes about because of the finite wavelength of the lasers used to generate the forces [69]. Close to the ground state, the motional wave function of the ion only overlaps with a small part of the optical wave, which can then be approximated as having a constant gradient over the wave function (Lamb-Dicke approximation). If the extend of the wave function grows in more excited motional states, this approximation breaks down and the sinusoidal shape of the light wave has to be taken into account. For driving a phase gate, the wave vector difference $\Delta k$ is adjusted so that the forces at the equilibrium positions $\pm x_0/2$ are the $F_i(t)$, with an integer number of periods $2\pi/\Delta k$ among them. $\Delta k$ can be adjusted by changing the direction(s) of the beam(s) in laser-based experiments. I choose $\Delta k$ so that the ions in the equilibrium position for the frequency $\omega/(2\pi) = 2$ MHz are placed in extrema of the sine function. In Fig. 3.5 (a) and (b), I depict the differential phase and worst case fidelity versus $t_f$ for this $x$-dependent force, starting in the motional ground state. The two curves correspond to the ions being eight periods apart at equilibrium, similar to [69], or four periods apart. As expected, the results degrade for very short times since the ions explore a broader region, where the forces deviate significantly from $F_i(t)$. The range of validity of the ideal results (the ones for a homogeneous force) in the limit $t_f\omega << 1$ is approximately given by $\frac{\Delta k}{\omega}\sqrt{\frac{\hbar}{t_f m}} << 1$, which may be found by estimating maximal amplitudes of $\alpha_\pm$ in Eq. (3.56), using Eq. (3.12) to calculate deviations from equilibrium positions and comparing them to half a lattice period

$\pi/\Delta k$. Note that, for eight periods, the phase does not really converge to the ideal value even at longer times, when the deviation is quite small compared to the period of the force. The reason is that the wave function width also implies that the ions do not strictly experience a homogeneous force, which can lead to squeezing of the state of motion rather than just a coherent displacement. Starting with the ground-state wave function in the harmonic approximation (i.e., a product of ground-state wave functions for each mode), we may calculate the width of the position of one ion as $\Delta x = \frac{1}{2}(1 + 1/\sqrt{3})^{1/2}\sqrt{\hbar/(m\omega)}$, see the Appendix E, which should be compared to $\pi/\Delta k$. For the parameters in Fig. 3.5 (a) and (b), the ratios $\Delta x \Delta k/\pi$ are 0.04 (eight oscillations) and 0.02 (four oscillations).

In Fig. 3.5 (c) and (d), I additionally consider that the evolved state begins in some excited Fock state so that the Lamb-Dicke approximation breaks down more easily. I only consider excitations of the stretch mode, $|n_- = 0, n_+\rangle$, as the full Hamiltonian only has nonzero cubic terms for this mode.

I also study the scaling with $t_f$ of spontaneous emission due to the fact that intense off-resonant fields may induce transitions. The transition rate will be proportional to the intensity of the field, and to the effective potential acting on the ions, i.e., to $|F|$. In Fig. 3.6, I have integrated this quantity over time for different values of $t_f$. Since $F \sim t_f^{-5/2}$, the result scales as $t_f^{-3/2}$. Arbitrary units are used as the scattering probability will depend on different factors, which are not explicitly considered here such as $\Delta k$ or the detuning.

## 3.6 Different masses

For different mass ions, $m_1 = m$, $m_2 = \mu m$, and $u_0 = m\omega_1^2 = \mu m\omega_2^2$. In this case, due to their different structure, both ions will react to different laser fields, thus, $F_1$ and $F_2$ can in principle be designed independently, such that $F_1 = \sigma_1^z F_a(t)$,
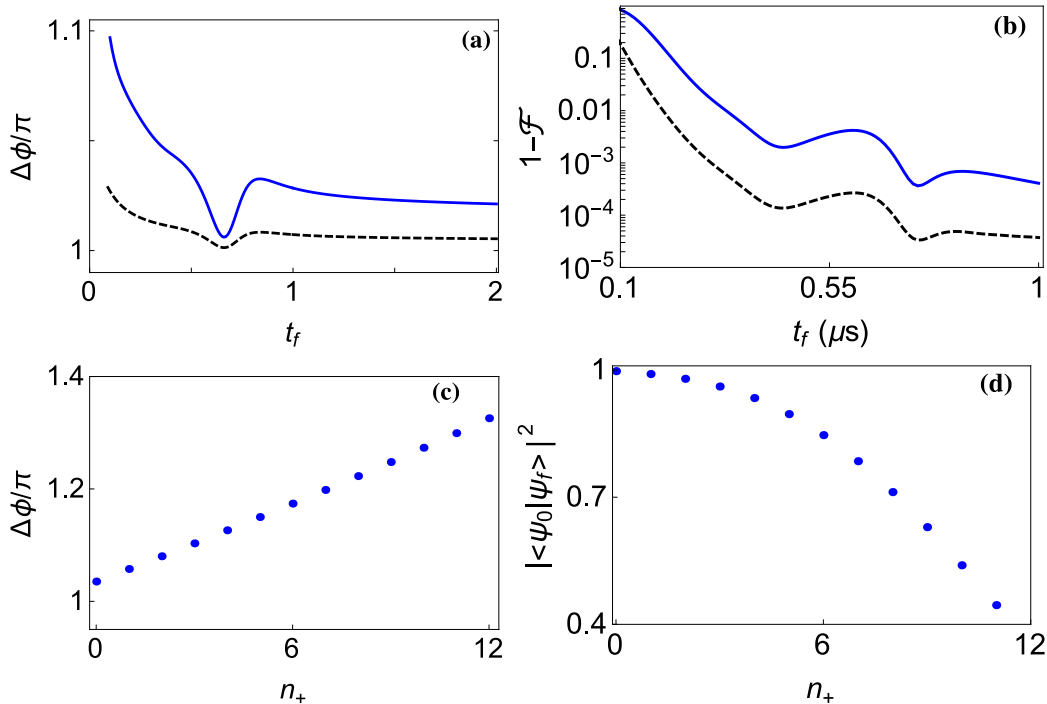
FIGURE 3.5:    Simulation of 2 $^9\text{Be}^+$ ions with trap frequency $\omega/(2\pi) = 2$ MHz.    Instead of homogeneous forces more realistic $x$-dependent forces $F_i(t)\sin(\Delta kx + \pi/2)$ are applied. In (a) and (b) the initial motional state is the ground state. $\Delta k = 8.67 \times 10^6$ m$^{-1}$: solid (blue) line (ions separated by 8 lattice periods at equilibrium); $\Delta k = 4.33 \times 10^6$ m$^{-1}$: dashed (black) line (ions separated by four lattice periods). In (a) we display the final phase vs the final time. In (b) the worst case infidelity (realized for antiparallel spins). In (c) and (d) the phase and worst case fidelity (corresponding to antiparallel spins) for different initial excited states are depicted, for a time $t_f = 0.5$ $\mu$s and the ions separated by eight lattice periods.

$F_2 = \sigma_2^z F_b(t)$ (more general cases are studied in Appendix B), yielding

$$
\begin{aligned}
f_\pm(\uparrow\uparrow) &= -f_\pm(\downarrow\downarrow) = \mp\frac{b_\mp}{\sqrt{m}}F_a \pm \frac{a_\mp}{\sqrt{\mu m}}F_b, \\
f_\pm(\uparrow\downarrow) &= -f_\pm(\downarrow\uparrow) = \mp\frac{b_\mp}{\sqrt{m}}F_a \mp \frac{a_\mp}{\sqrt{\mu m}}F_b,
\end{aligned}
\tag{3.62}
$$

which, as in the previous section, implies that

$$
\begin{aligned}
\alpha_\pm(\downarrow\uparrow) &= -\alpha_\pm(\uparrow\downarrow), \\
\alpha_\pm(\downarrow\downarrow) &= -\alpha_\pm(\uparrow\uparrow)
\end{aligned}
\tag{3.63}
$$
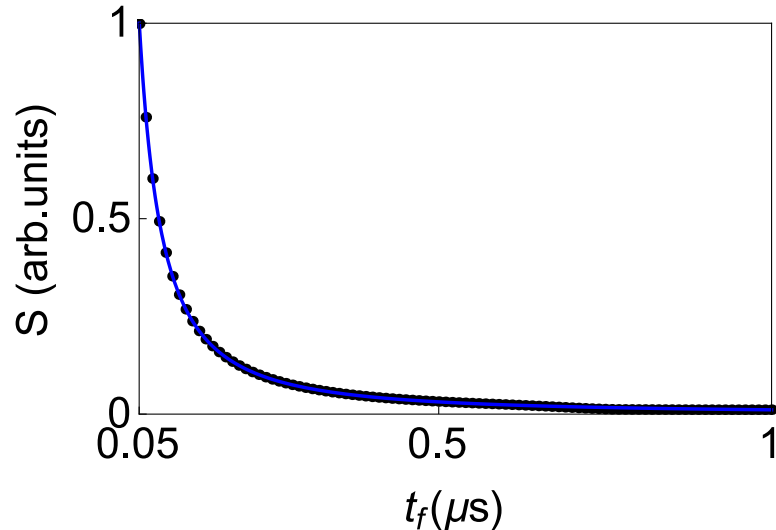
FIGURE 3.6: $S = \int_0^{t_f} dt |F(t)|$ (dots). $F(t)$ is designed for equal mass ions ($^9\text{Be}^+$ ions) according to Eq. (3.60) for a trap frequency $\omega/(2\pi) = 2$ MHz. The solid line is a fit proportional to $t_f^{-3/2}$.

[see Eqs. (3.14) and (3.20)], so if the protocol is designed to satisfy the boundary conditions for the $\uparrow\downarrow$ and $\uparrow\uparrow$ configurations, it will automatically satisfy the conditions for the remaining configurations. Inversely, from Eqs. (3.62) and (3.10),

$$
\begin{aligned}
F_a &= -\sqrt{m}[a_- f_-(\uparrow\downarrow) + a_+ f_+(\uparrow\downarrow)], \\
F_b &= \sqrt{\mu m}[b_- f_-(\uparrow\downarrow) + b_+ f_+(\uparrow\downarrow)].
\end{aligned} \tag{3.64}
$$

The procedure to design the forces is summarized in the following scheme,

$$
\alpha_\pm(\uparrow\downarrow) \dashrightarrow f_\pm(\uparrow\downarrow) \dashrightarrow F_a, F_b \dashrightarrow f_\pm(\uparrow\uparrow) \dashrightarrow \alpha_\pm(\uparrow\uparrow). \tag{3.65}
$$

To start with, ansatzes are proposed for $\alpha_+(\uparrow\downarrow)$ and $\alpha_-(\uparrow\downarrow)$,

$$
\begin{aligned}
\alpha_+(\uparrow\downarrow) &= a_0 + \sum_{n=1}^{4} a_n \cos\left[\frac{(2n-1)\pi t}{t_f}\right], \\
\alpha_-(\uparrow\downarrow) &= 0.
\end{aligned} \tag{3.66}
$$

It is also possible to design them so as to cancel $\alpha_+(\uparrow\downarrow) = 0$ instead of $\alpha_-(\uparrow\downarrow)$, as discussed in Appendix F. Similar to the previous section, $a_0$, $a_1$, and $a_2$ are fixed
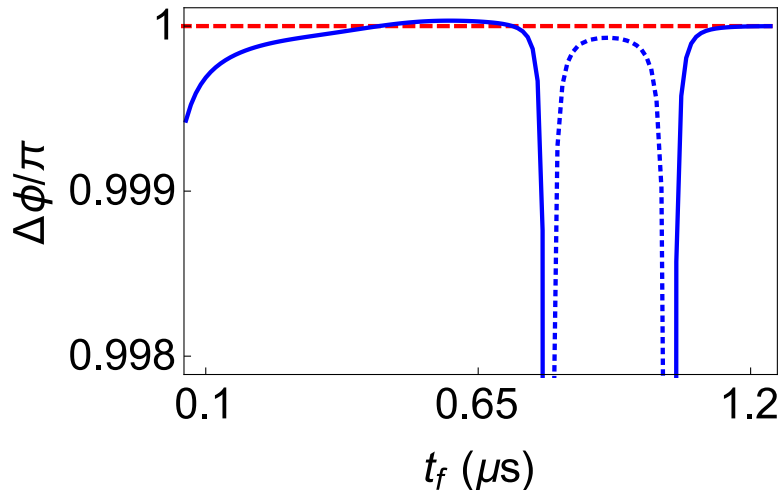
FIGURE 3.7:  Total final phase $\Delta\phi$ in Eq. (3.69) vs the final time (solid and dotted blue lines) for an exact wave function evolving with the Hamiltonian in Eq. (3.3), and the target value of this phase (dashed red line). The simulation is done for a $^9$Be$^+$ and a $^{25}$Mg$^+$ ion, initially in the motional ground state, within a trap of frequency $\omega_1/(2\pi) = 2$ MHz. At final times $t_f \sim 0.8$ $\mu$s and 1.03 $\mu$s, I change solutions [see the discussion below Eq. (3.72)]. The solid line is for $\gamma = -\pi$ and the dashed line for $\gamma = \pi$.

to satisfy the boundary conditions for $\alpha_+(\uparrow\downarrow)$ in Eqs. (3.29) and (3.31),

$$
\begin{aligned}
a_0 &= 0, \\
a_1 &= 2a_3 + 5a_4, \\
a_2 &= -3a_3 - 6a_4.
\end{aligned}
\tag{3.67}
$$

Introducing these ansatzes in Eq. (3.20), expressions for $f_\pm(\uparrow\downarrow;t)$ are found, in particular $f_-(\uparrow\downarrow) = 0$, and from these, expressions for the control functions $F_a(t), F_b(t)$ follow according to Eq. (3.64). Since $\alpha_+(t)(\uparrow\downarrow)$ is an odd function of $(t - t_f/2)$, the same symmetry applies to $F_a(t)$, $F_b(t)$, and to the spin-dependent forces $F_1$, $F_2$. Thus, the time integral of $\tilde{f}$ [see Eq. (3.14)] is zero for different masses as well, and does not contribute to the phase.

Using the last line of Eq. (3.14), the effective forces $f_\pm(\uparrow\uparrow)$ are found. Plugging these functions into Eq. (3.20), I solve the differential equations imposing the boundary conditions $\alpha_\pm(\uparrow\uparrow;t_b) = 0$ to fix the integration constants. At this point, the boundary conditions for $\ddot{\alpha}_\pm(\uparrow\uparrow;t_b)$ are automatically satisfied, and $\dot{\alpha}_\pm(\uparrow\uparrow;0) =$
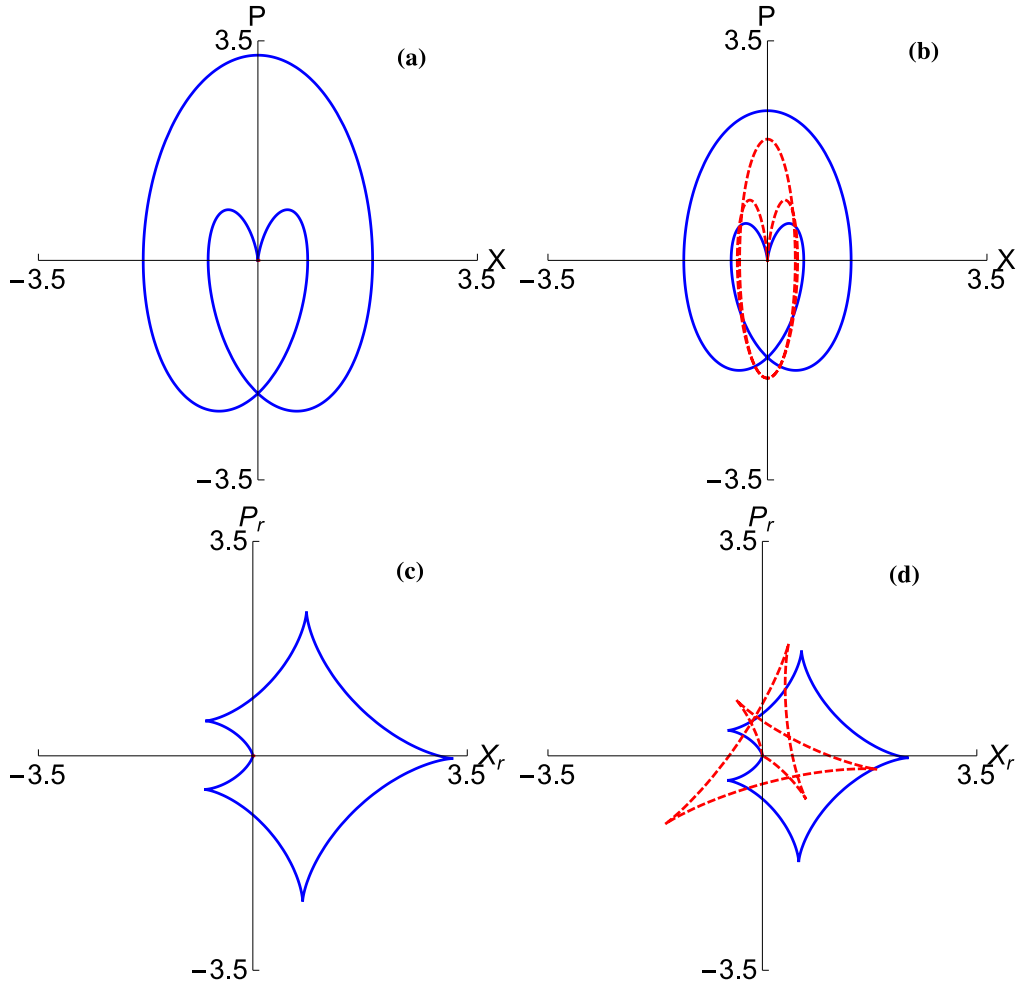
FIGURE 3.8: Parametric plots of the quadratures, $X = \sqrt{\frac{\Omega_\pm}{2\hbar}}\alpha_\pm$ and $P = \sqrt{\frac{1}{2\hbar\Omega_\pm}}\dot{\alpha}_\pm$. The quadratures in the rotating frame are defined as $X_r = \Re\mathrm{e}(e^{i\Omega_\pm t}Z)$, $P_r = \Im\mathrm{m}(e^{i\Omega_\pm t}Z)$, where $Z = X + iP$ at $t_f = 0.5$ $\mu$s. The solid blue lines represent the stretch $(+)$ mode and the dashed red lines the center-of-mass $(-)$ mode. (a) and (c) represent the phase space trajectory for $|\uparrow\downarrow\rangle$ and $|\downarrow\uparrow\rangle$, in the normal and the rotating frame respectively, while (b) and (d) represent the phase space trajectories for $|\uparrow\uparrow\rangle$, in the normal and rotating frames respectively. The other parameters are chosen as in Fig. 3.7.

$\dot{\alpha}_\pm(\uparrow\uparrow; t_f)$ by symmetry. Thus, imposing that the first derivatives vanish at the boundary times, $a_3$ is fixed as

$$a_3 = \frac{-25\pi^2 + t_f^2\Omega_-^2}{49\pi^2 - t_f^2\Omega_-^2}5a_4. \tag{3.68}$$

Once the $\alpha_\pm$ are given for both configurations, such that they do not produce any excitation in the modes at the final time, the final phase difference is, as in the

previous section,

$$
\begin{aligned}
\Delta\phi(t_f) &= 2[\phi(A) - \phi(P)] \\
&= -\frac{1}{\hbar} \sum_{\mu=\pm} \int_0^{t_f} dt[\dot{\alpha}_\mu^2(\uparrow\downarrow) - \Omega_\mu^2\alpha_\mu^2(\uparrow\downarrow)] \\
&\quad + \frac{1}{\hbar} \sum_{\mu=\pm} \int_0^{t_f} dt[\dot{\alpha}_\pm^2(\uparrow\uparrow) - \Omega_\mu^2\alpha_\mu^2(\uparrow\uparrow)].
\end{aligned}
\tag{3.69}
$$

The integrals can be evaluated, and give a function of $a_4$. This parameter is finally set by imposing some value to the phase difference, $\Delta\phi(t_f) = \gamma$,

$$
\begin{aligned}
a_4 &= \sqrt{\frac{\gamma\hbar(1 + (-1 + \mu)\mu)(-49\pi^2 + t_f^2\Omega_-^2)^2}{\Delta}}, \\
\Delta &= 6\mu(\Omega_- - \Omega_+)(\Omega_- + \Omega_+)t_f[2051\pi^4 + 11t_f^4\Omega_-^2\Omega_+^2 - 119\pi^2t_f^2(\Omega_-^2 + \Omega_+^2)].
\end{aligned}
\tag{3.70}
$$

The function $\Delta$ has zeros at

$$
\begin{aligned}
t_f^{(0)} &= 0, \\
t_f^{(1)} &= \pm\pi\sqrt{\frac{119(\Omega_-^2 + \Omega_+^2) - \delta}{22\Omega_-^2\Omega_+^2}}, \\
t_f^{(2)} &= \pm\pi\sqrt{\frac{119(\Omega_-^2 + \Omega_+^2) + \delta}{22\Omega_-^2\Omega_+^2}},
\end{aligned}
\tag{3.71}
$$

where

$$
\delta = \sqrt{7(2023\Omega_-^4 - 8846\Omega_-^2\Omega_+^2 + 2023\Omega_+^4)}.
\tag{3.72}
$$

Considering only the positive times, in the intervals $\left(t_f^{(0)}, t_f^{(1)}\right)$ and $t_f > t_f^{(2)}$, $\Delta$ is negative, so I chose $\gamma = -\pi$ to make $a_4$, and thus $F_a, F_b$, real. In the interval $\left(t_f^{(1)}, t_f^{(2)}\right)$ $\Delta$ is positive, so we can choose $\gamma = \pi$.
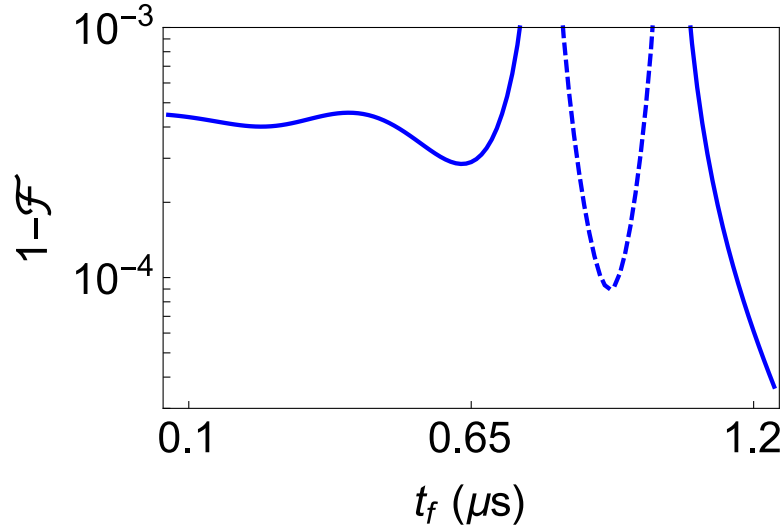
FIGURE 3.9: Infidelity vs final time for the worst case, which corresponds to antiparallel spins [see Eq. (D.8)]. Same parameters as in Fig. 3.7. The solid line is for $\gamma = -\pi$ and the dashed line for $\gamma = \pi$.

The explicit expressions for the control functions are finally, from Eq. (3.64),

$$
\begin{aligned}
F_a &= \left[ g_1^a + g_2^a \cos\left(\frac{2\pi t}{t_f}\right) + g_3^a \cos\left(\frac{4\pi t}{t_f}\right) \right] \\
&\times \frac{8 a_4 a_+ \sqrt{m} \cos\left(\frac{\pi t}{t_f}\right) \sin^2\left(\frac{\pi t}{t_f}\right)}{-49\pi^2 t_f^2 + t_f^4 \Omega_-^2}, \\
F_b &= -\frac{b_+ \sqrt{\mu}}{a_+} F_a,
\end{aligned}
\tag{3.73}
$$

where

$$
\begin{aligned}
g_1^a &= 3[401\pi^4 + t_f^4 \Omega_-^2 \Omega_+^2 - 9\pi^2 t_f^2 (\Omega_-^2 + \Omega_+^2)], \\
g_2^a &= 4[-181\pi^4 - t_f^4 \Omega_-^2 \Omega_+^2 + 19\pi^2 t_f^2 (\Omega_-^2 + \Omega_+^2)], \\
g_3^a &= (49\pi^2 - t_f^2 \Omega_-^2)(49\pi^2 - t_f^2 \Omega_+^2).
\end{aligned}
\tag{3.74}
$$

$F_a, F_b$ diverge for the final times in Eq. (3.71), so these times must be avoided. The positions of the divergences depend on the chosen ansatz. In particular, for a polynomial, rather than cosine ansatz, the only divergence is at $t_f = 0$. I have, however, kept the cosine ansatz as it needs fewer terms and it simplifies the results and the treatment of boundary conditions.

Figure 3.7 shows the phase numerically obtained with the exact Hamiltonian for $^9$Be (ion 1) and $^{25}$Mg (ion 2) in the Lamb-Dicke limit, beginning in the ground motional state. Figure 3.8 shows the quadratures for such a protocol at final time $t_f = 0.5$ $\mu$s, and Fig. 3.9 the worst case infidelities at final time, which, as in the previous section, correspond to initial states with antiparallel spin (see Appendix D). Around an oscillation period $2\pi/\omega_1 = 0.5$ $\mu$s, the results are slightly worse than in the previous section for equal mass ions, but still with a high fidelity. For final times close to $t_f^{(1)} \sim 0.8$ $\mu$s and $t_f^{(2)} \sim 1.03$ $\mu$s, the solutions change, with a drop in the stability of the phase (Fig. 3.7) and in the fidelity (Fig. 3.9). The phase and fidelity improve and stabilize again for times $t_f > 1.03$ $\mu$s.

In the limit were both ions are equal, $F_a = F_b = F$, the results of the previous section are recovered.

## 3.7 Discussion

In this chapter, I have designed simple and explicit protocols to perform fast and high fidelity phase gates with two trapped ions by using the invariant-based method to bypass adiabaticity. The scheme of the gate expands on methods that have been already tested in the laboratory. Experimentally, the state-dependent forces may be created by a standing wave with time-varying intensity produced by two crossed laser beams, whose amplitude is modulated following a smoothly designed trajectory to excite motion in both normal modes. In the limit of small oscillations, we can use both a normal mode harmonic approximation and the Lamb-Dicke limit and apply the inverse-design method assuming homogeneous forces. I have also numerically simulated the system dynamics and gate behavior without these approximations, namely, including the anharmonicity and the position dependence of the forces. Good fidelities are obtained at times around 1 $\mu$s, which is a significantly shorter time compared to the best experimental results so far, and close to the center of mass oscillation period which was assumed to be 0.5 $\mu$s in this work. Moreover, state-of-the-art technology allows for higher trap

frequencies than those used in our simulations, which should further improve the results. Expressions for the forces have been found for different scenarios, specifically, for equal or different masses, as well as for different proportionality factors between the spin-dependent forces.

Extensions of this work are possible in several directions. For example, the deviations from the ideal conditions may be taken into account to design the forces. The freedom offered by the approach may also be used to choose stable protocols with respect to different noises and perturbations.

# Chapter 4

# Fast expansions and compressions of trapped-ion chains

*"If not now, then when? If not you, then who?"*

Kailash Satyarthi

I investigate the dynamics under diabatic expansions/compressions of linear ion chains. Combining a dynamical normal-mode harmonic approximation with the invariant-based inverse-engineering technique, I design protocols that minimize the final motional excitation of the ions. This can substantially reduce the transition time between high and low trap-frequency operations, potentially contributing to the development of scalable quantum information processing.

## 4.1 Introduction

So far, I have only studied ion-transport related problems. In Chapters 1 and 2, I directly studied this problem for equal and different mass situations respectively. In Chapter 3 I designed the accelerated process that creates a $\pi$-phase gate. Physically, this is done by producing a displacement in the ions with state dependent forces, what makes the theoretical problem similar to that of the transport, but with the additional need of a precise control of the phase. In addition to ion transport [33, 42, 43, 52, 63, 82], chain expansions/compressions and ion-chain splitting and recombination [42, 45, 83, 84] are other important dynamical processes towards building a quantum processor in trapped ions. These operations can be performed on single or mixed-species ion chains [85], allowing for sympathetic ion cooling or quantum-logic spectroscopy [86].

The study of ion separation will be done in the following Chapter 5. The physical operation that I consider here is fast control of the motional frequencies of the trapped ions, which in the case of multiple ions leads to chain expansions and compressions. Several elementary protocols benefit from a high trap frequency, whereas others are better performed with low frequencies. Therefore, a fast transition between them without inducing final excitations is a worthwhile goal.

Operations that benefit from high motional frequencies (i.e. large potential curvature, small interion distance, and small Lamb-Dicke parameters) include:

- Doppler laser cooling, since the mean phonon number is lower for tighter traps [87];

- any operation where a single motional normal mode (NM) of an ion chain needs to be spectrally resolved, since the NM frequency splitting is proportional to the trap curvature [45];

- operations which make use of motional sidebands and whose fidelity is limited by off-resonantly driving carrier transitions on the qubit.

On the other hand, operations where a lower motional frequency is desired include:

- single-ion addressing in a multi-ion crystal;

- resolved sideband cooling, which cools at a rate proportional to the square of the Lamb-Dicke parameter [88];

- geometric phase gates [69], which are faster for larger Lamb-Dicke parameters.

In many cases a compromise will be optimal, depending on the dominant limitations for a particular experiment.

Fast expansions/compressions without final excitation have been designed in a number of different ways [31, 32, 39, 89–92]. Invariant-based engineering or scaling methods [32, 91] were realized experimentally for a noninteracting cold-atom cloud [93] and a Bose-Einstein condensate [93, 94]. However, the methods used rely on single particles, BEC dynamics, or equal masses, and are not directly applicable to an arbitrary interacting ion chain. I propose here a method to design trap expansions and compressions faster than adiabatically and without final motional excitation. Specifically I define dynamical normal modes similar to the ones defined for shuttling ion chains in Ref. [63] and apply invariant-based inverse-engineering techniques by either exact or approximate methods.

I first discuss two-ion chains in Sec. 4.2, both for ions of equal mass, and ions of different mass, and then extend the analysis in Sec. 4.3 to longer chains. In the examples only expansions of the trapping potential are considered, as compressions may be performed with the same time evolution of the spring constant, only time-reversed.

## 4.2   2-ion chain expansion

We will deal with a one-dimensional trap containing an $N$-ion chain whose Hamiltonian in terms of the positions $\{q_i\}$ and momenta $\{p_i\}$ of the ions in the

laboratory frame is

$$H = \sum_{i=1}^{N} \frac{p_i^2}{2m_i} + \sum_{i=1}^{N} \frac{1}{2} u_0(t) q_i^2 + \sum_{i=1}^{N-1} \sum_{j=i+1}^{N} \frac{C_c}{q_i - q_j}, \tag{4.1}$$

where $C_c = \frac{e^2}{4\pi\epsilon_0}$, with $\epsilon_0$ the vacuum permittivity. $u_0(t)$ is the common (time-dependent) spring constant that defines the oscillation frequencies $\omega_j(t)/(2\pi)$ for the different ions in the absence of Coulomb coupling: $u_0(t) = m_1\omega_1^2(t) = m_2\omega_2^2(t) = \cdots = m_N\omega_N^2(t)$. All ions are assumed to have the same charge $e$, and be ordered as $q_1 > q_2 > \cdots > q_N$, with negligible overlap of probability densities as a result of the Coulomb repulsion. The potential term $V(q_1, q_2) = H - \sum_i p_i^2/2m_i$ in the Hamiltonian (4.1) for two ions is minimal at the equilibrium points $q_1^{(0)} = x_0/2$, $q_2^{(0)} = -x_0/2$, where $x_0 \equiv x_0(t) = 2\sqrt[3]{\frac{C_c}{4u_0(t)}}$ is the equilibrium distance between the two ions. Instantaneous, mass-weighted, NM coordinates are defined by diagonalizing the matrix $V_{ij} = \frac{1}{\sqrt{m_i m_j}} \frac{\partial^2 V}{\partial q_i \partial q_j}(q_i^{(0)}, q_j^{(0)})$ [63]. The time-dependent eigenvalues are [59]

$$\lambda_\pm = \left(1 + \frac{1}{\mu} \pm \sqrt{1 - \frac{1}{\mu} + \frac{1}{\mu^2}}\right) \omega_1^2, \tag{4.2}$$

where I have relabeled $m_1 \to m$ and $m_2 \to \mu m$, and omitted the explicit time dependences to avoid a cumbersome notation, i.e., $\lambda_\pm \equiv \lambda_\pm(t)$ and $\omega_1 \equiv \omega_1(t)$. The time-dependent angular frequencies for each mode are

$$\Omega_\pm \equiv \Omega_\pm(t) = \sqrt{\lambda_\pm} = \left(1 + \frac{1}{\mu} \pm \sqrt{1 - \frac{1}{\mu} + \frac{1}{\mu^2}}\right)^{1/2} \omega_1, \tag{4.3}$$

and the eigenvectors corresponding to these eigenvalues are $v_{\pm} = (a_{\pm}, b_{\pm})^T$, where

$$
\begin{aligned}
a_+ &= \left( \frac{1}{1 + \left(1 - \frac{1}{\mu} - \sqrt{1 - \frac{1}{\mu} + \frac{1}{\mu^2}}\right)^2 \mu} \right)^{1/2}, \\
b_+ &= \left(1 - \frac{1}{\mu} - \sqrt{1 - \frac{1}{\mu} + \frac{1}{\mu^2}}\right) \sqrt{\mu} a_+, \\
a_- &= \left( \frac{1}{1 + \left(1 - \frac{1}{\mu} + \sqrt{1 - \frac{1}{\mu} + \frac{1}{\mu^2}}\right)^2 \mu} \right)^{1/2}, \\
b_- &= \left(1 - \frac{1}{\mu} + \sqrt{1 - \frac{1}{\mu} + \frac{1}{\mu^2}}\right) \sqrt{\mu} a_-.
\end{aligned} \tag{4.4}
$$

The instantaneous, dynamical normal-mode (mass-weighted) coordinates are finally

$$
\begin{aligned}
\mathsf{q}_+ &= a_+\sqrt{m}\left(q_1 - \frac{x_0}{2}\right) + b_+\sqrt{\mu m}\left(q_2 + \frac{x_0}{2}\right), \\
\mathsf{q}_- &= a_-\sqrt{m}\left(q_1 - \frac{x_0}{2}\right) + b_-\sqrt{\mu m}\left(q_2 + \frac{x_0}{2}\right).
\end{aligned} \tag{4.5}
$$

The quantum dynamics of a state $|\psi\rangle$ governed by $H$ in the laboratory frame may be transformed into the moving frame of NM coordinates by the unitary operator

$$
U = \int d\mathsf{q}_+ d\mathsf{q}_- dq_1 dq_2 |\mathsf{q}_+, \mathsf{q}_-\rangle\langle \mathsf{q}_+, \mathsf{q}_- | q_1, q_2\rangle\langle q_1, q_2 |, \tag{4.6}
$$

where $\langle \mathsf{q}_+, \mathsf{q}_- | q_1, q_2\rangle = \delta[q_1 - q_1(\mathsf{q}_+, \mathsf{q}_-)]\delta[q_2 - q_2(\mathsf{q}_+, \mathsf{q}_-)]$. The Hamiltonian in the dynamical equation for $|\psi'\rangle = U|\psi\rangle$ is given by

$$
\begin{aligned}
H' &= UHU^\dagger - i\hbar U(\partial_t U^\dagger) = \\
&= \sum_\nu \left( \frac{\mathsf{p}_\nu^2}{2} - \mathsf{p}_{0\nu}\mathsf{p}_\nu + \frac{1}{2}\Omega_\nu^2 \mathsf{q}_\nu^2 \right), 
\end{aligned} \tag{4.7}
$$

where cubic and higher order terms in the coordinates have been neglected, $\nu = \pm$, $\mathsf{p}_\pm$ are (mass-weighted) momenta conjugate to $\mathsf{q}_\pm$, and

$$
\mathsf{p}_{0\pm} = -\dot{\mathsf{q}}_\pm = \frac{2}{3}(-a_\pm\sqrt{m_1} + b_\pm\sqrt{m_2})\sqrt[3]{\frac{C_c}{4m_1\omega_1^5}}\dot{\omega}_1 \tag{4.8}
$$

are functions of time with the same dimensions as the mass-weighted momenta. They appear because of the time dependence of the NM coordinates through $x_0$, which is a function of $\omega_1(t)$. These $\mathsf{p}_{0\pm}$ functions act as momentum shifts in a further unitary transformation which suppresses the terms linear in $\mathsf{p}_\pm$,

$$
\begin{aligned}
\mathcal{U} &= e^{-i(\mathsf{p}_{0+}\mathsf{q}_+ + \mathsf{p}_{0-}\mathsf{q}_-)/\hbar}, \\
|\psi''\rangle &= \mathcal{U}|\psi'\rangle, \\
H'' &= \mathcal{U}H'\mathcal{U}^\dagger - i\hbar\mathcal{U}(\partial_t\mathcal{U}^\dagger) = \\
&= \sum_\nu \left[ \frac{\mathsf{p}_\nu^2}{2} + \frac{1}{2}\Omega_\nu \left( \mathsf{q}_\nu + \frac{\dot{\mathsf{p}}_{0\nu}}{\Omega_\nu^2} \right)^2 \right].
\end{aligned}
\tag{4.9}
$$

This Hamiltonian corresponds to two effective harmonic oscillators with time-dependent frequencies and a time-dependent moving center. Note that the "motion" of the harmonic oscillators is in the normal-mode-coordinate space, and that the actual center of the external trap in the laboratory frame is fixed. According to Eqs. (4.3) and (4.8) both the NM harmonic oscillators' centers $(-\dot{\mathsf{p}}_{0\pm}/\Omega_\pm^2)$ and the frequencies $(\Omega_\pm)$ depend on $\omega_1(t)$. This is important as, to solve the dynamics for given $\omega_1(t)$, the oscillators are effectively independent. However, from an inverse-engineering perspective, their time-dependent parameters cannot be designed independently. This "coupling" is here more involved than for the transport of two ions in a rigidly moving harmonic trap [63], where $\mathsf{p}_{0\pm}(t)$ take different forms which depend on the trap position but not on the trap frequency. A different approach is thus required.

The Lewis-Riesenfeld invariants [76] of the two oscillators are

$$
\begin{aligned}
I_\pm &= \frac{1}{2}[\rho_\pm(\mathsf{p}_\pm - \dot{\alpha}_\pm) - \dot{\rho}_\pm(\mathsf{q}_\pm - \alpha_\pm)]^2 \\
&+ \frac{1}{2}\Omega_{0\pm}^2 \left( \frac{\mathsf{q}_\pm - \alpha_\pm}{\rho_\pm} \right)^2,
\end{aligned}
\tag{4.10}
$$

where $\Omega_{0\pm} = \Omega_\pm(0)$. The invariants depend on the auxiliary functions $\rho_\pm$ (scaling factors of the expansion modes) and $\alpha_\pm$ (mass-scaled centers of the dynamical

modes of the invariant). They satisfy the auxiliary (Ermakov and Newton) equations

$$\ddot{\rho}_\pm + \Omega_\pm^2 \rho_\pm = \frac{\Omega_{0\pm}^2}{\rho_\pm^3}, \tag{4.11}$$

$$\ddot{\alpha}_\pm + \Omega_\pm^2 \alpha_\pm = \dot{\mathsf{p}}_{0\pm}. \tag{4.12}$$

Dynamical expansion modes $|\psi''_{n\pm}\rangle$ (not to be confused with normal modes) may be found. These are exact time-dependent solutions of the Schrödinger equation and also instantaneous eigenstates of the invariant [33],

$$\langle \mathsf{q}_\pm | \psi''_{n\pm} \rangle = e^{\frac{i}{\hbar}\left[\frac{\dot{\rho}_\pm \mathsf{q}_\pm^2}{2\rho_\pm} + (\dot{\alpha}_\pm \rho_\pm - \alpha_\pm \dot{\rho}_\pm)\frac{\mathsf{q}_\pm}{\rho_\pm}\right]} \frac{\Phi_n(\sigma_\pm)}{\rho_\pm^{1/2}}, \tag{4.13}$$

where $\sigma_\pm = \frac{\mathsf{q}_\pm - \alpha_\pm}{\rho_\pm}$ and $\Phi_n(\sigma_\pm)$ are the eigenfunctions of the static harmonic oscillator at time $t = 0$. Within the harmonic approximation the NM wave functions $|\psi''_\pm\rangle$ evolve independently with $H''$. They may be written as combinations of the expansion modes, $|\psi''_\pm(t)\rangle = \sum_n c_{n\pm} |\psi''_{n\pm}\rangle$ with normalized constant amplitudes. The average energies of the $n$th expansion mode for two NM are

$$\begin{aligned} E''_{n\pm} &= \langle \psi''_{n\pm} | H'' | \psi''_{n\pm} \rangle \\ &= \frac{(2n+1)\hbar}{4\Omega_{0\pm}} \left( \dot{\rho}_\pm^2 + \Omega_\pm^2 \rho_\pm^2 + \frac{\Omega_{0\pm}^2}{\rho_\pm^2} \right) \\ &+ \frac{1}{2}\dot{\alpha}_\pm^2 + \frac{1}{2}\Omega_\pm^2(\alpha_\pm - \dot{\mathsf{p}}_{0\pm}/\Omega_{0\pm}^2)^2. \end{aligned} \tag{4.14}$$

In numerical examples, the initial ground state is, in the harmonic approximation, of the form $|\psi''_{0+}(0)\rangle|\psi''_{0-}(0)\rangle$, so the time-dependent energy is given by $E''(t) = E''_{0+} + E''_{0-}$. Note that if we impose both unitary operators $U(t)$ and $\mathcal{U}(t)$ to be 1 at $t = 0$ and $t_f$, the transformed wave function $|\psi''\rangle$ and the laboratory wave function $|\psi\rangle$ will be the same at both these times and the energy $E''(t = 0, t_f)$ will be the same as the laboratory-frame energy. Both unitary transformations satisfy this provided that $\dot{\omega}_1(t_b) = 0$, where $t_b = 0, t_f$, as long as the quadratic approximation in the Hamiltonian (4.9) is valid.

For a single harmonic oscillator without the independent term in Eq. (4.12),
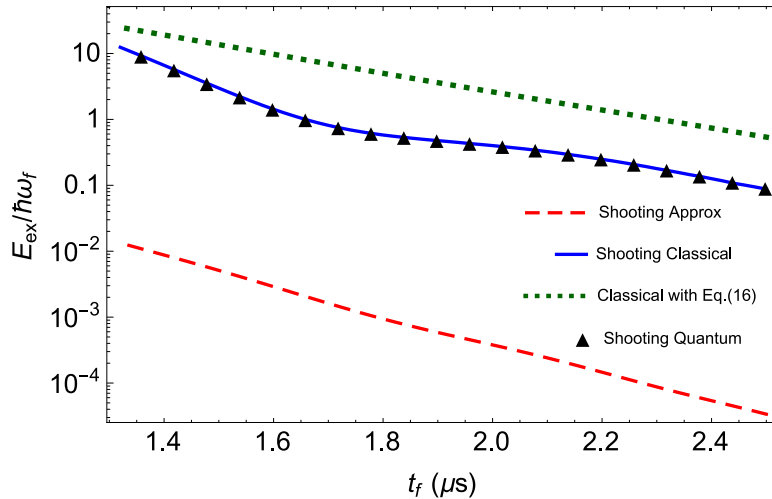
FIGURE 4.1: Final excitation energy at $t_f$ for the expansion of two $^{40}\text{Ca}^+$ ions, with respect to the final ground state (quantum) or the final equilibrium energy (classical). The initial state is the ground state (quantum) or the equilibrium state (classical) for the initial trap. The dashed red line is the excitation in the harmonic approximation, using Eq. (4.14) for the NM energies, with the protocol obtained by the shooting method; the solid blue line (classical) and black triangles (quantum) are for the same protocol but with the dynamics driven by the full Hamiltonian (4.1). The dotted green line is for the protocol (4.16) with the full Hamiltonian. The parameters used are $\omega_0/(2\pi) = 1.2$ MHz and $\gamma^2 = 3$.

i.e. with a fixed center, the frequency in a trap expansion was already inverse engineered in [32]. For this case we can use the same notation as before but no subindices for the auxiliary functions. $\alpha$ is zero for all times, and in the Ermakov equation the conditions $\rho(0) = 1$, $\rho(t_f) = \gamma = \sqrt{\omega_0/\omega_f}$, and $\dot{\rho}(t_b) = \ddot{\rho}(t_b) = 0$, suffice to avoid any excitation (since $[H(t_b), I(t_b)] = 0$) and ensure continuity of the oscillator frequency. Any interpolated function $\rho(t)$ satisfying these conditions provides a valid $\Omega(t)$. Similarly, in harmonic transport of an ion (with the trap moving rigidly from 0 to $d$ with a constant frequency [33]) the auxiliary equation for $\rho$ becomes trivially satisfied by $\rho = 1$ and, to avoid excitations and ensure continuity, $\alpha$ may be any interpolated function satisfying $\alpha(0) = 0$, $\alpha(t_f) = d$, $\dot{\alpha}(t_b) = \ddot{\alpha}(t_b) = 0$ [33]. Instead of these simpler settings, when inverse engineering the expansion of the ion chain the auxiliary equations (4.11) are nontrivially coupled and have to be solved consistently with Eq. (4.12), since $\Omega_\pm$ and $\mathsf{p}_{0\pm}$ are functions of the same frequency $\omega_1$. In other words, only interpolated auxiliary functions $\rho_\pm(t)$, $\alpha_\pm(t)$ consistent with the same $\omega_1(t)$ are valid.
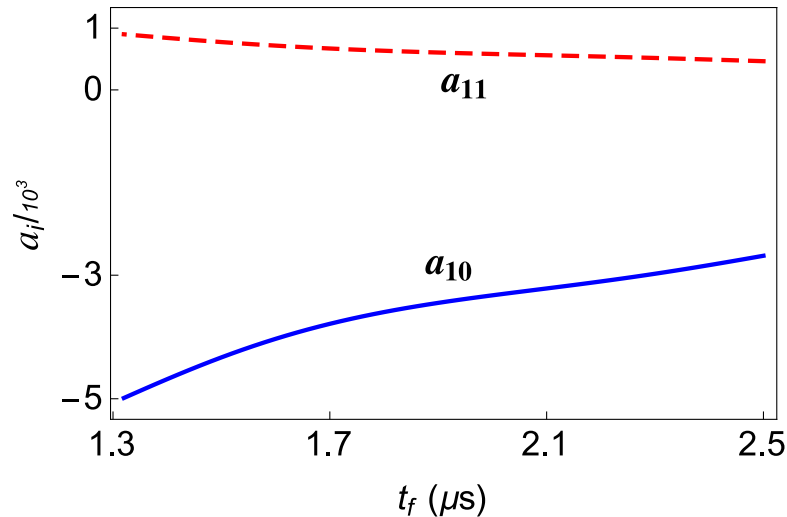
FIGURE 4.2: Values of the optimizing free parameters in the two-ion expansion $a_{10}$ (solid blue line) and $a_{11}$ (dashed red line) in the expansion of two $^{40}\text{Ca}^+$ ions starting in the ground state. $\omega_0/(2\pi) = 1.2$ MHz, $\gamma^2 = 3$.

For both NM, I impose for Eq. (4.11) the boundary conditions (BC) $\rho_\pm(0) = 1$, $\rho_\pm(t_f) = \gamma$, $\dot{\rho}_\pm(t_b) = \ddot{\rho}_\pm(t_b) = 0$. Here $\omega_0 = \omega_1(0)$ and $\omega_f = \omega_1(t_f)$. The BC for the second set of equations are $\alpha_\pm(t_b) = \dot{\alpha}_\pm(t_b) = \ddot{\alpha}_\pm(t_b) = 0$. Eq. (4.12) with Eq. (4.8) implies that at the boundaries we must have $\frac{5}{3}\frac{\dot{\omega}_1^2(t_b)}{w_1(t_b)} - \dddot{\omega}_1(t_b) = 0$. This is satisfied by imposing $\dot{\omega}_1(t_b) = 0$, $\ddot{\omega}_1(t_b) = 0$. Substituting these conditions in Eq. (4.11) one finally gets the extra BC $\rho_\pm^{(3)}(t_b) = \rho_\pm^{(4)}(t_b) = 0$.

To engineer the auxiliary functions I proceed as follows: first I design $\rho_-(t)$[1] so as to satisfy the 10 BC for $\rho_-(t_b)$ and their derivatives. They could be satisfied with a ninth-order polynomial, but I shall use higher-order polynomials so that free parameters are left. These may be chosen to satisfy the equations for the remaining BC for $\alpha_\pm$ and $\rho_+$. $\omega_1(t)$ is deduced from the polynomial using Eq. (4.11) so it becomes a function of the free parameters. There are different ways to fix the free parameters so as to satisfy the remaining BC and design the other auxiliary functions. In practice, I have used a shooting method [95]. The BC used for the shooting are $\alpha_\pm(0) = \dot{\alpha}_\pm(0) = \dot{\rho}_+ = 0$ and $\rho_+(0) = 1$. Note that if $\alpha_\pm(t_b) = 0$, then $\ddot{\alpha}_\pm(t_b) = 0$ since we impose $\dot{\omega}_1(t_b) = \ddot{\omega}_1(t_b) = 0$. The differential equations (4.11) for $\rho_+(t)$ and (4.12) for $\alpha_\pm$ are now solved forward in time.

---

[1] I choose $\rho_-$ instead of $\rho_+$ since $\Omega_+ > \Omega_-$. The effective trap for the plus (+) mode is thus tighter and less prone to excitation than the minus (−) mode. Designing first $\rho_-$ guarantees that this 'weakest' minus mode will not be excited.

In the following, one must distinguish between single-species and mixed-species ion chains. A consequence of having equal mass ions is that $\alpha_-(t)$ is 0 at all times (because the ion chain is symmetric, and thus the center of mass remains static) so we only have to design the three auxiliary functions $\rho_\pm(t)$ and $\alpha_+(t)$. When both ions are of different species, the chain is not symmetric anymore, so we also need to design $\alpha_-$ taking into account its BC.

The MatLab function "fminsearch" [95] is used to find the free parameters that minimize the total final energy for the approximate Hamiltonian, $E_{0+}''(t_f) + E_{0-}''(t_f)$ [see Eq. (4.14)]. For equal mass ions, an 11th order polynomial $\rho_-(t) = \sum_{n=0}^{11} a_n t^n / t_f^n$, i.e. two free parameters, is enough to achieve negligible excitation in a range of times for which the harmonic approximation is valid. Only two free parameters are needed to satisfy the BC $\alpha_+(t_f) = \dot{\alpha}_+(t_f) = 0$, whereas $\rho_+(t_f) = \gamma$ is also nearly satisfied for all values of these free parameters because the evolution of this scaling factor is close to being adiabatic. $\omega_1(t)$ is then a function of the free parameters $a_{10}, a_{11}$. Figure 4.1 depicts the final excitation energy for optimized parameters in the harmonic approximation, using Eq. (4.9), and with the full Hamiltonian (4.1), whereas in Fig. 4.2 the values of the optimizing free parameters are represented. The quantum simulations (triangles in Fig. 4.1) are performed starting from the ground state of the Hamiltonian (4.1) at $t = 0$, which is calculated numerically. For the corresponding classical simulations I solve Hamilton's equations for the two ions in the laboratory frame with Eq. (4.1): the excitation energy is calculated as the total energy minus the minimal energy of the ions in equilibrium. The initial conditions correspond as well to the ions in equilibrium. As the potential is effectively nearly harmonic and the evolution of wave packet's width ($\rho_\pm$) is close to being adiabatic, the classical excitation energy reproduces accurately the quantum excitation energy, as demonstrated in Fig. 4.1. Quantum calculations are very demanding, in particular with three or more ions, so that we shall only perform classical calculations from now on.

For two different ions, we use a 13th order polynomial $\rho_-(t) = \sum_{n=0}^{13} a_n t^n / t_f^n$, which is enough to nearly satisfy $\alpha_\pm(t_f) = \dot{\alpha}_\pm(t_f) = 0$ and $\rho_+(t_f) = \gamma$ by finding suitable values for the four free parameters $a_{10-13}$. As before, $\rho_+(t_f) = \gamma$ is
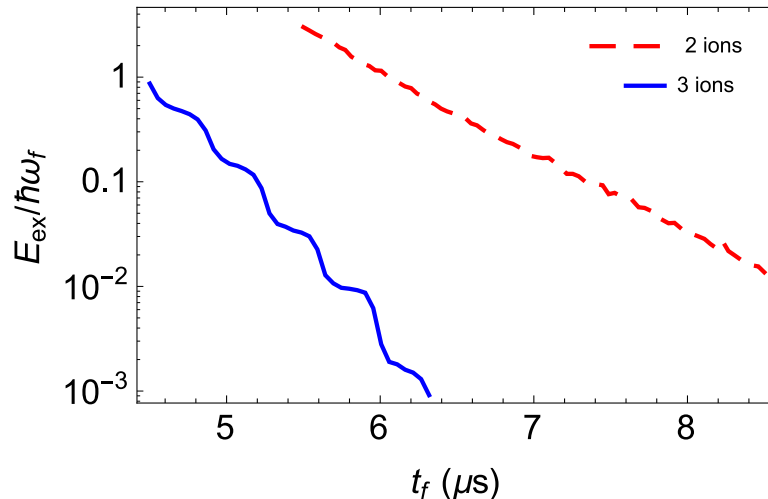
FIGURE 4.3: Final excitation energy for the expansion of a $^9\text{Be}^+$-$^{40}\text{Ca}^+$ ion chain (dashed red line) and a $^9\text{Be}^+$-$^{40}\text{Ca}^+$-$^9\text{Be}^+$ chain (solid blue line) starting in the equilibrium configuration. The protocols are optimized with four (for $^9\text{Be}^+$-$^{40}\text{Ca}^+$) and two (for $^9\text{Be}^+$-$^{40}\text{Ca}^+$-$^9\text{Be}^+$) free parameters, see the main text. $\omega_0/(2\pi) = 1.2$ MHz, $\gamma^2 = 3$.

nearly satisfied without any special design. Figure 4.3 shows the final excitation for a chain of two different ions. The excitation is higher than for equal masses. Both for the equal mass and different mass expansions, the (exact) excitation energy increases at short times, where the quadratic approximation to set the NM Hamiltonians fails, see Figs. 4.1 and 4.3. Further simulations indicate that the larger the ratio between the masses, the higher the excitation.

A less accurate, approximate treatment is based on the simpler polynomial ansatz $\rho_- = \sum_{n=0}^{9} a_n t^n$ without free parameters,[2]

$$
\begin{aligned}
\rho_- & = 126(\gamma - 1)s^5 - 420(\gamma - 1)s^6 + 540(\gamma - 1)s^7 \\
& - 315(\gamma - 1)s^8 + 70(\gamma - 1)s^9 + 1,
\end{aligned}
\tag{4.15}
$$

$s = t/t_f$. While the BC of $\rho_+$ and $\alpha_\pm$ are in general not accounted for exactly, an advantage of this procedure is that there is no need to perform any numerical minimization. This is useful to generalize the method for larger ion chains. For equal masses, both $\alpha_- = 0$ and $\rho_-(t)$ are correctly designed, so that the center of

---

[2]As in the transport of two ions [63], an alternative ansatz to the polynomial is $\rho_-(t) = \frac{1+\gamma}{2} + \frac{\gamma-1}{256} \sum_{n=1}^{3} a_n \cos\left(\frac{(2n-1)\pi t}{t_f}\right)$, where $a_n = (-150, 25, -3)$. In numerical calculations the polynomial ansatz (4.15) performs slightly better than the cosine-based one.
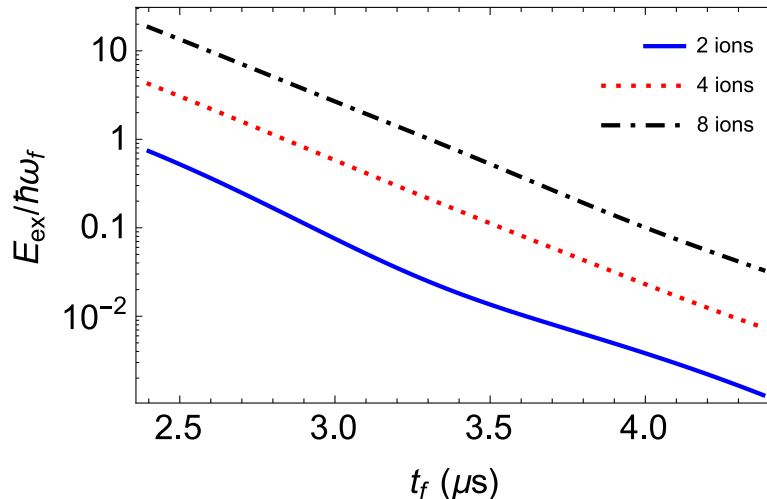
FIGURE 4.4: Final excitation vs final times for expansions of two-equal ions (solid blue line), four-equal ions (red dots) and eight-equal ions (dash-dotted black line). The simulations are performed according to the approximate protocol in Eq. (4.16) and by solving the classical equations of motion for $^{40}Ca^+$ ions. The initial ion chain is at equilibrium. $\omega_0/(2\pi) = 1.2$ MHz, $\gamma^2 = 3$.

mass is not excited. From Eq. (4.11), $\omega_1(t)$ is given by

$$\omega_1 = \sqrt{\frac{\omega_0^2}{\rho_-^4} - \frac{\ddot{\rho}_-}{A_-^2 \rho_-}}, \tag{4.16}$$

where $A_- = \Omega_-/\omega_1$ is a constant [see Eq. (4.3)]. In Fig. 4.1 I compare the performance of this approximate protocol and the one that satisfies all the BC in the two-equal-ion expansion.

## 4.3 N-ion chain expansion

I now proceed to extend the results in the previous section to larger ion chains governed by the Hamiltonian (4.1). The equilibrium positions can be written in the form [96]

$$q_i^{(0)}(t) = l(t)u_i, \tag{4.17}$$

where

$$l^3(t) = \frac{C_c}{u_0(t)} \tag{4.18}$$
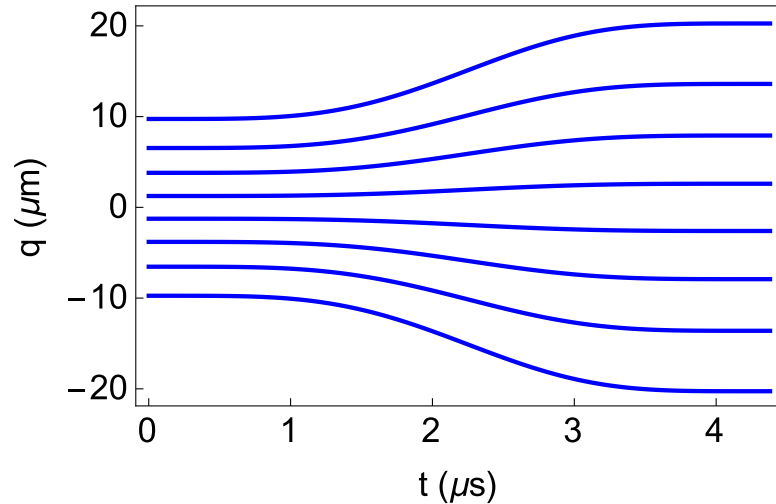
FIGURE 4.5: Classical trajectories of eight expanding $^{40}$Ca$^+$ ions. The evolution is performed according to Eq. (4.16). $\omega_0/(2\pi) = 1.2$ MHz, $\gamma^2 = 3$, $t_f = 4.4$ μs.

and the $u_i$ are the solutions of the system

$$u_i - \sum_{j=1}^{i-1} \frac{1}{(u_i - u_j)^2} + \sum_{j=i+1}^{N} \frac{1}{(u_i - u_j)^2} = 0. \tag{4.19}$$

The NM coordinates are thus defined as [85]

$$\mathsf{q}_\nu = \sum_i a_{\nu i} \sqrt{m_j}(q_i - q_i^{(0)}), \tag{4.20}$$

where the NM subscript $\nu$ runs now from 1 to $N$. Conventionally the $\nu$ are ordered from the lowest to the highest frequency [96]. As for two ions we define $V(q_1, q_2, q_3, ..., q_N)$ as the coordinate-dependent part of the Hamiltonian (4.1). The $a_{\nu i}$ are the components of the $\nu$th eigenvector of the symmetric matrix $V_{ij} = \frac{1}{\sqrt{m_i m_j}} \frac{\partial^2 V}{\partial q_i \partial q_j}(q_i^{(0)}, q_j^{(0)})$, that, together with the eigenvalues $\lambda_\nu = \Omega_\nu^2$, will usually be determined numerically [96]. They are normalized as $\sum_i a_{\nu i}^2 = 1$. As $u_0$ is common to all ions, it can be shown that $\Omega_\nu(t) = A_\nu \omega_1(t)$, where $A_\nu$ is a constant.
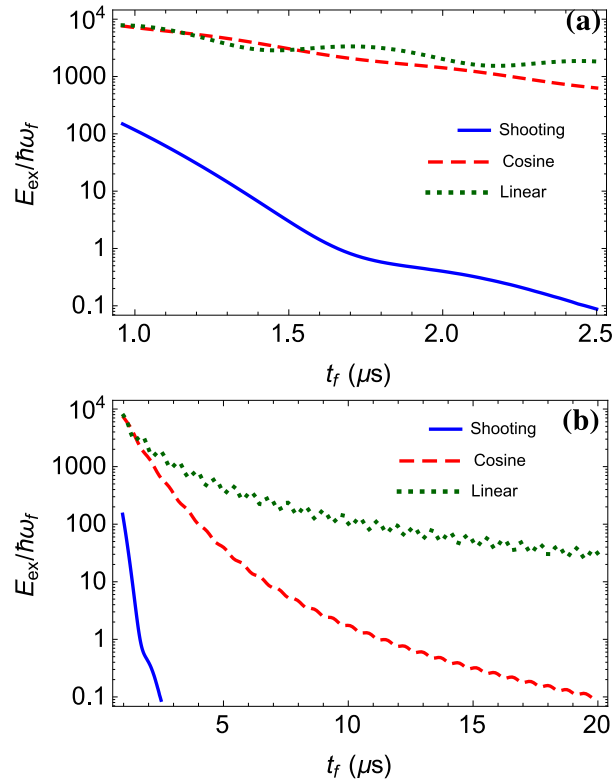
FIGURE 4.6: Comparison of final excitation quanta (classical simulation as in Fig. 4.1) vs final time in the expansion of two $^{40}Ca^+$ ions following the shooting protocol (solid blue), linear protocol in Eq. (4.24) (dotted green), and cosine protocol in Eq. (4.25) (dashed red). In (a) I plot in logarithmic scale up to times where only the shooting protocol reaches the level of 0.1 excitation quanta. In (b) I extend the analysis up to longer final times, so that the best of the cosine protocol reaches also 0.1 final excitation quanta. $\omega_0/(2\pi) = 1.2$ MHz, $\gamma^2 = 3$.

Generalizing the steps leading to Eq. (4.7), the Hamiltonian in a NM frame up to quadratic terms becomes

$$H' = \sum_\nu \left[ \frac{\mathsf{p}_\nu^2}{2} + \frac{1}{2}\Omega_\nu^2 \mathsf{q}_\nu^2 + \mathsf{p}_{0\nu}\mathsf{p}_\nu \right], \tag{4.21}$$

where the $\mathsf{p}_\nu$ are momenta conjugate to the $\mathsf{q}_\nu$, and $\mathsf{p}_{0\nu} = -\sum_i a_{\nu i}\sqrt{m_i}\dot{q}_i^{(0)}$. As for two ions, all the $\mathsf{p}_{0\nu}$ are proportional to $\dot{\omega}_1/\omega_1^{5/3}$. We now apply the unitary transformation $\mathcal{U} = e^{-i\sum_\nu \mathsf{p}_{0\nu}\mathsf{q}_\nu/\hbar}$ and find the effective Hamiltonian

$$H'' = \sum_\nu \left[ \frac{\mathsf{p}_\nu^2}{2} + \frac{1}{2}\Omega_\nu^2 \left( \mathsf{q}_\nu + \frac{\dot{\mathsf{p}}_{0\nu}}{\Omega_+^2} \right)^2 \right]. \tag{4.22}$$

This Hamiltonian is similar to the one for two ions (4.9). The corresponding set of auxiliary equations is also similar to Eqs. (4.11) and (4.12),

$$
\begin{aligned}
\ddot{\rho}_\nu + \Omega_\nu^2 \rho_\nu &= \frac{\Omega_{0\nu}^2}{\rho_\nu^3}, \\
\ddot{\alpha}_\nu + \Omega_\nu^2 \alpha &= \dot{\mathsf{p}}_{0\nu}.
\end{aligned}
\tag{4.23}
$$

The BC for inverse engineering read $\rho_\nu(0) = 1$, $\rho_\nu(t_f) = \gamma$, $\dot{\rho}_\nu(t_b) = \ddot{\rho}_\nu(t_b) = 0$, $\alpha_\nu(t_b) = \dot{\alpha}_\nu(t_b) = \ddot{\alpha}_\nu(t_b) = 0$. When introducing the BC for the $\alpha_\nu$ in the set of Newton's equations, we get from all of them the same condition $\frac{\dot{\omega}_1(t_b)}{\omega_1(t_b)} + \ddot{\omega}_1(t_b) = 0$, which is satisfied for $\dot{\omega}_1(t_b) = \ddot{\omega}_1(t_b) = 0$.

Figure 4.4 depicts the excitation for expansions of single-species ion chains, with approximate (nonoptimized) protocols that use Eqs. (4.15) and (4.16), but with the lowest-frequency mode, $\nu = 1$, instead of the *minus* $(-)$ mode. The longer the chain, the lower the fidelity of the protocol, as more terms are neglected in the NM approximation and more boundary conditions are disregarded. However, the protocol still provides little excitation at long enough final times in the most demanding simulation that we examined, $N = 8$. Figure 4.5 shows the position of the ions, and the trap frequency along the evolution time for the eight-ion chain, ending up with a separation between ions twice as large as the initial one, in times shorter than 4 $\mu$s (Fig. 4.4) without any significant final excitation.

In Fig. 4.3 the excitation for an expansion of the two-species chain $^9\text{Be}^+$-$^{40}\text{Ca}^+$-$^9\text{Be}^+$ is depicted. The minimization technique was used with two free parameters, that is, with an 11th-order polynomial ansatz for $\rho_{\nu=1}(t)$. The excitation is smaller than for the shorter chain $^9\text{Be}^+$-$^{40}\text{Ca}^+$ (with a 13th-order polynomial for $\rho_-$) due to the symmetry in the three-ion chain, which leaves two of the NM static and unexcited.

## 4.4 Discussion

I have designed fast diabatic protocols for the time dependence of the trap frequency that suppress the final excitation of different ion-chain expansions or compressions. Unlike the simpler single-ion expansion [32], the inverse design problem of the trap frequency for an ion chain involves coupled Newton and Ermakov equations for each dynamical normal mode. I found ways to deal with this inverse problem by applying a shooting technique in the most accurate protocols, and effective, simplifying approximations.

These protocols work for process times for which the quadratic approximation for the Hamiltonian is valid. Longer and more asymmetric chains need larger times than shorter and symmetrical ones. The examples show that these times are compatible with current quantum information protocols, so many processes may benefit by the described trap-frequency time dependencies.

The designed protocols provide a considerable improvement in final time and excitation energy with respect to simple, naive protocols. For the expansion of two $^{40}$Ca$^+$ considered in Fig. 4.1 I compare in Fig. 4.6 the excitation energy of the shooting protocol with two simple protocols that drive the frequency $\omega_1$ linearly,

$$\omega_1(t) = \omega_0 + \frac{\omega_f - \omega_0}{t_f} t, \tag{4.24}$$

and following a cosine function,

$$\omega_1(t) = \frac{\omega_0 + \omega_f}{2} + \frac{\omega_0 - \omega_f}{2} \cos\left(\frac{\pi t}{t_f}\right). \tag{4.25}$$

The simulations are classical, as described in Sec. 4.2. Figure 4.6 (a) compares the excitations at short times. For $t_f \sim 2.5$ $\mu$s, the shooting protocol reaches a low excitation of 0.1 vibrational quanta, four orders of magnitude smaller than the excitations due to the simple methods. In Fig. 4.6 (b) the excitations are represented for longer protocol times. The smoother cosine protocol behaves better than the linear one and finally reaches an excitation of approximately 0.1 quanta

for $t_f \sim 20 \; \mu$s. That means that the optimized protocol gets an improvement by a factor of 8 in final time. The results presented on this chapter were published in [97].

# Chapter 5

# Fast separation of two trapped ions

*"A creative man is motivated by the desire to achieve, not by the desire to beat others."*

Ayn Rand

I design fast protocols to separate or recombine two ions in a segmented Paul trap. By inverse engineering the time evolution of the trapping potential composed of a harmonic and a quartic term, it is possible to perform these processes in a few microseconds without final excitation. These times are much shorter than the ones reported so far experimentally. The design is based on dynamical invariants and dynamical normal modes. Anharmonicities beyond the harmonic approximation at potential minima are taken into account perturbatively. The stability versus an unknown potential bias is also studied.

## 5.1 Introduction

Separating ion chains is in the toolkit of basic operations required. (Merging chains is the corresponding reverse operation so we shall only refer to separation hereafter.) It has been used to implement two-qubit quantum gates [57]; also to purify entangled states [98, 99], or teleport material qubits [100]. Moreover, as is a common theme in this thesis, ion chain separation/merging could be an important operation in the scheme to build an architecture for processing information scalable to many ions in multisegmented traps [23].

Ion-chain separation is known to be a difficult operation [101]. Experiments have progressed towards lower final excitations and shorter times but much room for improvement still remains [26, 42, 84]. Problems identified include anomalous heating, so devising short-time protocols via shortcuts-to-adiabaticity (STA) techniques was proposed as a way out worth exploring [83]. STA methods intend to speed up different adiabatic operations [31, 32] without inducing final excitations. An example of an elementary (fast quasi-adiabatic) STA approach [32] was already applied for fast chain splitting in [42]. Here, I design, using a more general and efficient STA approach based on dynamical normal modes (NM) [63, 97], protocols to effectively separate two equal ions, initially in a common electrostatic linear harmonic trap, into a final configuration where each ion is in a different well. The motion is assumed to be effectively one dimensional due to tight radial confinement. The external potential for an ion at $q$ is approximated as

$$V_{ext} = \alpha(t)q^2 + \beta(t)q^4, \tag{5.1}$$

which is experimentally realizable with state-of-art segmented Paul Traps [101, 102].

Using dynamical NM [63, 97], a Hamiltonian will be set which is separable in a harmonic approximation around potential minima. By means of Lewis-Riesenfeld invariants [76], I shall design first the approximate dynamics of an unexcited splitting, taking into account anharmonicities in a perturbative manner, and from that

inversely find the corresponding protocol, i.e. the $\alpha(t)$ and $\beta(t)$ functions.

The Hamiltonian of the system of two ions of mass $m$ and charge $e$ is, in the laboratory frame,

$$
\begin{aligned}
H &= \frac{p_1^2}{2m} + \frac{p_2^2}{2m} + V, \\
V &= \alpha(t)(q_1^2 + q_2^2) + \beta(t)(q_1^4 + q_2^4) + \frac{C_c}{q_1 - q_2},
\end{aligned}
\tag{5.2}
$$

where $p_1, p_2$ are the momentum operators for both ions, $q_1, q_2$ their position operators, and $C_c = \frac{e^2}{4\pi\epsilon_0}$, $\epsilon_0$ being the vacuum permittivity. I use on purpose a c-number notation since I shall also consider classical simulations. The context will make clear if $c-$numbers or $q-$numbers are required. I suppose that, due to the strong Coulomb repulsion, $q_1 > q_2$. By minimizing the potential part of the Hamiltonian $V$, I find for the equilibrium distance between the two ions, $d(t)$, the quintic equation [101]

$$
\beta(t)d^5(t) + 2\alpha(t)d^3(t) - 2C_c = 0,
\tag{5.3}
$$

which will be quite useful for inverse engineering the ion-chain splitting, even without an explicit solution for $d(t)$. At $t = 0$ a single external well is assumed, $\beta(0) = 0$ and $\alpha(0) > 0$, whereas in the final double-well configuration $\beta(t_f) > 0, \alpha(t_f) < 0$. At some intermediate time $t_i$ the potential becomes purely quartic ($\alpha(t_i) = 0$). My aim is to design the functions $\alpha(t)$ and $\beta(t)$ so that each of the
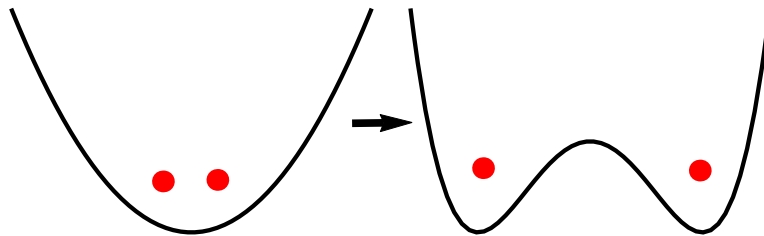


FIGURE 5.1: Scheme of the separation process. At $t = 0$ (left), both ions are trapped within the same external harmonic potential. At final time $t_f$ (right), the negative harmonic term, and a quartic term build a double well external potential. The aim of the process is to set each of the ions in a different well without any residual excitation.

ions ends up in a different external well as shown in Fig. 5.1, in times as short as possible, and without any final excitation.

## 5.2 Dynamical Normal Modes

To define dynamical NM coordinates, I calculate first at equilibrium (the point $\{q_1^{(0)}, q_2^{(0)}\}$ in configuration space where the potential is a minimum, $\partial V/\partial q_1 = \partial V/\partial q_2 = 0$) the matrix $V_{ij} = \frac{1}{m}\frac{\partial^2 V}{\partial q_i \partial q_j}\big|_{\text{eq}}$. The equilibrium positions are $q_1^{(0)} = \frac{d(t)}{2}$, $q_2^{(0)} = -\frac{d(t)}{2}$, and the matrix takes the form

$$V_{ij} = \frac{1}{m}\begin{pmatrix} 2\alpha + 12\beta\frac{d^2}{4} + \frac{2C_c}{d^3} & -\frac{2C_c}{d^3} \\ \frac{-2C_c}{d^3} & 2\alpha + 12\beta\frac{d^2}{4} + \frac{2C_c}{d^3} \end{pmatrix}. \tag{5.4}$$

The eigenvalues are

$$\begin{aligned} \lambda_- &= \frac{1}{m}(2\alpha + 3\beta d^2), \\ \lambda_+ &= \frac{1}{m}\left(2\alpha + 3\beta d^2 + \frac{4C_c}{d^3}\right), \end{aligned} \tag{5.5}$$

which define the NM frequencies as $\Omega_\pm = \sqrt{\lambda_\pm}$ corresponding to center-of-mass $(-)$ and relative (stretch) motions $(+)$. These relations, with Eq. (5.3) written as

$$\beta(t) = \frac{2C_c}{d^5(t)} - \frac{2\alpha(t)}{d^2(t)}, \tag{5.6}$$

allow to write $\alpha(t)$ and $d(t)$ as functions of the NM frequencies:

$$\alpha(t) = \frac{1}{8}m\left(3\Omega_+^2 - 5\Omega_-^2\right), \tag{5.7}$$

$$d(t) = \sqrt[3]{\frac{4C_c}{m\left(\Omega_+^2 - \Omega_-^2\right)}}. \tag{5.8}$$

Substituting these expressions into Eq. (5.6), $\beta(t)$ may also be written in terms of NM frequencies.

The normalized eigenvectors are

$$
\begin{aligned}
v_- &= \frac{1}{\sqrt{2}} \begin{pmatrix} 1 \\ 1 \end{pmatrix}, \\
v_+ &= \frac{1}{\sqrt{2}} \begin{pmatrix} 1 \\ -1 \end{pmatrix},
\end{aligned}
\tag{5.9}
$$

which I denote as $v_\pm = \begin{pmatrix} a_\pm \\ b_\pm \end{pmatrix}$. The (mass-weighted) dynamical NM coordinates are defined in terms of the laboratory coordinates as

$$
\mathsf{q}_\pm = a_\pm \sqrt{m}(q_1 - q_1^{(0)}) + b_\pm \sqrt{m}(q_2 - q_2^{(0)}).
\tag{5.10}
$$

The unitary transformation of coordinates is

$$
U = \int d\mathsf{q}_+ d\mathsf{q}_- dq_1 dq_2 |\mathsf{q}_+, \mathsf{q}_-\rangle \langle \mathsf{q}_+, \mathsf{q}_- | q_1, q_2 \rangle \langle q_1, q_2 |,
\tag{5.11}
$$

where $\langle \mathsf{q}_+, \mathsf{q}_- | q_1, q_2 \rangle = \delta[q_1 - q_1(\mathsf{q}_+, \mathsf{q}_-)]\delta[q_2 - q_2(\mathsf{q}_+, \mathsf{q}_-)]$. The Hamiltonian in the dynamical equation for $|\psi'\rangle = U|\psi\rangle$, where $|\psi\rangle$ is the lab-frame time-dependent wave function evolving with $H$, is given by

$$
\begin{aligned}
H' &= UHU^\dagger - i\hbar U(\partial_t U^\dagger) = \\
&= \frac{\mathsf{p}_+^2}{2} + \frac{1}{2}\Omega_+^2 \mathsf{q}_+^2 + \frac{\dot{d}}{\sqrt{2}}\sqrt{m}\,\mathsf{p}_+ \\
&+ \frac{\mathsf{p}_-^2}{2} + \frac{1}{2}\Omega_-^2 \mathsf{q}_-^2,
\end{aligned}
\tag{5.12}
$$

plus qubic and higher order terms in the potential that we neglect by now (they will be considered in Sec. 5.4 below). Similarly to [63, 97], I apply a further unitary transformation $\mathcal{U} = e^{-i\sqrt{m}\dot{d}\mathsf{q}_+/(\sqrt{2}\hbar)}$ to write down an effective Hamiltonian for $|\psi''\rangle = \mathcal{U}|\psi'\rangle$ with the form of two independent harmonic oscillators in NM space, $H'' = \mathcal{U}H'\mathcal{U}^\dagger - i\hbar\mathcal{U}(\partial_t \mathcal{U}^\dagger)$,

$$
\begin{aligned}
H'' &= \frac{\mathsf{p}_+^2}{2} + \frac{1}{2}\Omega_+^2 \left( \mathsf{q}_+ + \frac{\sqrt{m}\ddot{d}}{\sqrt{2}\Omega_+^2} \right)^2 \\
&+ \frac{\mathsf{p}_-^2}{2} + \frac{1}{2}\Omega_-^2 \mathsf{q}_-^2 = H_+'' + H_-''.
\end{aligned}
\tag{5.13}
$$

These oscillators have dynamical invariants of the form [76]

$$
\begin{aligned}
I_\pm &= \frac{1}{2}[\rho_\pm(\mathsf{p}_\pm - \dot{x}_\pm) - \dot{\rho}_\pm(\mathsf{q}_\pm - x_\pm)]^2 \\
&+ \frac{1}{2}\Omega_{0\pm}^2\left(\frac{\mathsf{q}_\pm - x_\pm}{\rho_\pm}\right)^2,
\end{aligned}
\tag{5.14}
$$

where the auxiliary functions $\rho_\pm$ and $x_+$ satisfy

$$
\ddot{\rho}_\pm + \Omega_\pm^2\rho_\pm = \frac{\Omega_{0\pm}^2}{\rho_\pm^3}, \tag{5.15}
$$

$$
\ddot{x}_+ + \Omega_+^2 x_+ = -\sqrt{\frac{m}{2}}\ddot{d}, \tag{5.16}
$$

with $\Omega_{0\pm} = \Omega_\pm(0)$, and, due to symmetry, $x_- = 0$. In this chapter, I used the notation $x_\pm$ for the auxiliary function satisfying Newton's equation instead of $\alpha_\pm$ as in the rest of the chapters because $\alpha$ is already used to define the harmonic term in the potential. This is done because it is a tradition in the field to name the harmonic term as $\alpha$.

The physical meaning of the auxiliary functions may be grasped from the solutions of the time-dependent Schrödinger equations (for each NM Hamiltonian $H_\pm''$ in Eq. (5.13)) proportional to the invariant eigenvectors [33]. They form a complete basis for the space spanned by each Hamiltonian $H_\pm''$ and take the form

$$
\langle \mathsf{q}_\pm|\psi_{n\pm}''(t)\rangle = e^{\frac{i}{\hbar}\left[\frac{\dot{\rho}_\pm \mathsf{q}_\pm^2}{2\rho_\pm} + (\dot{x}_\pm\rho_\pm - x_\pm\dot{\rho}_\pm)\frac{\mathsf{q}_\pm}{\rho_\pm}\right]}\frac{\Phi_n(\sigma_\pm)}{\rho_\pm^{1/2}}, \tag{5.17}
$$

where $\sigma_\pm = \frac{\mathsf{q}_\pm - x_\pm}{\rho_\pm}$, and $\Phi_n(\sigma_\pm)$ are the eigenfunctions of the static harmonic oscillator at time $t = 0$. Thus, $\rho_\pm$ are scaling factors proportional to the state "width" in NM coordinates, whereas the $x_\pm$ are the dynamical-mode centers in the space of NM coordinates. Within the harmonic approximation, there are dynamical states of the factorized form $|\psi''(t)\rangle = |\psi_+''(t)\rangle|\psi_-''(t)\rangle$ for the ion chain dynamics, where the NM wave functions $|\psi_\pm''(t)\rangle$ evolve independently with $H_\pm''$. They may be written as combinations of the form $|\psi_\pm''(t)\rangle = \sum_n C_{n\pm}|\psi_{n\pm}''(t)\rangle$, with constant amplitudes $C_{n\pm}$. The average energies of the $n$th-basis states for the two

NM are $E''_{n\pm} = \langle \psi''_{n\pm} | H''_{\pm} | \psi''_{n\pm} \rangle$,

$$
\begin{aligned}
E''_{n-} &= \frac{(2n+1)\hbar}{4\Omega_{0-}} \left( \dot{\rho}_-^2 + \Omega_-^2 \rho_-^2 + \frac{\Omega_{0-}^2}{\rho_-^2} \right), \\
E''_{n+} &= \frac{(2n+1)\hbar}{4\Omega_{0+}} \left( \dot{\rho}_+^2 + \Omega_+^2 \rho_+^2 + \frac{\Omega_{0+}^2}{\rho_+^2} \right) \\
&\quad + \frac{1}{2}\dot{x}_+^2 + \frac{1}{2}\Omega_+^2 \left( x_+ - \frac{\sqrt{m}\ddot{d}}{\sqrt{2}\Omega_+^2} \right)^2 .
\end{aligned}
\tag{5.18}
$$

## 5.3  Design of the Control Parameters

Once the Hamiltonian and Lewis-Riesenfeld invariants are defined, I proceed to apply the invariant-based inverse-engineering technique and design shortcuts to adiabaticity. The results for the simple harmonic oscillator in [32] serve as a reference, but have to be extended here since the two modes are not really independent from the perspective of the inverse problem. This is because a unique protocol, i.e., a single set of $\alpha(t)$ and $\beta(t)$ functions has to be designed.

I first set the initial and target values for the control parameters $\alpha(t)$ and $\beta(t)$. At time $t = 0$, the external trap is purely harmonic, with (angular) frequency $\omega_0$. From Eq. (5.5), we find that $\Omega_-(0) = \omega_0$ and $\Omega_+(0) = \sqrt{3}\omega_0$. The equilibrium distance is $d(0) = \sqrt[3]{\frac{2C_c}{m\omega_0^2}}$. For the final time, I set a tenfold expansion of the equilibrium distance, $d(t_f) = 10d(0)$, and $\Omega_-(t_f) = \omega_0$. This also implies $\Omega_+(t_f) = \sqrt{1.002}\,\omega_0 \approx \Omega_-(t_f)$, i.e., the final frequencies of both NM are essentially equal, the Coulomb interaction is negligible, and the ions can be considered to oscillate in independent traps.

The inverse problem is somewhat similar to the expansion of a trap with two equal ions in Ref. [63], but complicated by the richer structure of the external potential. The Hamiltonian (5.13) and the invariant (5.14) must commute at both boundary times $[H(t_b), I(t_b)] = 0$,

$$
t_b = 0, t_f,
\tag{5.19}
$$
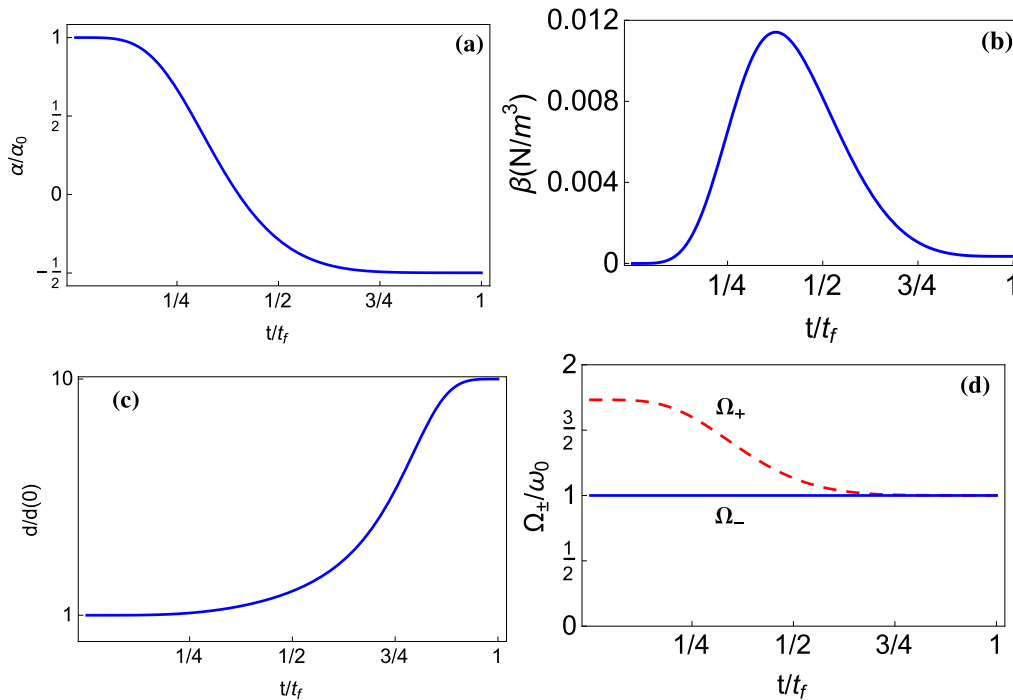
FIGURE 5.2: Evolution of (a) $\alpha(t)$; (b) $\beta(t)$; and (c) d(t). In (d), the NM frequencies, solid line for the '-' and dashed line for the '+' are depicted. Two $^9Be^+$ ions were separated in the simulation, with $\omega_0/(2\pi) = 2$ MHz, $t_f = 5.2$ $\mu$s, $\alpha_0 = m\omega_0^2/2$, and $d(0) = 5.80$ $\mu$m.

to drive initial levels into final levels via a one-to-one mapping. This is achieved by applying appropriate boundary conditions (BC) to the auxiliary functions $\rho_\pm$, $x_\pm$ and their derivatives:

$$\rho_\pm(0) = 1, \qquad \rho_\pm(t_f) = \gamma_\pm, \tag{5.20}$$

$$\dot{\rho}_\pm(t_b) = \ddot{\rho}_\pm(t_b) = 0, \tag{5.21}$$

$$x_+(t_b) = \dot{x}_+(t_b) = \ddot{x}_+(t_b) = 0, \tag{5.22}$$

where $\gamma_\pm = \sqrt{\frac{\Omega_\pm(0)}{\Omega_\pm(t_f)}}$. Let me recall that $x_- = 0$ for all times so this parameter does not have to be considered further.

Inserting the BC for $x_+(t_b)$ and $\ddot{x}_+(t_b)$ in Eq. (5.16), we find that $\dddot{d}(t_b) = 0$. Additionally, $\dot{d}(t_b) = 0$ is to be imposed so that $\mathcal{U}(t_b) = 1$. According to Eq. (5.8), $\ddot{d}(t_b) = \dddot{d}(t_b) = 0$ by imposing $\dot{\Omega}_\pm(t_b) = \ddot{\Omega}_\pm(t_b) = 0$. With $\dot{d}(t_b) = \ddot{d}(t_b) = 0$, the Hamiltonians and wave functions coincide at the boundaries, $H'(t_b) = H''(t_b)$,

$|\psi'(t_b)\rangle = |\psi''(t_b)\rangle\rangle$, which simplifies the calculation of the excitation energy.

From Eq. (5.15), the NM frequencies may be written as

$$\Omega_\pm = \sqrt{\frac{\Omega_{0\pm}^2}{\rho_\pm^4} - \frac{\ddot{\rho}_\pm}{\rho_\pm}}. \qquad (5.23)$$

Thus, the BC $\dot{\Omega}_\pm(t_b) = \ddot{\Omega}_\pm(t_b) = 0$ are satisfied by imposing on the auxiliary functions the additional BC

$$\dddot{\rho}_\pm(t_b) = \ddddot{\rho}_\pm(t_b) = 0. \qquad (5.24)$$

We may now design ansatzes for the auxiliary functions $\rho_\pm$ that satisfy the ten BC in Eqs. (5.20,5.21,5.24), plus the BC for $x_+(t_b)$ and $\dot{x}_+(t_b)$ in Eq. (5.22) (since $\ddot{d}(t_b) = 0$, $\ddot{x}_+(t_b) = 0$ is then automatically satisfied [see Eq. (5.16)]). Finally, from the NM frequencies given by Eq. (5.23) we can inverse engineer the control parameters $\alpha(t)$ and $\beta(t)$ from Eqs. (5.6), (5.7), and (5.8).

A simple choice for $\rho_-(t)$ is a polynomial ansatz of 9th order $\rho_- = \sum_{i=0}^{9} b_i s^i$, where $s = t/t_f$. Substituting this form in the ten BC in Eqs. (5.20), (5.21), (5.24), we finally get

$$\begin{aligned}\rho_- &= 126(\gamma_- - 1)s^5 - 420(\gamma_- - 1)s^6 + 540(\gamma_- - 1)s^7 \\ &- 315(\gamma_- - 1)s^8 + 70(\gamma_- - 1)s^9 + 1.\end{aligned} \qquad (5.25)$$

For $\rho_+$ I use an 11th order polynomial $\rho_+ = \sum_{n=0}^{11} a_n s^n$ to satisfy as well $x_+(t_b) = \dot{x}_+(t_b) = 0$. The parameters $a_{0-9}$ are fixed so that the 10 BC for $\rho_+$ are fulfilled (see the Appendix G), whereas $a_{10}, a_{11}$ are left free, and will be numerically determined by a shooting program [103] ('fminsearch' in MATLAB, which uses the Nelder-Mead simplex method for optimization), so that the remaining BC for $x_+(t_b)$ and $\dot{x}_+(t_b)$ are also satisfied. Specifically, for each pair $\{a_{10}, a_{11}\}$, $\Omega_\pm(t)$ and $d(t)$ are determined from Eqs. (5.8) and (5.15), to solve Eq. (5.16) for $x_+(t)$ with initial conditions $x_+(0) = \dot{x}_+(0) = 0$. The free constants are changed until $x_+(t_f) = 0$

and $\dot{x}_+(t_f) = 0$ are satisfied. Numerically, a convenient way to find the solution is to minimize the energy $E''_{n+}(t_f)$ in Eq. (5.18).

Figures 5.2 (a) and (b) depict the control parameters $\alpha(t)$ and $\beta(t)$ found with this method, using Eqs. (5.6) and (5.7), for some value of $t_f$ and $\omega_0$, see the caption, while Fig. 5.2 (c) represents the equilibrium distance between ions as a function of time (5.8), and Fig. 5.2 (d) the NM frequencies. In Fig. 5.3 (a) the excitation energy is shown versus final time for the optimized parameters given in Fig. 5.3 (b). The initial state is the ground state of the two ions. It is calculated by propagating an initial guess of the wave function in imaginary time until it relaxes to the lowest eigenfunction [81]. The excitation energy is $E_{ex} = E(t_f) - E_0(t_f)$, where $E(t_f)$ is the final energy, calculated in the lab frame, and $E_0(t_f)$ is the final ground-state energy. The wave function evolution is calculated using the "Split-Operator Method" with the full Hamiltonian (5.2). If the harmonic approximation were exact, there would not be any excitation with this STA method, $E(t_f) = E''_{0+}(t_f) + E''_{0-}(t_f) = E_0(t_f)$ [see Eq. (5.18)]. The actual result is perturbed by the anharmonicities and NM couplings. The final ground state is also calculated with an "imaginary-time evolution". The corresponding final ground-state energy is essentially twice the harmonic-oscillator ground-state energy plus the (negligible) Coulomb repulsion at distance $d(t_f)$. For the final times of all the examples, as it was noted in previous works [52, 63, 63, 83], classical simulations (solving Hamilton's equations from the equilibrium configuration instead of Schrödinger's equation) give indistinguishable results in the scale of Fig. 5.3 (a).

The excitation energy in Fig. 5.3(a) (solid line) increases at short times since the harmonic NM approximation fails [63, 97]. However, it goes down rapidly below one excitation quantum at times which are still rather small compared to experimental values used so far [42, 84]. In the following section, I shall apply a perturbative technique to minimize the excitation further.
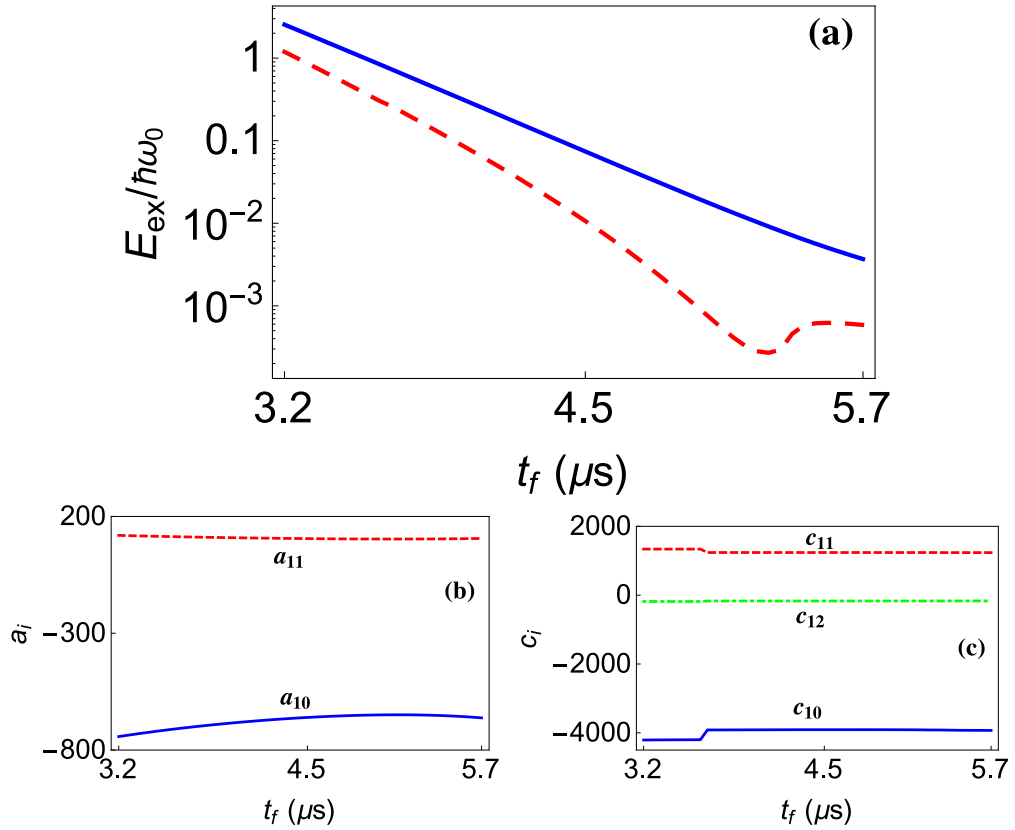
FIGURE 5.3: (a) Final excitation energy vs final time using the inverse-engineering design of Sec. 5.3 (solid blue), and the design that takes into account anharmonicities in Sec. 5.4 (dashed red). (b) Values of the free parameters $a_{10}$ (solid blue) and $a_{11}$ (dashed red) that minimize the excitation energy for the 11th order polynomial (G.1). (c) Parameters $c_{10}$ (solid blue), $c_{11}$ (dashed red) and $c_{12}$ (dash-dotted green) that minimize the excitation energy for the 12th order polynomial (G.2). Two $^9$Be$^+$ ions were splitted, with $\omega_0/(2\pi) = 2$ MHz.

## 5.4 Beyond the harmonic approximation

An improvement of the protocol is to consider the perturbation of the higher order terms neglected in the Hamiltonian (5.13). These "anharmonicities" [59] are cubic and higher order terms in the Taylor expansion of the Coulomb term $C_c/(q_1 - q_2)$,

$$
\begin{aligned}
\delta V &= \sum_{j=3}^{\infty} \delta V^{(j)} \\
&= \sum_{j=3}^{\infty} \frac{(-1)^j C_c}{d^{j+1}} \left[ \left( q_2 - q_2^{(0)} \right) - \left( q_1 - q_1^{(0)} \right) \right]^j .
\end{aligned}
\tag{5.26}
$$

In NM coordinates, the terms take the simple form

$$\delta V^{(j)} = (-1)^{j+1} \frac{C_c}{d^{j+1}} \left( \sqrt{\frac{2}{m}} \mathsf{q}_+ \right)^j, \qquad (5.27)$$

which may be regarded as a perturbation to be added to $H''_+$ in Eq. (5.13). (The perturbation does not couple the center-of-mass and relative subspaces.) To first order, the excess energy due to these perturbative terms at final time is given by

$$\delta E_{n+}^{(j)} = \langle \psi''_{n+}(t_f)|\delta V^{(j)}|\psi''_{n+}(t_f)\rangle, \qquad (5.28)$$

where the $|\psi''_{n+}\rangle$ are the unperturbed states in Eq. (5.17). Inverse engineering the splitting process may now be carried out by considering a 12th order polynomial for $\rho_+$ (see (G.2)), with three free parameters so as to fix the BC for $x_+$ and also minimize the excitation energy. In practice, I used MATLAB's 'fminsearch' function for the shooting to minimize $E_{0+}(t_f)+\delta E_{0+}^{(3)}$ as no significant improvement occurs by including higher order terms. Figure 5.3 (a) compares the performance of such a protocol with the simpler one with the 11th-order polynomial (G.1). Figure 5.3 (c) gives the values of optimized parameters at different final times.

## 5.5   Discussion

A large quartic potential is desirable to control the excitations produced at the point where the harmonic term changes its sign [83]. At this point, the harmonic potential switches from confining to repulsive, which reduces the control of the system and potentially increases diabaticities and heating. In the inverse approach proposed here, there is no special design of the protocol at this point, but the method naturally seeks high quartic confinements there. In Fig. 5.2 (b) $\beta$ reaches its maximum value right at the time where $\alpha$ changes sign (see Fig. 5.2 (a)). However, the maximum value that $\beta$ can reach will typically be limited in a Paul trap [101]. In Table 5.1 I summarize the different maximal values of $\beta$, and critical

| $\omega_0$ (MHz) | $\beta_{max}$ ($10^{-3}$N/m$^3$) | $t_{crit}$ ($\mu$s) |
|:---:|:---:|:---:|
| 3 | 44.2 | 2.9 |
| 2 | 11.4 | 4.4 |
| 1.2 | 2.082 | 7.4 |
| 0.8 | 0.539 | 11.2 |

TABLE 5.1: Maximum values of $\beta$, and critical times (final times at which excitations below 0.1 quanta are reached) for different values of $\omega_0$. The calculations were performed with the 11th order polynomial for $\rho_+$.

times (final times at which excitations below 0.1 quanta are reached) for different values of $\omega_0$ using the 11th-order polynomial (G.1) for $\rho_+$.

The maximum $\beta$ decreases with $t_f$, such that the shortest possible $t_f$ at a given maximum tolerable excitation energy is limited by the achievable $\beta$. The trap used in Ref. [84] yields a maximum $\beta$ of about $10^{-4}$ N/m$^3$, at $\pm 10$ V steering range. In a recent experiment reported in [104], where although the purpose was not ion separation a double well potential was produced, the value used was $\beta \approx 5 \times 10^{-3}$ N/m$^3$. The numbers reported in the Table are thus within reach, as the $\beta$ coefficients scale with the inverse 4th power of the overall trap dimension, and technological improvements on arbitrary waveform generators may allow for operation at an increased voltage range.

Another potential limitation the method could encounter in the laboratory is due to biases (a linear slope) in the trapping potential, $V_{ext} = \alpha q^2 + \beta q^4 + \lambda q$, with $\lambda$ constant and unknown [83]. Figure 5.4 represents the excitation energy versus the energy difference between the two final minima of the external potential, $\Delta E$ (also vs $\lambda$). To calculate the results, $\alpha(t)$ and $\beta(t)$ are designed as if $\lambda = 0$, but the dynamics is carried out with a nonzero $\lambda$, in particular the initial state is the actual ground state, including the perturbation. Note that $\Delta E$ should be more than a thousand vibrational quanta to excite the final energy by one quantum. In Ref. [84] an energy increase of ten phonons at about 150 zN and 80 $\mu$s separation
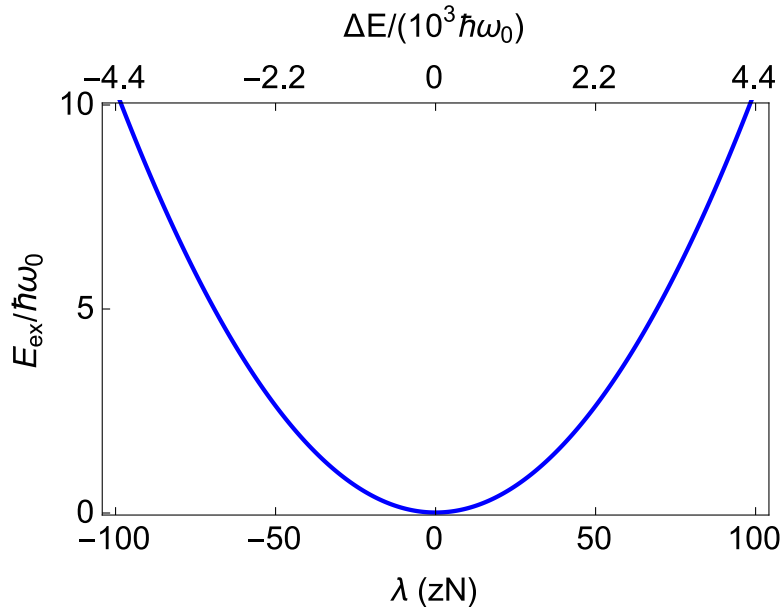
FIGURE 5.4: Excitation energy vs. different tilt values of the external potential in terms of the energy difference between both wells (upper axis) and values of the $\lambda$ parameter (lower axis), when using the 11th order polynomial in the evolution. Same parameters as in Fig. 5.2.

time was reported, so the STA ramps definitely improve the robustness against bias.

Further experimental limitations may be due to random fluctuations in the potential parameters, or higher order terms in the external potential. I leave these important issues for a separate study but note that the structure of the STA techniques used here is well adapted to deal with noise or perturbations [44, 56, 105].

Finally, I compare in Fig. 5.5 the performance of the protocols based on the polynomials (5.25) and (G.1) with a simple non-optimized protocol based on those experimentally used in [84]. There, the equilibrium distance $d$ is first designed as $d(t) = d(0) + [d(t_f) - d(0)]s^2 \sin(s\pi/2)$, where $s = t/t_f$. From the family of possible potential ramps consistent with this function, I chose a polynomial that drives $\alpha$ from $\alpha(0) = \alpha_0$ to $\alpha(t_f) = -\alpha_0/2$ (as in Fig. 5.2) and whose first derivatives are 0 at both boundary times. $\beta$ is given by Eq. (5.3). For the times analysed in Fig. 5.5, the method based on Eqs. (5.25) and (G.1) clearly outperforms the nonoptimized ramp. To get excitations below the single motional excitation
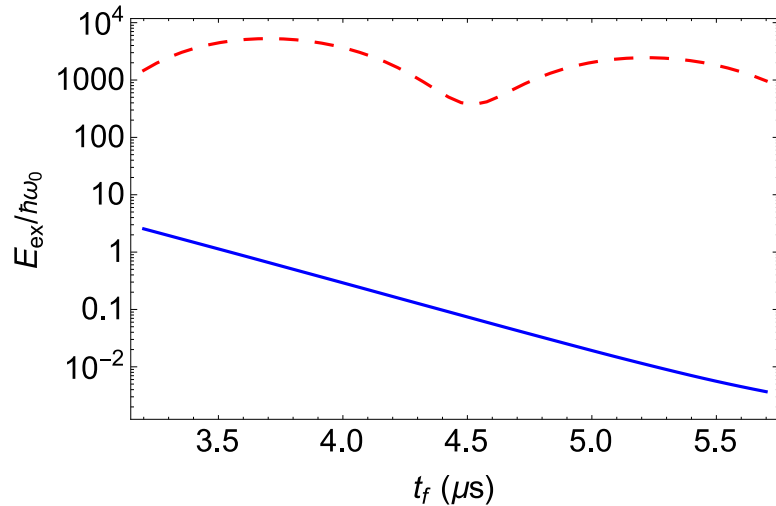
FIGURE 5.5: Excitation energy vs. final time comparing the 11th order polynomial (solid blue) and a non optimized trajectory experimentally used in [84] (dashed red) in the evolution. Same parameters as in Fig. 5.2.

quantum with the nonoptimized protocol, final times as long as $t_f \sim 80\,\mu s$ would be needed, which is in line with current experiments.

I conclude that the method presented here, could bring a clear improvement with respect to the best results experimentally reported so far [42, 84]. The parameters required are realistic in current trapped ions laboratories. The simulations show that, under ideal conditions, the separation of two ions could be performed in a few oscillation periods, at times similar to those required for other operations as transport [63] or expansions [97], studied before in this thesis (Chapters 2 and 4 respectively). The results obtained in this chapter were published in [106].

# Chapter 6

# Shortcuts to adiabaticity for an ion in a rotating radially-tight trap

> Merlin:  *There's only one thing to it. Learn! Learn why the world wags, and what wags it.*
>
> Arthur:  *How could I learn if I couldn't think?....*
>
> Merlin:  *Yes...thinking, boy, is something you should definitely get into the habit of making use of as often as possible.*
>
> From the film "Camelot" (1967)

I engineer the fast rotation of an effectively one-dimensional ion trap for a predetermined rotation angle and time, avoiding the final excitation of the trapped ion. Different schemes are proposed with different speed limits that depend on the control capabilities. I also make use of trap rotations to create squeezed states without manipulating the trap frequencies.

## 6.1 Introduction

In this chapter I study rotations of a single ion as depicted in Fig. 6.1. My aim is to inverse engineer the time dependence of the control parameter(s) to implement a fast process, free from final excitations. I assume for simplicity that the ion is trapped in a linear, harmonic trap, tightly confined in a radial direction so that it moves effectively along a one-dimensional axial direction, hereafter "the line". The trapping line is set horizontally and is rotated in a time $t_f$ up to an established final angle ($\theta_f = \pi/2$ in all examples) with respect to a vertical axis that crosses the center of the trap. Such an operation would be useful to drive atoms through corners and junctions in a scalable quantum processor [107, 108]. It is also a first step towards the more complicated problem of rotating an ion chain [107, 109, 110], which would facilitate scalability in linear segmented traps, and be useful to rearrange the ions, e.g., to locate a cooling ion at the right position in the chain [110]. Opposite to other operations studied in this thesis, like transport (Chapters 1 and 2) or expansion (Chapter 4), rotation of a single ion was never studied before, so I shall first design the rotation process for a single ion in this chapter, and then I will extend the analysis to ion chains in Chapter 7.

I shall first find the classical Hamiltonian. Let $s$ denote a point on the line.
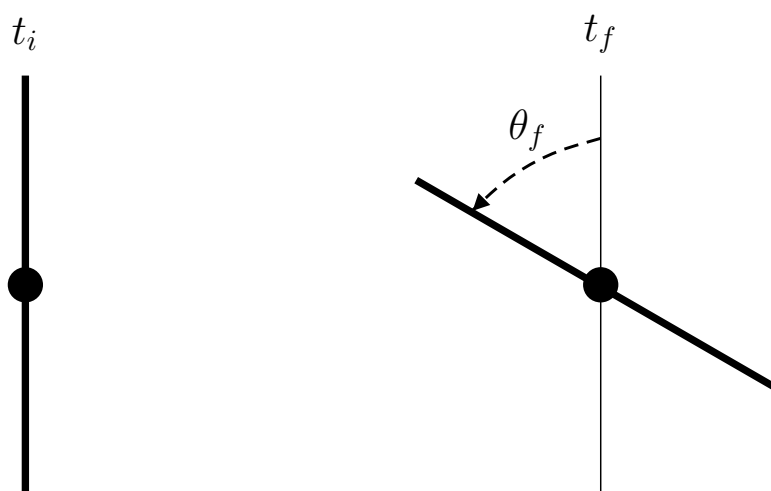


FIGURE 6.1: Schematic representation of the rotation process. The ion is confined along a line (where it is subjected to an effective one-dimensional longitudinal potential), which is rotated by an angle $\theta$ up to $\theta_f$ in a time $t_f$, so that the final state is not excited.

$s$ may take positive and negative values. A time-dependent trajectory $s(t)$ has Cartesian, laboratory frame components $x = x(s,t)$, $y = y(s,t)$,

$$
\begin{aligned}
x &= s\cos(\theta), \\
y &= s\sin(\theta),
\end{aligned} \tag{6.1}
$$

where $\theta = \theta(t)$ is the rotation angle. The kinetic energy is $K = \frac{1}{2}m(\dot{x}^2 + \dot{y}^2)$, where $m$ is the ion mass, and the potential energy is assumed by now to be harmonic, $\frac{1}{2}m\omega_0^2 s^2$ (this will be relaxed below and in Sec. 6.2), where $\omega_0$ is the angular frequency of the external confining trap in the (longitudinal) direction of the line. This gives the Lagrangian

$$
\begin{aligned}
L &= \frac{1}{2}m\dot{s}^2 - \frac{1}{2}m\omega^2 s^2, \tag{6.2} \\
\omega^2 &= \omega_0^2 - \dot{\theta}^2. \tag{6.3}
\end{aligned}
$$

Note that the angular velocity of the rotation $\dot{\theta}$ must be real but could be negative, whereas $\omega^2$ may be positive or negative, making $\omega$ purely imaginary in the later case. Unless stated otherwise, the following physically motivated boundary conditions are also assumed: the initial and final trap should be at rest, and I also impose continuity of the angular velocity,

$$
\begin{aligned}
\theta(0) &= 0, \quad \theta(t_f) = \theta_f, \tag{6.4} \\
\dot{\theta}(0) &= \dot{\theta}(t_f) = 0, \tag{6.5} \\
\omega(0) &= \omega(t_f) = \omega_0, \tag{6.6}
\end{aligned}
$$

where the last line follows from the second one using Eq. (6.3). By a Legendre transformation we finally get the Hamiltonian[1]

$$
H = \dot{s}\frac{\partial L}{\partial \dot{s}} - L = \frac{1}{2}m\dot{s}^2 + \frac{1}{2}m\omega^2 s^2. \tag{6.7}
$$

At this point, I quantize this Hamiltonian by substituting $m\dot{s}$ by the momentum

---

[1]This is easily generalized for a potential $U(s)$, not necessarily harmonic, as $H = \frac{1}{2}m\dot{s}^2 + U(s) - \frac{1}{2}m\dot{\theta}^2 s^2$

operator $p$ and by considering $s$ as the position operator, which becomes a $c$-number in coordinate representation,

$$H = \frac{1}{2m}p^2 + \frac{1}{2}m\omega^2 s^2. \tag{6.8}$$

I will from now on work with this quantum Hamiltonian (possibly with a more general potential) and corresponding quantum states. It represents formally a harmonic oscillator with time-dependent frequency, but there are significant differences with an actual harmonic oscillator when the inverse engineering of $\omega(t)$ is considered. For an actual harmonic oscillator, a fast and safe expansion or compression in a time $t_f$ should take the system from an initial value to a final value of $\omega$ without final excitation, in principle without further conditions. By contrast, in the rotation process, according to Eq. (6.6), the initial and final effective frequencies are the same, but the conditions in Eqs. (6.4) and (6.5) must be satisfied. This implies an integral constraint on $\omega$,

$$\theta(t_f) = \int_0^{t_f} \dot{\theta} dt' = \int_0^{t_f} [\omega_0^2 - \omega^2]^{1/2} dt', \tag{6.9}$$

where the square root branch should be chosen to satisfy continuity. One further difference is that in a physical expansion/compression $\omega(t)$ is controlled directly, whereas in the rotation there are several options. If $\omega_0$ is constant, only $\dot{\theta}(t)$ is controlled, so that $\omega(t)$ is an 'effective' frequency. In general, both $\omega_0$ and $\dot{\theta}$ could be controlled as time-dependent functions, see the next section. As for the final excitation, the expression for the energy of a state that begins in the $n$th eigenstate of the trap at rest can be found making use of the Lewis-Riesenfeld invariants [32, 76], see the corresponding time-dependent wave function in the Appendix H,

$$\langle H(t) \rangle_n = \frac{(2n+1)\hbar}{4\omega(0)} \left( \dot{\rho}^2 + \omega^2(t)\rho^2 + \frac{\omega(0)^2}{\rho^2} \right). \tag{6.10}$$

Here $\rho$ is a scaling factor, proportional to the width of the invariant eigenstates, that satisfies the Ermakov equation

$$\ddot{\rho} + \omega^2(t)\rho = \frac{\omega^2(0)}{\rho^3}. \tag{6.11}$$

To avoid any final excitation, it is required that

$$\rho(t_f) = 1, \quad \dot{\rho}(t_f) = 0 \tag{6.12}$$

for the initial conditions $\rho(0) = 1$, $\dot{\rho}(0) = 0$. The boundary conditions for $\rho$ and Eqs. (6.4), (6.5), (6.6) imply that $H(0) = H(t_f)$ commutes with the corresponding Lewis-Riesenfeld invariant [76], so that the $n$th initial eigenstate is dynamically mapped onto itself (but rotated) at time $t_f$. In Eqs. (6.10) and (6.11), both the excitation energy and the wave packet width are mass independent, so that inverse-engineered rotation protocols will be independent of the species. In the following sections, I shall analyze different methods to perform the rotation without final excitation.

## 6.2 Control of trap frequency and angular velocity

If both the trap angular frequency $\omega_0$ and the angular velocity $\dot{\theta}$ are controllable functions of time, a simple family of solutions to the inverse problem is found by setting a $\dot{\theta}(t)$ that satisfies Eqs. (6.4) and (6.5), and compensating the time dependence of $\dot{\theta}^2$ with a corresponding change in $\omega_0^2(t)$, so that $\omega^2(t) = \omega^2(0)$ remains constant during the whole process. From the point of view of the effective harmonic oscillator, 'nothing happens' throughout the rotation, so that the effective state remains unexcited at all times.

I may apply the Lewis-Leach theory of quadratic in momentum invariants [58, 111] to extend the above results to arbitrary potentials[2]. The family of Hamiltonians

$$H = \frac{p^2}{2m} + \frac{1}{2}m\Omega^2 s^2 + \frac{1}{\rho^2}U\left(\frac{s}{\rho}\right), \tag{6.13}$$

---

[2]The theory was first formulated for classical systems in [58] but is applicable to quantum systems as well [111]. Incidentally, this means that the rotation protocols designed in this chapter (in this and the following sections) are valid for classical particles as well. The difference appears only when considering which states are valid or not for classical and quantum particles, e.g., when using phase-space formulations of quantum states and classical ensembles.

where $U$ is an arbitrary function, and $\Omega$ depends on time, has the invariant

$$I = \frac{\pi^2}{2m} + \frac{1}{2}m\Omega_0^2 s^2 + U\left(\frac{s}{\rho}\right), \tag{6.14}$$

where $\pi = \rho p - m\dot{\rho}s$, and $\Omega_0$ is a constant, provided the Ermakov equation

$$\ddot{\rho} + \Omega^2\rho = \frac{\Omega_0^2}{\rho^3} \tag{6.15}$$

is satisfied. Consider the simple case $\Omega_0 = 0$, i.e., from Eq. (6.15),

$$\Omega^2(t) = -\frac{\ddot{\rho}}{\rho}. \tag{6.16}$$

If we set $\rho(t) = 1$ as a constant for all times, it follows that $\Omega(t) = 0$. However, as we saw in the previous section, the rotation of a line with the potential $U(s)$ produces in the line frame a centrifugal term $-\dot{\theta}^2 s^2 m/2$. To cancel the total harmonic term, we have to add to the trap potential a compensating harmonic term, $\omega_c^2 s^2 m/2$, such that $\omega_c^2 = \dot{\theta}^2$. In other words, $\Omega^2 = \omega_c^2 - \dot{\theta}^2 = 0$. The resulting Hamiltonian and invariant (in this case they are equal) are simply

$$H = I = \frac{p^2}{2m} + U(s), \tag{6.17}$$

i.e., time independent. No excitation occurs at any time in spite of the fact that a rotation is taking place.

For some applications, it may be interesting to consider in Eq. (6.13) the more general case in which $\rho$ depends on time (for example to achieve a squeezed state as will be studied later in Sec. 6.6), and $\omega^2 = \omega_c^2 - \dot{\theta}^2$, corresponding to an auxiliary harmonic term and the centrifugal term. The inverse engineering in this case proceeds by designing $\theta(t)$, so that $\dot{\theta}(0) = \dot{\theta}(t_f) = 0$, and then $\rho(t)$ obeying

the boundary conditions

$$\rho(0) = \rho(t_f) = 1, \tag{6.18}$$

$$\dot{\rho}(0) = \dot{\rho}(t_f) = 0, \tag{6.19}$$

$$\ddot{\rho}(0) = \ddot{\rho}(t_f) = 0, \tag{6.20}$$

(or more generally, $\rho(t_f) = \gamma$) that guarantee the commutation between invariant and Hamiltonian at boundary times. Once $\theta$ and $\rho$ are set, I design the auxiliary harmonic term considering, as before, $\Omega_0 = 0$ in Eq. (6.15):

$$\omega_c^2 = \Omega^2 + \dot{\theta}^2 = -\frac{\ddot{\rho}}{\rho} + \dot{\theta}^2. \tag{6.21}$$

The auxiliary harmonic term vanishes at both boundary times according to the boundary conditions imposed on $\ddot{\rho}$ and $\dot{\theta}$. In fact $\Omega^2$ vanishes as well at the boundary times so that before and after the rotation the atom is confined only in the potential $U(s)$. This type of protocols, where both the rotation speed and the potential have to be controlled (the latter in space and time) may be quite demanding experimentally. In the rest of the chapter, I shall assume the simpler scenario in which only the rotation speed $\dot{\theta}$ is controlled, and the trap potential is purely harmonic with constant angular frequency $\omega_0$.

## 6.3 Bang-bang

It is possible to perform rotations without final excitation satisfying Eqs. (6.4) and (6.5) keeping $\dot{\theta}$ constant or piecewise constant. Here, I consider the simplest one-step case,

$$\dot{\theta}(t) = \begin{cases} 0, & t \leq 0, \\ c, & 0 < t \leq t_f, \\ 0, & t \geq t_f. \end{cases} \tag{6.22}$$

Note that Eqs. (6.5) and (6.6) are only satisfied now as one-sided limits. A bang-bang approach may admittedly be difficult to implement because of the sharp

changes involved, but it sets a useful, simple reference for orders of magnitude estimates of rotation speeds, which may be compared to smoother approaches that will be presented later. Integrating $\dot{\theta}$, one finds

$$\theta_f = ct_f. \tag{6.23}$$

For a constant $\dot{\theta} = c$, $\omega$ remains constant from $t = 0$ to $t = t_f$, and equal to $\omega_1 = (\omega_0^2 - c^2)^{1/2}$, whereas $\omega = \omega_0$ in the initial and final time regions. For this configuration, and $0 < t < t_f$,

$$\rho(t) = \sqrt{\frac{\omega_0^2 - \omega_1^2}{\omega_1^2} \sin^2(\omega_1 t) + 1}, \tag{6.24}$$

$$\dot{\rho}(t) = \frac{\sin(\omega_1 t) \cos(\omega_1 t)(\omega_0^2 - \omega_1^2)}{\omega_1 \rho(t)}, \tag{6.25}$$

to satisfy the boundary conditions $\rho(0) = 1$, $\dot{\rho}(0) = 0$. The shortest final time to satisfy the conditions (6.12) at $t_f$ is $\pi/\omega_1$. From Eq. (6.23), this gives the value of $c$ needed,

$$c = \frac{\theta_f \omega_0}{[\pi^2 + \theta_f^2]^{1/2}}, \tag{6.26}$$

whereas

$$t_f = \frac{\pi}{\omega_1} = \frac{\pi}{\sqrt{\omega_0^2 - c^2}} = \frac{\pi}{\omega_0} f, \tag{6.27}$$

$$f := \sqrt{1 + \frac{\theta_f^2}{\pi^2}}. \tag{6.28}$$

As $c < \omega_0$, the effect of this bang-bang protocol is to expand the effective trap during the rotation time interval. $\rho$ increases first, and then decreases during half an oscillation period of the effective trap. This does not, in general, coincide with half an oscillation period of the actual nonrotating trap $\pi/\omega_0$, because of the $f$ factor, but it is not too different for relevant values of $\theta_f$. In particular, for $\theta_f = \pi/2$, $f = 1.118$. The maximum of $\rho(t)$ at $t_f/2$ is precisely $f$. For example, for a frequency $\omega_0/(2\pi) = 2$ MHz, this implies a final time $t_f = 0.28$ $\mu$s.

# 6.4 Optimal Control by Pontryagin's maximum Principle

While the previous bang-bang method with just one time segment provides a simple guidance, I am also interested in knowing the absolute time minimum that could in principle be achieved (even if the "optimal" protocol ends up being hardly realizable). Unlike ordinary expansions/compressions, the shortest time protocol for bounded control is not of a bang-bang form. To find it, I first rescale the time with $\omega_0$ by setting $\sigma = \omega_0 t$ for $t \in [0, t_f]$. Now, I set the variables

$$
\begin{aligned}
x_1(\sigma) &= \rho(t) = \rho\left(\frac{\sigma}{\omega_0}\right), \\
x_2(\sigma) &= \frac{1}{\omega_0}\dot\rho\left(\frac{\sigma}{\omega_0}\right), \\
x_3(\sigma) &= \int_0^\sigma u(\tau)d\tau,
\end{aligned} \tag{6.29}
$$

where $u(\sigma) = u(\omega_0 t) = \frac{1}{\omega_0}\dot\theta(t)$, with $\sigma \in [0, \omega_0 t_f]$. Then, one can write a control system describing the Ermakov equation (6.15) and the constraints in (6.4), (6.5) and (6.6), and formulate the time-optimal control (OC) problem for rotation of a quantum particle on a line as

$$
\begin{aligned}
\min_u J &= \int_0^T 1 d\tau, \\
\text{such that} \quad x_1' &= x_2, \\
x_2' &= \frac{1}{x_1^3} + (u^2 - 1)x_1, \\
x_3' &= u,
\end{aligned} \tag{6.30}
$$

where $T = \omega_0 t_f$, and the prime is a derivative with respect to $\sigma$, with the boundary conditions

$$
\begin{aligned}
x_1(0) &= 1, & x_1(T) &= 1, \\
x_2(0) &= 0, & x_2(T) &= 0, \\
x_3(0) &= 0, & x_3(T) &= \theta_f.
\end{aligned} \tag{6.31}
$$

Note that I assume that the boundary conditions for $u$ at $t = 0$ and $t = t_f$ can be fulfilled by the use of a sudden switch.

## 6.4.1   Unbounded Control

I apply the Pontrygin's maximum principle [112] to solve the time-OC problem (6.30), where the Hamiltonian is given by

$$H(t, x, u, \lambda) = \lambda_0 + \lambda_1 x_2 + \lambda_2 \left[ \frac{1}{x_1^3} + (u^2 - 1)x_1 \right] + \lambda_3 u, \qquad (6.32)$$

in which $\lambda = (\lambda_0, \lambda_1, \lambda_2, \lambda_3)$ and $\lambda_0$ is either 0 or 1. The necessary condition $\frac{\partial H}{\partial u} = 0$ gives

$$u^* = -\frac{\lambda_3}{2\lambda_2 x_1}, \qquad (6.33)$$

which minimizes the Hamiltonian and where the co-states $\lambda_1, \lambda_2, \lambda_3 : [0, T] \to \mathbb{R}$ satisfy $\lambda_i' = -\frac{\partial H}{\partial x_i}$, $i = 1, 2, 3$, i.e.,

$$\begin{aligned}
\lambda_1' &= \left[ \frac{3}{x_1^4} - (u^2 - 1) \right] \lambda_2, \\
\lambda_2' &= -\lambda_1, \\
\lambda_3' &= 0.
\end{aligned} \qquad (6.34)$$

Solutions are found by solving the equation system composed by Eqs. (6.30), (6.33) and (6.34) with the boundary conditions at $\sigma = 0$ in Eq. (6.31). We have the freedom of choosing different initial values for the $\lambda_i(0)$ to satisfy the boundary conditions at $T$ in Eq. (6.31). I applied a shooting method and numerically minimize $[x_1(T) - 1]^2 + x_2(T)^2 + [x_3(T) - \theta_f]^2$ for these parameters using MATLAB's 'fminsearch' function with $\theta_f = \pi/2 = 1.5708$. The best results obtained are for $T = 2.2825$, which, for the external trap frequency $\omega_0/(2\pi) = 2$ MHz used in other examples, implies a final time $t_f = 0.18$ $\mu$s. The solution found is not exact, $(x_1(T), x_2(T), x_3(T)) = (1.0765, 0.0842, 1.5650)$, which might be an indication that the system is not controllable. Figure 6.2 (a) shows the time evolution of $u$ for this case following Eq. (6.33), but forcing it to be 0 in the boundary times.
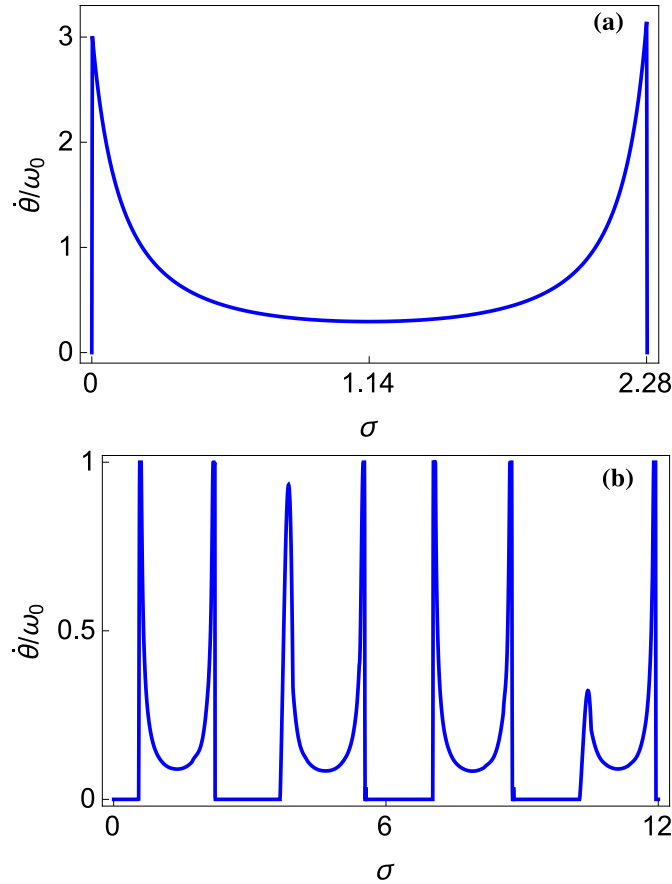
FIGURE 6.2: Time evolution $\dot{\theta}(t)$ for the optimal unbounded (a) and bounded (b) control. The rotation angle is $\theta_f = \frac{\pi}{2}$.

## 6.4.2 Bounded Control

Now, consider a bounded control with $u(\sigma) \in [0,1]$ for all $\sigma \in [0,T]$. Because the Hamiltonian (6.32) is quadratic in $u$, the OC that minimizes $H$ is of the form

$$u_b^* = \min\left\{ \max\left\{ -\frac{\lambda_3}{2\lambda_2 x_1}, 0 \right\}, 1 \right\}. \tag{6.35}$$

The bounded time-OC, and the resulting optimal trajectory, are illustrated in Fig. 6.2 (b). The minimum (dimensionless) time that completes the desired rotation is $T = 11.9984$, and the calculated final state following the OC is $(x_1(T), x_2(T), x_3(T)) = (1.0083, 0.0382, 1.5708)$. For $\omega_0/(2\pi) = 2$ MHz, the minimal time is 0.95 $\mu$s. Since $u(\sigma) \in [0,1], \forall \sigma \in [0,T]$, from Eq. (6.30), we see that $\dot{\theta} > 0$, and hence, the rotation is always forward. In this case, $x_3$ reaches the desired $\theta_f = \pi/2$ at $\sigma = 11.9028$, and the control is turned off. Then, the states $x_1$ and $x_2$ are oscillating to reach
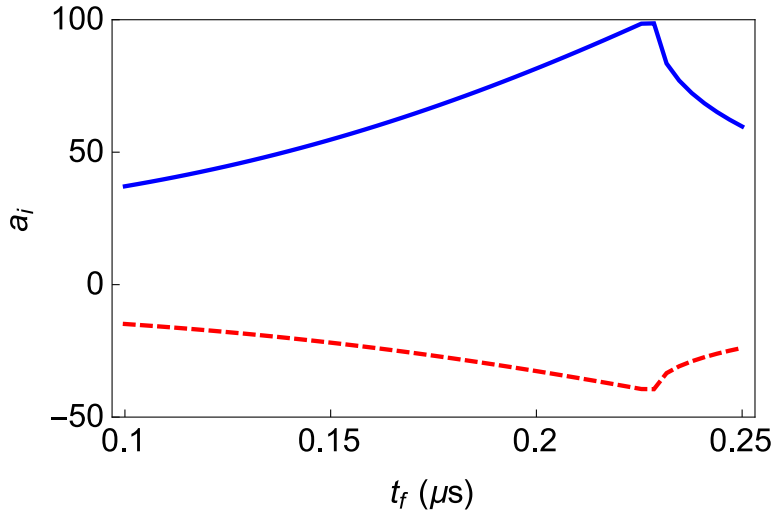
FIGURE 6.3: Values of the optimizing parameters $a_4$ (thick blue line) and $a_5$ (dashed red line) for different rotation times $t_f$. The trap frequency is $\omega_0/(2\pi) = 2$ MHz, and the final angle $\theta_f = \frac{\pi}{2}$.

the desired terminal state $(1,0)$. Figure 6.2 (b) shows the time evolution of $u$ for this solution.

## 6.5    Smooth inverse engineering

An alternative inversion route, that provides smooth solutions, is depicted in the following scheme:

$$\theta \xrightarrow{\hspace{1cm}} \dot{\theta} \longrightarrow \omega \longrightarrow E[\rho(t_f), \dot{\rho}(t_f)] \ .$$
$$\underset{minimize\ E}{\xleftarrow{\hspace{3cm}}}$$

First, $\theta(t)$ is designed to satisfy Eq. (6.4) and Eq. (6.5) with some free parameters. The corresponding $\dot{\theta}$ and final energy are calculated, and the parameters are changed until the minimum energy (and excitation) is found.

A convenient choice for $\theta$ is a fifth order polynomial ansatz $\theta = \sum_{n=0}^{5} a_n t^n / t_f^n$. In order to satisfy the boundary conditions in Eqs. (6.4) and (6.5), we need to fix parameters $a_{0-3} = (0, 0, a_4 + 2a_5 + 3\theta_f, -2a_4 - 3a_5 - 2\theta_f)$. The other two parameters, $a_4, a_5$, are left free in order to satisfy the remaining two boundary conditions in Eq. (6.12), and suppress the final excitation energy. In practice, I
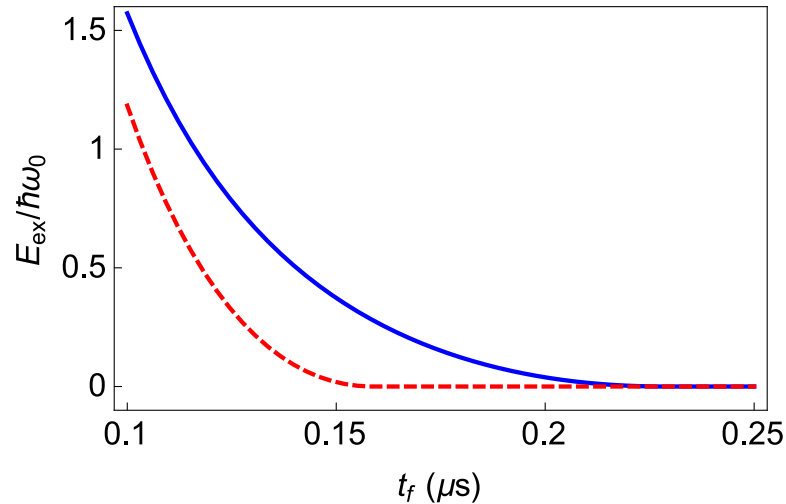
FIGURE 6.4: Final excitation energy vs final time for the optimized protocol without (solid blue line) and with final squeezing ($\gamma^2 = 3$, dashed red line). The trap frequency is $\omega_0/(2\pi) = 2$ MHz, and the final rotation angle $\theta_f = \frac{\pi}{2}$. The initial state is the ground state of the trap.

solve numerically Eq. (6.11) to find the final energy (6.10) for each pair $a_4, a_5$, and use MATLAB's 'fminsearch' function to find the values of the free parameters that minimize the final excitation energy.

In Fig. 6.3, the values of the free parameters that result from this process are given, and in Fig. 6.4 I depict the corresponding excess energy with respect to the ideal target state (as in previous examples, $\omega_0/(2\pi) = 2$ MHz). Vanishing residual excitations are found for times shorter than half an oscillation period up to a time $t_f \sim 0.23$ $\mu$s, not much larger than the unbounded-OC minimum of 0.18 $\mu$s. Figure 6.5 depicts the difference between the ideal value of $\rho(t_f)$ and the actual value, and makes evident the sharp change that marks the shortest time

| | bang-bang | OC(unbounded) | OC(bounded) | inverse engineering |
|---|---|---|---|---|
| $t_f$ ($\mu$s) | 0.28 | 0.18 | 0.95 | 0.23 |

TABLE 6.1: Minimal rotation times for the different methods. Trap frequency $\omega_0/(2\pi) = 2$ MHz. In bounded OC, $0 \leq \dot{\theta} \leq \omega_0$.
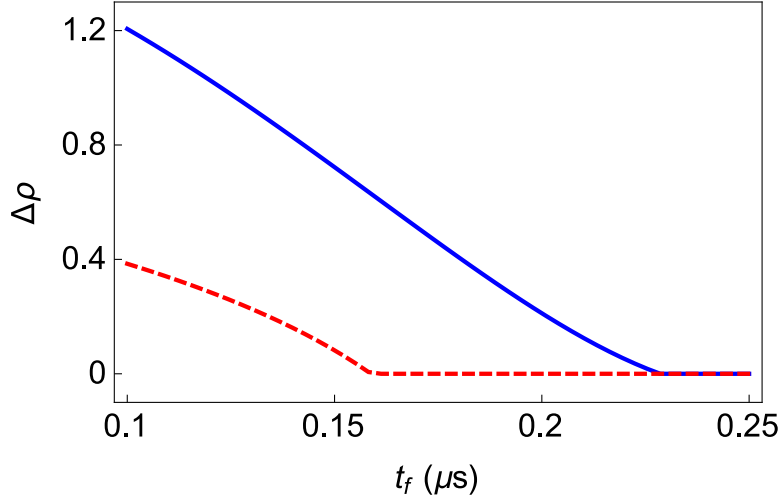
FIGURE 6.5: Difference between the ideal and actual value of $\rho$ at the end of the rotation vs final time for the optimized inverse-engineered protocol for rotations without (solid blue line) and with final squeezing ($\gamma^2 = 3$, dashed red line). The trap frequency is $\omega_0/(2\pi) = 2$ MHz, and the final rotation angle $\theta_f = \frac{\pi}{2}$.

for which a solution exists. Since I have limited the possible solutions by imposing a functional form of the function $\theta(t)$, this time is larger than the one found via OC. Note also that the shortest final time is slightly better than the one provided by the simple bang-bang protocol. Table 6.1 summarizes the results.

## 6.6 Wave packet squeezing

Consider now a trap rotation with constant trap frequency $\omega_0$ satisfying the conditions (6.4)-(6.6), and $\rho$ satisfying

$$
\begin{aligned}
\rho(0) &= 1, \quad \dot{\rho}(0) = 0, \\
\rho(t_f) &= \gamma, \quad \dot{\rho}(t_f) = 0.
\end{aligned} \tag{6.36}
$$

Unlike the previous sections, $\rho$ ends in a value $\gamma$ different from 1.

According to Eq. (H.3), each initial state $\phi_n(0)$ will evolve into $e^{-i(n+1/2)\omega_0 g}\phi_{n,sq}$ at $t_f$, where $g = g(t_f) = \int_0^{t_f} dt'/\rho^2(t')$, and $\phi_{n,sq}$ is the normalized eigenstate for
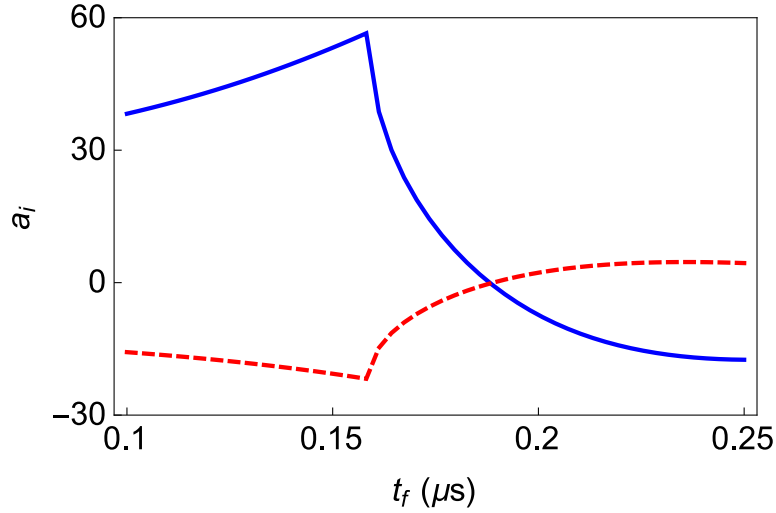
FIGURE 6.6: Values of the optimizing parameters $a_4$ (thick blue line) and $a_5$ (dashed red line) for different rotation times to generate a squeezed vaccum state with $\gamma^2 = 3$. The trap frequency is $\omega_0/(2\pi) = 2$ MHz, and the rotation angle $\theta_f = \frac{\pi}{2}$.

the trap with angular frequency $\omega_{sq} = \omega_0/\gamma^2$. (This is a virtual trap, let me recall that the actual trap has angular frequency $\omega_0$.)

A coherent state at time $t = 0$,

$$|\alpha\rangle = e^{-|\alpha|^2/2} \sum_{n=0}^{\infty} \frac{\alpha^n}{\sqrt{n!}} |\phi_n(0)\rangle, \qquad (6.37)$$

will thus evolve into

$$|\psi(t_f)\rangle = e^{-i\omega_0 g/2} e^{-|\tilde{\alpha}|^2/2} \sum_{n=0}^{\infty} \frac{\tilde{\alpha}^n}{\sqrt{n!}} |\phi_{n,sq}\rangle, \qquad (6.38)$$

where $\tilde{\alpha} = \alpha e^{-i\omega_0 g}$. This is a coherent state for the virtual frequency $\omega_{sq}$, and therefore, a minimum-uncertainty product state. However, since the actual trap has frequency $\omega_0$, it is also a squeezed coherent state with respect to the actual trap, $|[r, \tilde{\alpha}]\rangle$, see [113], where $r = -\ln\gamma$, up to a global phase factor. The final and initial coordinate and momentum widths are related by $\Delta_{s,t_f} = \gamma\Delta_{s,0}$, $\Delta_{p,t_f} = \Delta_{p,0}/\gamma$. We may rewrite the state at time $t_f$ in terms of the squeezing and displacement operators as

$$|\psi(t_f)\rangle = e^{-i\omega_0 g/2} S(r)|\tilde{\alpha}\rangle = e^{-i\omega_0 g/2} S(r) D(\tilde{\alpha})|0\rangle = e^{-i\omega_0 g/2}|[r, \tilde{\alpha}]\rangle, \qquad (6.39)$$

where $S(r) = e^{\frac{r}{2}(a^2 - a^{\dagger 2})}$, $a$ and $a^{\dagger}$ are annihilation and creation operators for the $\omega_0$-harmonic trap, and $D(z) = e^{za^{\dagger} - z^* a}$ is the displacement operator. Note that the phase at $t_f$, $\arg(\tilde{\alpha})$, is controllable by means of the $g$-function that depends on the process history, whereas the squeezing parameter $1/\gamma$ is controlled by the imposed boundary condition. If necessary, a controlled tilt of the squeezed state in phase space is easy to achieve by letting it evolve, after its formation at $t_f$, in the fixed, nonrotating trap.

As a simple example, let me consider the generation of squeezed vacuum states starting from the ground state of the initial trap, so that $\alpha = 0$. To design the squeezing process, one may follow a similar procedure as in the previous section, but minimizing the cost function

$$
\begin{aligned}
F &= \dot{\rho}(t_f)^2 + \omega^2(t_f)\tilde{\rho}(t_f)^2 + \frac{\omega(0)^2}{\tilde{\rho}(t_f)^2}, \\
\tilde{\rho} &= \rho - \gamma + 1,
\end{aligned}
\tag{6.40}
$$

which is minimal for $\tilde{\rho}(t_f) = 1$ and $\dot{\tilde{\rho}}(t_f) = 0$, so that $\rho(t_f) = \gamma$ and $\dot{\rho}(t_f) = 0$.

Since, due to the centrifugal force during the rotation, the wave packet tends to spread first, the squeezed states with $\gamma > 1$ may be achieved in shorter times than the ones needed without squeezing in the previous section. Figure 6.6 depicts the free parameters that optimize a rotation with a final squeezed state for the same parameters in the previous subsection, but $\gamma^2 = 3$, and Fig. 6.4 the excess energy with respect to the target state. The excitation in a process with a final moderate squeezing is smaller than for the simple rotation without squeezing. Figure 6.5 depicts the difference between the target value of the function $\rho$ (proportional to the width of the wave packet) and its actual value at final time for rotations without and with squeezing. Again, the minimizations change suddenly to a different solution that cannot satisfy the conditions at a critical time, see also Figs. 6.3 and 6.6.

## 6.7   Discussion

I have worked out different schemes to perform fast rotations of a one-dimensional trap without any final excitation of the confined particle, which I have considered to be an ion (for being the common platform in this thesis) throughout, but could be a neutral particle as well by setting the proper trapping interaction. Apart from excitation-free rotations, it is also possible to generate squeezed states in a controllable way. For an arbitrary trap, the fast processes could in principle be performed in an arbitrarily short time if an auxiliary harmonic potential with time-dependent frequency could be implemented. In a simpler setting, where only the rotation speed may be controlled, the rotation time cannot be arbitrarily short, as demonstrated by inverse engineering or bang-bang approaches, and confirmed by optimal-control theory. Bang-bang and OC protocols provide useful information and time bounds, but are difficult to implement experimentally due to the sudden kicks required in the angular velocity of the trap. Smooth protocols designed by invariant-based inverse engineering have also been worked out. They achieve negligible excitations for times close to the minimum times given by OC theory.

The analysis may be generalized for a two-dimensional trap, but it becomes considerably more involved [114]. The 1D approximation used here will be valid for total energies well below the transversal confinement energy $E_\perp = \hbar\omega_\perp$. For the shortest final times considered in my simulations, excitation energies are never larger than $2\hbar\omega_0$, so that $\omega_\perp \gg \omega_0$ would be enough for their validity.

Rotations are elementary manipulations, which, together with transport, splitting and expansions, may help build a scalable quantum information architecture. In particular, they provide a mechanism for connecting sites by changing transport directions in 2D networks. Rotations have been demonstrated experimentally for trapped ions [110], and improving the capability to control the parameters involved is feasible with state-of-the-art trapped-ion technology. To extend the present analysis to ion chains [110], an approach similar to that in [63, 97, 106] will be applied in Chapter 7, working out the dynamical modes of the system and taking into account the dipole-dipole interaction due to the rotation of the charged

particles. The present results set a first step towards accurately controlling rotating ion chains, which would allow for fast reordering. The results obtained in this chapter were published in [115].

# Chapter 7

# Shortcuts to adiabatic rotation of two ions on a line

> *"Our goal is to make the best devices in the world, not to be the biggest."*
>
> Steve Jobs

I engineer the fast rotation of two trapped ions confined in an effectively one-dimensional, harmonic trap, for a predetermined rotation angle and time, avoiding final excitation. Different approaches are used when the ions are of the same species or of different species, but in both cases it is possible to get a clear improvement with respect to the adiabatic protocol.

## 7.1   Introduction

In this chapter, I extend the analysis done in [115] and in Chapter 6, and study rotations of two ions as depicted in Fig. 7.1. My aim is to inverse engineer the time-dependence of the control parameter(s) to implement a fast process, free from final excitations. I assume that the ions are trapped in a linear, harmonic trap, tightly confined in a radial direction so that they move effectively along a one-dimensional axial direction, hereafter "the line". I also assume the ions to never change the ordering within the trap frame, due to the strong Coulomb repulsion. The trapping line is set horizontally and is rotated in a time $t_f$ up to an established final angle ($\theta_f = \pi$ in all examples) with respect to a vertical axis that crosses the center of the trap. Such an operation was adiabatically performed by Splatt et al [110], where the objective was simply showing the reordering of small ion chains was possible, or with an optimized faster approach in [116]. This is important, for example, when topologically encoding a qubit [117], where the ion chain reordering is essential. A better experimental control of these rotations will involve improvements in the filtering, voltage and noise control. In this chapter, I explore the fundamental limitations for such an operation, more specifically the time scale that could be reached under the ideal conditions of an effective external potential that rotates rigidly, with strong radial confinement, so that the two ions move effectively along a rotating one-dimensional line. I am thus ignoring features that depend strongly on the electrode configuration, such as the possible effects of micromotion.

Following the same procedure as in Chapter 6, I shall first find the classical Hamiltonian from the corresponding classical Lagrangian and then quantize the result. Let $s_i$ denote the points on the line where each ion lays. $s_i$ may take positive and negative values. A time dependent trajectory $s_i(t)$ has cartesian (lab frame) components $x_i = x_i(s,t)$, $y_i = y_i(s,t)$,

$$x_i = s_i \cos(\theta), \quad y_i = s_i \sin(\theta), \tag{7.1}$$
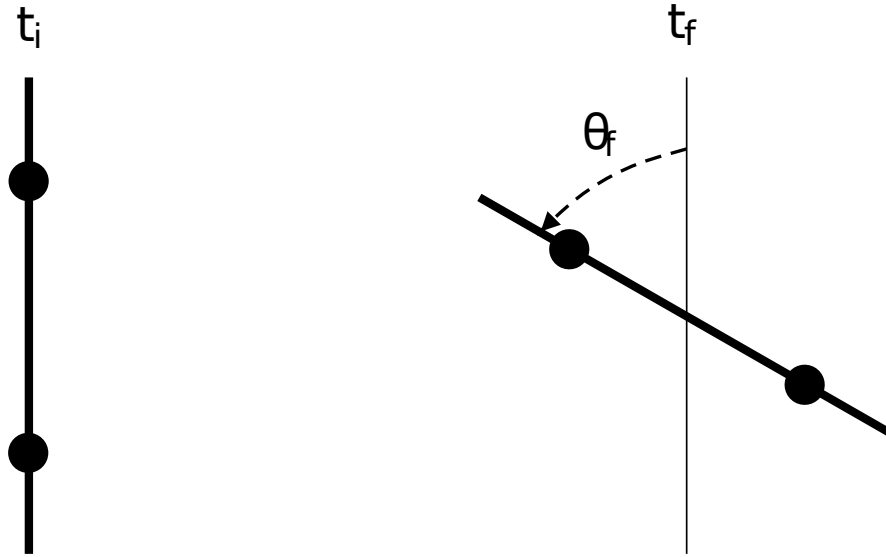
FIGURE 7.1: Schematic representation of the rotation process studied here. The atom is confined along a line (where it is subjected to a one-dimensional potential), which is rotated by an angle $\theta$ up to a time $t_f$ so that the final state is not excited.

where $\theta = \theta(t)$ is the rotation angle. For two equal ions, the kinetic energy is $K = \frac{1}{2}m(\dot{x}_1^2 + \dot{y}_1^2) + \frac{1}{2}m(\dot{x}_2^2 + \dot{y}_2^2)$, and the potential energy is assumed by now to be harmonic plus a Coulomb interaction between both ions, $V = \frac{1}{2}u_0(s_1^2 + s_2^2) + \frac{C_c}{s_2 - s_1}$, where $u_0 = m\omega_0^2$ and $C_c = \frac{e^2}{4\pi\epsilon_0}$, $\epsilon_0$ being the vacuum permittivity, $e$ the electric charge of a single electron and $\omega_0$ the external harmonic frequency for both ions in the (longitudinal) direction of the line and $m$ the mass of each ion. This gives the Lagrangian

$$L = \frac{1}{2}m\dot{s}_1^2 + \frac{1}{2}m\dot{s}_2^2 - \frac{1}{2}m\omega^2(s_1^2 + s_2^2) - \frac{C_c}{s_2 - s_1}, \tag{7.2}$$

$$\omega^2 = \omega_0^2 - \dot{\theta}^2. \tag{7.3}$$

Note that the angular velocity of the rotation $\dot{\theta}$ must be real but could be negative, whereas $\omega^2$ may be positive or negative, making $\omega$ purely imaginary in the later case. The following physically motivated boundary conditions are also assumed: the initial and final trap should be at rest, and I also impose continuity of the

angular velocity,

$$\theta(0) \;=\; 0, \quad \theta(t_f) = \theta_f, \tag{7.4}$$

$$\dot{\theta}(0) \;=\; \dot{\theta}(t_f) = 0, \tag{7.5}$$

$$\omega(0) \;=\; \omega(t_f) = \omega_0, \tag{7.6}$$

where the last line follows from the second one using Eq. (7.3). By a Legendre transformation we finally get the Hamiltonian

$$H = \sum_i \dot{s}_i \frac{\partial L}{\partial \dot{s}_i} - L = \frac{1}{2}m(\dot{s}_1^2 + \dot{s}_2^2) + \frac{1}{2}m\omega^2(s_1^2 + s_2^2) + \frac{C_c}{s_2 - s_1}. \tag{7.7}$$

At this point, I quantize this Hamiltonian by substituting $m\dot{s}_i$ by the momentum operator $p_i$ and by considering $s_i$ as the position operator, which becomes a $c$-number in coordinate representation,

$$H = \frac{1}{2m}(p_1^2 + p_2^2) + \frac{1}{2}m\omega^2(s_1^2 + s_2^2) + \frac{C_c}{s_2 - s_1}. \tag{7.8}$$

I will from now on work with this quantum Hamiltonian and corresponding quantum states. It represents formally two coupled harmonic oscillators with (the same) time-dependent frequency. For this kind of system, we cannot apply the usual tools of inverse engineering through dynamical invariants, so I will define the normal modes to get an approximate Hamiltonian as it was done in previous chapters.

## 7.2 Normal modes

In order to get the normal modes [59], we first need to calculate the equilibrium position of both ions $\{s_i^{(0)}\}$ by solving the equation system $\{\partial V/\partial s_i = 0\}$, where $V$ is the potential part in the Hamiltonian (7.8). These are given by

$$s_1^{(0)} = -s_2^{(0)} = -\frac{x_0}{2}, \tag{7.9}$$
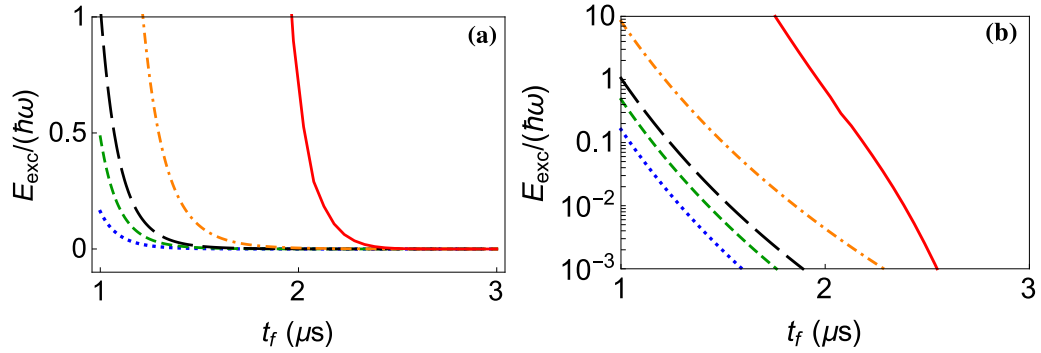
FIGURE 7.2: Exact energy excess evolving the full Hamiltonian (7.8) according to Eq. (7.26) for the parameters $c_{3-6}$ that minimize the excitation in the normal modes. (a) represents this excitation in a linear scale, whereas (b) shows the same excitation in a logarithmic scale. The dotted blue line is for the protocol using all 4 free parameters to minimize the energy. The short-dashed green line fixes $c_6 = 0$ and minimizes the energy using 3 parameters. The long-dashed black line fixes $c_5 = c_6 = 0$ and minimizes the energy using 2 parameters. The dash-dotted orange line fixes $c_4 = c_5 = c_6 = 0$ and minimizes the energy using 1 parameter. The solid red line fixes is the excitation given by a non-optimized protocol after fixing $c_{3-6} = 0$ in Eq. (7.26). The evolution was done for two $^{40}$ Ca$^+$ ions, with an external trap frequency $\omega_0/(2\pi) = 1.41$ MHz and a total rotation angle $\theta_f = \pi$.

where

$$x_0 = \left( \frac{2C_c}{m\omega^2} \right)^{1/3}. \tag{7.10}$$

Diagonalize the matrix $V_{ij} = \frac{1}{m} \frac{\partial^2 V}{\partial s_i \partial s_j}\big|_{\{s_i,s_j\}=\{s_i^{(0)},s_j^{(0)}\}}$, the eigenvalues are

$$\lambda_\pm = (2 \pm 1)\omega^2. \tag{7.11}$$

The effective frequencies of the approximated harmonic oscillators in the normal modes are given by

$$\Omega_\pm = \sqrt{\lambda_\pm}. \tag{7.12}$$

The eigenvectors $v_\pm = \begin{pmatrix} a_\pm \\ b_\pm \end{pmatrix}$ are

$$
\begin{aligned}
a_+ &= \frac{1}{\sqrt{2}}, & b_+ &= -\frac{1}{\sqrt{2}}; \\
a_- &= \frac{1}{\sqrt{2}}, & b_- &= \frac{1}{\sqrt{2}}.
\end{aligned} \tag{7.13}
$$

The (mass-weighted) normal mode coordinates are subsequently defined as,

$$
\begin{aligned}
s_+ &= a_+\sqrt{m}(s_1 + \frac{x_0}{2}) + b_+\sqrt{m}(s_2 - \frac{x_0}{2}), \\
s_- &= a_-\sqrt{m}(s_1 + \frac{x_0}{2}) + b_-\sqrt{m}(s_2 - \frac{x_0}{2}).
\end{aligned}
\tag{7.14}
$$

To transform the Hamiltonian to the new set of coordinates, we apply the unitary operator

$$
U = \int ds_+ ds_- ds_1 ds_2 |s_+, s_-\rangle\langle s_+, s_-|s_1, s_2\rangle\langle s_1, s_2|,
\tag{7.15}
$$

where $\langle s_+, s_-|s_1, s_2\rangle = \delta[s_1 - s_1(s_+, s_-)]\delta[s_2 - s_2(s_+, s_-)]$. Since what we have is effectively a two-ion expansion as in [97], the transformation is obtained as it was there,

$$
\begin{aligned}
H' &= UHU^\dagger - i\hbar U(\partial_t U^\dagger) \\
&= \sum_\nu \left( \frac{p_\nu^2}{2} - p_{0\nu}p_\nu + \frac{1}{2}\Omega_\nu^2 s_\nu^2 \right),
\end{aligned}
\tag{7.16}
$$

where I only considered terms up to the harmonic in the approximation, $\nu = \pm$, $p_\pm$ are the conjugate momenta of the normal mode coordinates and

$$
\begin{aligned}
p_{0+} &= \frac{2\sqrt{2m}}{3} \sqrt[3]{\frac{C_c}{4m\omega^5}}\dot{\omega}, \\
p_{0-} &= 0.
\end{aligned}
\tag{7.17}
$$

This latter terms appear after the unitary transformation of the Hamiltonian due to the time dependence of the equilibrium positions of the ions, $x_0$, as seen in Eq. (7.10). A further unitary transformation allows us to transform the term linear in $p_\pm$ into a term linear in $s_\pm$,

$$
\begin{aligned}
\mathcal{U} &= e^{-i(p_{0+}s_+ + p_{0-}s_-)/\hbar}, \\
H'' &= \sum_\nu \left[ \frac{p_\nu^2}{2} + \frac{1}{2}\left( s_\nu + \frac{\dot{p}_{0\nu}}{\Omega_\nu^2} \right)^2 \right].
\end{aligned}
\tag{7.18}
$$

This Hamiltonian is effectively the sum of two independent harmonic oscillators, that expand or compress through the time dependence of $\Omega_\pm$ and that have a

virtual transport through $\dot{p}_{0\pm}$. This Hamiltonian is very similar to the one in [97] for simple trap expansions, except for $\omega$ (the effective lab frequency) being now given by Eq. (7.3), while in [97] $\omega$ was the time-dependent frequency of the external trap, which was directly controlled in the lab. Here, its time dependence comes through $\theta(t)$, which is our control parameter. Thus, it is not enough to design an $\omega$ that leaves the normal modes unexcited as done in [97]. We additionally need to inverse engineer this parameter to get an expression of $\theta$ that still satisfies the conditions in Eqs. (7.4) and (7.5). This inverse engineering was already problematic in Chapter 6 for a single ion rotation, because it implies a square root, $\dot{\theta} = \sqrt{\omega_0^2 - \omega^2}$, which can be imaginary if the effective frequency $\omega$ (which, in principle, has no physical limitation for not being a "real" frequency) happens to be larger than the external trap frequency $\omega_0$.

The Hamiltonian (7.18) has a dynamical invariant [76]

$$
\begin{aligned}
I &= \sum_{\nu} \frac{1}{2} [\rho_\nu (p_\nu - \dot{\alpha}_\nu) - \dot{\rho}_\nu (s_\nu - \alpha_n u)]^2 \\
&+ \frac{1}{2} \Omega_{0\nu}^2 \left( \frac{s_\nu - \alpha_n u}{\rho_\nu} \right)^2 ,
\end{aligned}
\tag{7.19}
$$

where $\nu$ stands for $\pm$ as in previous equations, $\Omega_{0\pm} = \Omega_\pm(0)$, and $\rho_\pm$ (scaling factors of the expansion modes) and $\alpha_\pm$ (classical trajectories of the normal modes) are auxiliary functions that have to satisfy respectively the Ermakov and Newton equations,

$$
\ddot{\rho}_\pm + \Omega_\pm^2 \rho_\pm = \frac{\Omega_{0\pm}^2}{\rho_\pm^3}
\tag{7.20}
$$

$$
\ddot{\alpha}_\pm + \Omega_\pm^2 \alpha_\pm = \dot{p}_{0\pm}.
\tag{7.21}
$$

The Schrödinger equation is solvable, and the wave functions are known and analytic for such a Hamiltonian [33]

$$
|\psi''_{n\pm}\rangle = e^{\frac{i}{\hbar}[\frac{\dot{\rho}_\pm s_\pm^2}{2\rho_\pm} + (\dot{\alpha}_\pm \rho_\pm - \alpha_\pm \dot{\rho}_\pm)\frac{s_\pm}{\rho_\pm}]} \frac{1}{\rho_\pm^{1/2}} \Phi_n(\sigma_\pm) ,
\tag{7.22}
$$

where $\sigma_\pm = \frac{s_\pm - \alpha_\pm}{\rho_\pm}$ and $\Phi_n$ are the eigenfunctions for the static harmonic oscillators. The average energy for the $n$th mode are also known [97, 106],

$$
\begin{aligned}
E''_{n\pm} &= \langle \psi''_{n\pm} | H'' | \psi''_{n\pm} \rangle \\
&= \frac{(2n+1)\hbar}{4\Omega_{0\pm}} \left( \dot{\rho}_\pm^2 + \Omega_\pm^2 \rho_\pm^2 + \frac{\Omega_{0\pm}^2}{\rho_\pm^2} \right) \\
&= \frac{1}{2} \dot{\alpha}_\pm^2 + \frac{1}{2} \Omega_\pm^2 \left( \alpha_\pm - \frac{\dot{p}_{0\pm}}{\Omega_{0\pm}^2} \right)^2 .
\end{aligned}
\tag{7.23}
$$

## 7.3 Inverse engineering

The usual way of solving the dynamics via invariant-based inverse engineering is by first imposing commutativity between Hamiltonian and invariant both at initial $t = 0$ and final times $t = t_f$. This guarantees that our Hamiltonian will drive the system in such a way that at final time we will recover the same eigenstate we had at the beginning, although we might have diabatic excitations at intermediate times, where the commutation between Hamiltonian and invariant is not guaranteed. Commutativity at boundary times amounts to imposing the boundary conditions

$$
\begin{aligned}
\dot{\rho}_\pm(t_b) &= \ddot{\rho}_\pm(t_b) = 0, \\
\dot{\alpha}_\pm(t_b) &= \ddot{\alpha}_\pm(t_b) = 0,
\end{aligned}
\tag{7.24}
$$

being $t_b = 0, t_f$. Additionally, we impose

$$
\begin{aligned}
\rho_\pm(t_b) &= 0, \\
\alpha_\pm(t_b) &= 0,
\end{aligned}
\tag{7.25}
$$

so that the external trap has the same frequency at the boundary times, $\omega_0(0) = \omega_0(t_f)$. The control parameters are the rotation angle $\theta$ and in principle the external trap frequency $\omega_0$, although I will leave $\omega_0$ constant for a rigid rotation. To make sure that the square root that defines the rotation frequency remains positive, similarly to [115], I proceed by setting an ansatz for $\theta$ that satisfies the boundary

conditions (7.4) and (7.5), and additionally leaves some free parameters. Then, I solve the differential Eqs. (7.20) and (7.21), and fix the free parameters so that they satisfy the boundary conditions that leave the normal modes excitationless [Eqs. (7.24) and (7.25)]. I use several ansatzes with up to 4 free parameters,

$$
\begin{aligned}
\theta(t) &= \frac{1}{16}(32c_3 + 80c_4 + 144c_5 + 224c_6 - 9\theta_f)\cos\left(\frac{\pi t}{t_f}\right) \\
&- \frac{1}{16}(48c_3 + 96c_4 + 160c_5 + 240c_6 - \theta_f)\cos\left(\frac{3\pi t}{t_f}\right) \\
&+ c_3\cos\left(\frac{5\pi t}{t_f}\right) + c_4\cos\left(\frac{7\pi t}{t_f}\right) \\
&+ c_5\cos\left(\frac{9\pi t}{t_f}\right) + c_6\cos\left(\frac{11\pi t}{t_f}\right) + \frac{\theta_f}{2}
\end{aligned}
\tag{7.26}
$$

This gives us an expression of $\dot{\theta}$, from which we obtain $\omega$ as in Eq. (7.3). We introduce $\omega$ in (7.12) to get the normal mode frequencies $\Omega_\pm$ and these in Eqs. (7.20) and (7.21). I proceeded by fixing the values of the free parameters $c_{3-6}$, solving the auxiliary Eqs. (7.20) and (7.21) numerically and then recursively repeating the process for different values in order to find the set of parameters that minimize a given function. This minimization, known as a shooting process [103], was done using the MatLab function 'fminsearch', and the function we minimized was the total energy of the ground state of the normal mode [Eq. (7.23)] at final time $E''(t_f) = E''_{0+}(t_f) + E''_{0-}(t_f)$.

Once the free parameters are defined such that the design of $\theta$ minimizes the excitation energy of the normal modes, the evolution of the quantum state is calculated with the full Hamiltonian (7.8) to check the performance of the designed protocol. The method used to do the evolution is the "Split-Operator Method", and I chose the ground state as the initial state, which was calculated performing an evolution in imaginary time [81]. Figure 7.2 shows the final excitation, i.e., the excess energy with respect to the initial energy after performing the evolution of the full Hamiltonian (7.8). In Fig. 7.2 (a), I show this excitation in a linear scale, and in Fig. 7.2 (b) in a logarithmic scale. The figures demonstrate the improvement achieved by adding more free parameters. Even when using a single optimizing parameter, the results are clearly better than the protocol with no
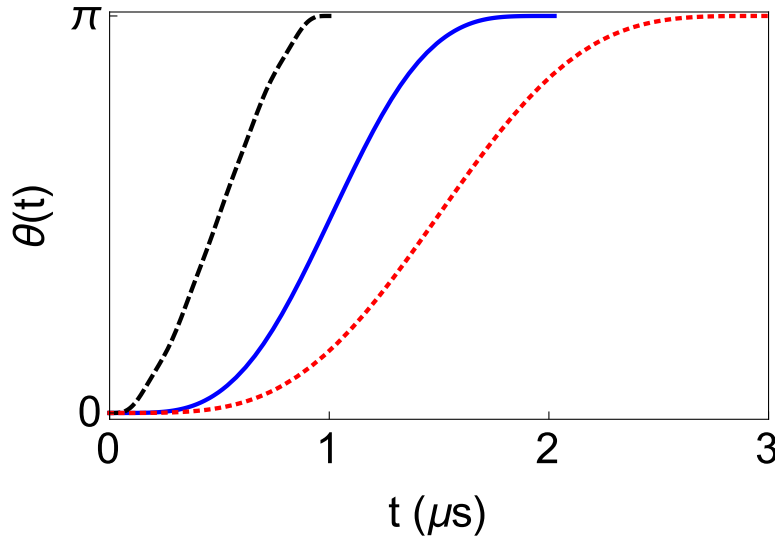
FIGURE 7.3:   Evolution of the control parameter $\theta(t)$ for different final times when designed using all 4 free parameters. The dashed black line has $t_f = 1$ $\mu$s, and the optimization parameters are $c_{3-6} = (5.134, -5.360, 59.577, 91.234) \times 10^{-4}$. The solid blue line has $t_f = 2$ $\mu$s, and the optimization parameters are $c_{3-6} = (3.093, 0.971, 3.386, -6.036) \times 10^{-4}$. The dotted red line has $t_f = 3$ $\mu$s, and the optimization parameters are $c_{3-6} = (1.400, -0.270, 0.182, -0.117) \times 10^{-4}$. Other parameters as in Fig. 7.2.

free parameters. Figure 7.3 shows some examples of the protocol that leads to these results. The best protocol (4 free parameters) reaches the threshold of 0.1 motional excitation quanta at a final time $t_f = 1.05$ $\mu$s, whereas without free parameters the same threshold is reached at $t_f = 2.23$ $\mu$s. That means that using our shortcut-to-adiabaticity protocol, one can accelerate the rotation of two ions by a factor of over 2.

## 7.4   Magnetic vs electric force

In the lab frame, during the rotation, the velocities of the two charged particles have perpendicular components to their alignment direction, so a magnetic force appears of magnitude

$$|F_{mag}| = \left| \frac{\mu_0}{4\pi} \frac{e^2}{r^2} \vec{v}_1 \times (\vec{v}_2 \times \hat{r}) \right|, \tag{7.27}$$
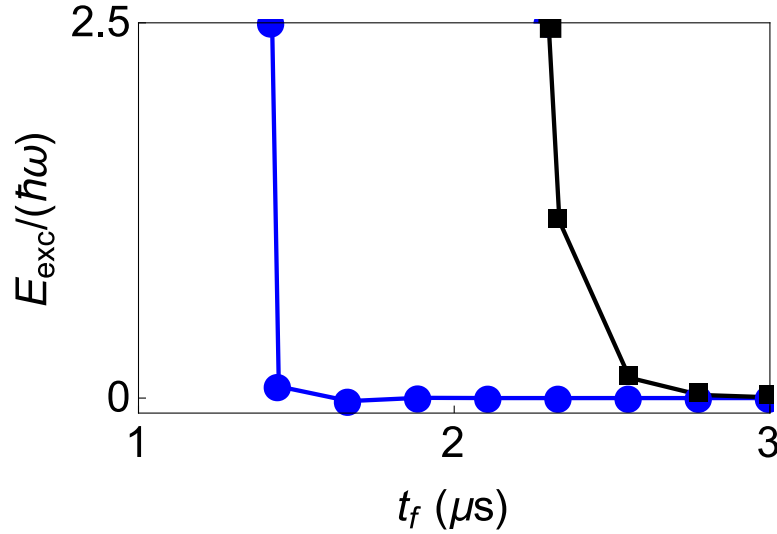
FIGURE 7.4: Exact energy excess with the full Hamiltonian (7.32) according to Eq. (7.26) for the parameters $c_{3-6}$ that minimize this excitation by a brute-force approach. The blue line with circles is using all of the 4 optimizing parameters. The black line with squares is the excitation fixing $c_{3-6} = 0$ in Eq. (7.26). Using 2 and 3 optimizing parameters we get very similar results to those for 4 optimizing parameters. The evolution was done for a $^{40}$Ca$^+$ and a $^9$Be$^+$ ion, with an external trap frequency for the Ca$^+$ ion of $\omega_1/(2\pi) = 1.41$ MHz and a final rotation angle $\theta_f = \pi$.

where $\mu_0$ is the permeability constant, $\vec{v}_i$ the velocity vectors of each ion and $\vec{r} = \vec{r}_2 - \vec{r}_1$ the relative position vector of both ions in the lab frame, $r_i = (x_i, y_i)$. This is to be compared with the Coulomb interaction, which is the only one considered so far, and gives a force

$$|F_{el}| = \left| \frac{C_c}{r^2} \right|. \tag{7.28}$$

The ratio of these two forces is

$$R = \frac{|F_{mag}|}{|F_{el}|} = \frac{\frac{\mu_0}{4\pi} \frac{e^2}{r^2} |\vec{v}_1 \times (\vec{v}_2 \times \hat{r})|}{\frac{1}{4\pi\epsilon_0} \frac{e^2}{r^2}}. \tag{7.29}$$

Using $\vec{v}_1 = -\vec{v}_2 = \frac{\vec{r}}{2}\dot{\theta}$ and $\mu_0\epsilon_0 = \frac{1}{c^2}$, being $c$ the speed of light in the vacuum, we finally get

$$R = \frac{r^2\dot{\theta}^2}{4c^2}. \tag{7.30}$$

In the protocols of the previous section, the maximum values in the simulations are $\dot{\theta}_{max} = 5 \times 10^6$ s$^{-1}$ and $r_{max} = 5.5 \times 10^{-6}$ m, so $R_{max} \sim \frac{1}{c^2}$. For these parameters, the magnetic interaction is negligible with respect to the electric one.

## 7.5  Two different ions

In the scheme of ion chains that have to be reordered, tackling the rotation of two different ions is of even more interest that the rotation of equal ions. However, a shortcut cannot be designed using the same method. Even if the masses are different, the spring constant will be the same for both ions, that is, $m_1\omega_1^2 = m_2\omega_2^2$, being $m_i$ the mass of each ion and $\omega_i$ the effective external trap frequency. For this case, the Lagrangian in Eq. (7.2) will be

$$
\begin{aligned}
L &= \frac{1}{2}m_1\dot{s}_1^2 + \frac{1}{2}m_2\dot{s}_2^2 \\
&\quad - \frac{1}{2}m_1\omega_a^2 s_1^2 - \frac{1}{2}m_2\omega_b^2 s_2^2 - \frac{C_c}{s_2 - s_1}, \\
\omega_a^2 &= \omega_1^2 - \dot{\theta}^2, \\
\omega_b^2 &= \omega_2^2 - \dot{\theta}^2.
\end{aligned}
\tag{7.31}
$$

Instead of Eq. (7.8), the Hamiltonian is

$$
H = \frac{p_1^2}{2m_1} + \frac{p_2^2}{2m_2} + \frac{1}{2}u_1 s_1^2 + \frac{1}{2}u_2 s_2^2 + \frac{C_c}{s_2 - s_1},
\tag{7.32}
$$

where $u_1 = m_1\omega_a^2$, $u_2 = m_2\omega_b^2$. Effectively, this is still an expansion of a two-ion chain, however, the effective spring constants of both ions are different, unlike in [97]. For this Hamiltonian, the equilibrium positions of both ions are

$$
\begin{aligned}
s_1^{(0)} &= -\frac{u_2}{u_1}s_2^{(0)}, \\
s_2^{(0)} &= \sqrt[3]{\frac{C_c}{\left(1 + \frac{u_2}{u_1}\right)^2 u_2}},
\end{aligned}
\tag{7.33}
$$
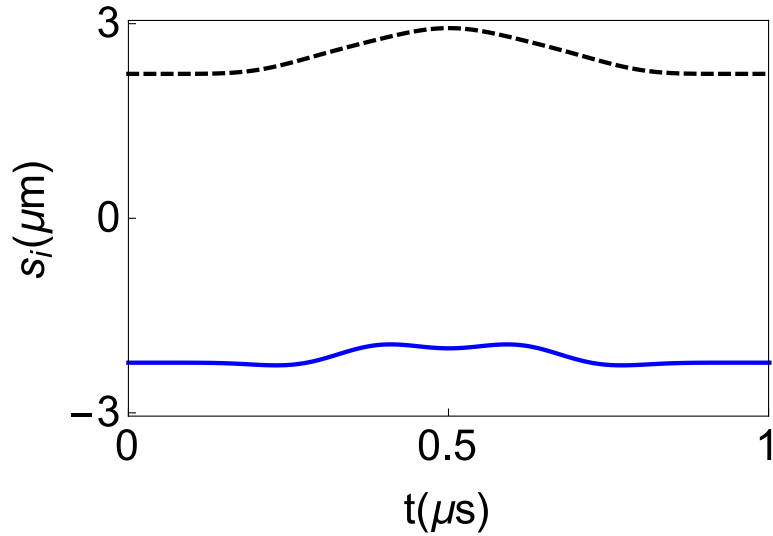
FIGURE 7.5: Position of each of the ions, $s_1$ (Calcium ion) as the solid blue line and $s_2$ (Berilium ion) in dashed black, at final time $t_f = 1$ $\mu$s and for the optimizing parameters $c_{3-6} = (1.757, 1.824, 1.120, -0.234) \times 10^{-2}$ when evolving the Hamiltonian (7.32) under the protocol in Eq. (7.26).

which are not symmetrical with respect to the external trap center anymore. The new eigenvalues of the matrix $V_{ij}$ are

$$
\begin{aligned}
\lambda_\pm &= \frac{u_1}{2m_1} + \frac{u_2}{2m_2} + \frac{(m_1 + m_2)u_1 u_2}{m_1 m_2 (u_1 + u_2)} \\
&\pm \frac{1}{2m_1 m_2 (u_1 + u_2)} \\
&\times \sqrt{16 m_1 m_2 u_1^2 u_2^2 + [m_1 u_2 (3u_1 + u_2) + m_2 u_1 (u_1 + 3u_2)]^2}.
\end{aligned}
$$

(7.34)

The eigenvectors also have a complicated dependence with $u_1$, $u_2$, that is, they depend on time. I will not display the explicit expressions here because they are rather lengthy, but they are analytic. As it happened for example in [106], when the coefficients $a_\pm$, $b_\pm$ are time-dependent, the normal mode transformation leads to crossed terms. That means that we cannot write the Hamiltonian as two independent time-dependent one-dimensional harmonic oscillators, and thus the Lewis-Riesenfeld invariants [76] are of no direct use here. Instead, I use a direct numerical optimization of the protocol using same ansatz for the control $\theta$ as in Eq. (7.26). I try initially random values for the free parameters $c_{3-6}$, but instead of some differential equations as for the equal ion case, we solve the full dynamics

for the Hamiltonian (7.32) and calculate the excess energy. As in Sec. 7.3, using the function 'fminsearch' from MatLab recursively repeat the process for different values of the free parameters until I get the minimum of the excitation energy. In Fig. 7.4 I show this final excitation, optimizing the result using 4 free parameters for the $\theta$ as well as the results for no free parameters. The times achieved are slightly longer than the ones for the protocols based in minimizing the normal mode energy for equal ions in Sec. 7.3. The best protocol (4 optimizing parameters) gives an excitation below 0.1 quanta at a final time $t_f = 1.4$ $\mu$s, whereas the protocol with no optimization needs $t_f = 2.6$ $\mu$s. That is, we get an improvement of almost a factor of 2. The computational time required is dramatically longer than in the previous section, as I had to solve the full dynamics of the system at every iteration of the shooting method, whereas in the normal mode based method we only needed to solve a simple system of differential equations at each iteration. It is important to note that the squeezing plays an important role here, and so it is not possible to use classical dynamics (which are much faster) to calculate the energy instead of the quantum dynamics. Figure 7.5 shows the positions of both ions during the evolution for $t_f = 1$ $\mu$s.

## 7.6 Discussion

In this chapter, I have designed protocols to rotate a linear trap containing two ions, such that at final time we recover the same state we initially had in the trap frame. This provides a way to reorder ions without producing any additional excitation energy. For two equal ions, independent normal modes may be defined, and Lewis-Riesenfeld invariants may be used to design a protocol that leads to negligible excitations in times around two oscillation periods of the external trap. For two different ions, the modes are not independent, so I applied a direct numerical minimization of the excitation energy. This minimization requires a much longer calculation time. For any of the methods, the shortcut supposes a clear improvement, which helps in the task of accelerating dynamical processes for a viable quantum computing architecture based on trapped ions. Possible future

extensions of this work are considering a time dependent external trap frequencies, or designing the voltage supply evolution for a given trap architechture. Also, specific protocols could be designed to simultaneously rotate longer chains of ions, although it is always possible to sequentially rotate them in groups of 2 using the protocols designed here.

# Conclusions

The common thread of this thesis has been the design of various fast dynamical processes for trapped ions using shortcuts to adiabaticity, with the aim of accelerating these processes such that they reach the desired final state without any final excitation. The operations studied, namely, transport, 2-qubit phase gates, expansion, ion separation and rotation, are basic elements, or at least useful processes to implement a scalable quantum processor based on the technology of trapped ions. Compared to previous work on shortcuts, the contribution of this thesis has been extending the technique of invariant-based inverse engineering to few-body systems with Coulomb interactions. This was done by introducing the concept of "dynamical normal modes" [118] and using Lewis-Riesenfeld invariants for each of them in a consistent manner, so that only one physical set of control parameters manages to satisfy the no-final excitation condition for every mode.

All the processes designed here are "experimentally friendly" in the sense that the Hamiltonians considered are doable in the labs, and that limitations on the values of the control parameters, and sometimes even typical deviations were considered. Moreover, the parameter values considered in all the examples are similar to those they work with in state-of-art laboratories. That gives a fair view of the validity of the methods here developed, and makes the shortcuts have the potential of an immediate impact. In fact, many of the works were done in direct collaboration with several laboratories, and I expect some of these protocols to be experimentally realized soon.

Possibly, the greatest leap is that brought by the transport protocols, Chapters 1 and 2, and the related phase-gate in Chapter 3. The transport is known to be the

most time consuming process when adiabatically driven. For both cases I managed to design protocols that drive the system well bellow the 100 $\mu$s threshold that is usually the limit in ion traps before the anomalous heating turns into a problem, with final negligible excitation. For different mass ions, $4 - 5$ $\mu$s were enough, implying an improvement of over a factor of 20 with respect to the most naive linear driving. Phase gates were shown to potentially work at even shorter times. Another challenging operation is the ion separation, studied in Chapter 5. Here, I showed how the performance of the shortcut protocol depends on the maximum value certain control parameter (the quartic part of the potential) can reach. For a range of reasonable maximum values of this parameter, it was shown that it could work for final times between 3 and 11 $\mu$s, whereas an adiabatic protocol used for comparison needed around 80 $\mu$s. The quickest reported time reached in the lab for similar parameters has been 55 $\mu$s, although it had excitation higher (2 quanta per ion) than the one used here as the threshold for negligible excitation (0.1 quanta). Expansions, in Chapter 4, and rotation, in Chapters 6 and 7, are not as time consuming protocols. Nevertheless, these chapters show how it is possible to design shortcut protocols that further improve these final time performances. In an architecture based on moving trapped ions, one should potentially perform many repetitions of each operation, so any improvement in the time required, even if it is by a small factor, has potentially a major impact. During the realization of this work, there has been a phenomenal progress in the technical ability of the laboratories to improve on time and spatial resolution of the applied potentials and on their stability, getting close to the accuracy level needed to implement the fast protocols.

Shortcuts to adiabaticity contribute to fight decoherence, possibly the most serious stumbling block towards practical quantum computation and comercial applications in two ways: Shortening the process time is one of them, as noise and perturbations have less time for spoiling the quantum state. The other way is to make use of the ample freedom to design the shortcut so as to make it more robust versus specific perturbations. I have put the emphasis on the first aspect, but the route towards increasing the stability has been already explored

in different systems and could be applied in this context as well. An example is in Chap. 5, where I have implemented a protocol perturbatively stable with respect to anharmonicities.

In short, I have demonstrated that shortcut-to-adiabaticity techniques can be applied to trapped ion systems, and provide useful fast and safe protocols. A shortcut-toolkit was developed for a number of different dynamical operations needed for a scalable architecture. Simulations show a clear final time improvement in all of them, giving this shortcut-toolkit the potential to have an impact in the effort to develop a scalable quantum processor.

# Appendices

# Appendix A

# N-Ion transport

In this Appendix, I show that for $N$ equal ions in a harmonic trap the trap trajectory appears only in the CM part. In a harmonic trap with $N$ equal ions, the Hamiltonian is given by $N$ coordinates for the positions of each of the ions $(\mathsf{q}_1, \mathsf{q}_2, \mathsf{q}_3, \ldots, \mathsf{q}_\mathsf{N})$ and the corresponding momenta

$$
\begin{aligned}
\widehat{H}(\{\widehat{\mathsf{q}}_i, \widehat{\mathsf{p}}_i\}) &= \frac{1}{2m}\sum_{i=1}^{N}\widehat{\mathsf{p}}_i^2 + \frac{1}{2}m\omega^2\sum_{i=1}^{N}(\widehat{\mathsf{q}}_i - Q_0)^2 \\
&+ \sum_{i=1}^{N-1}\sum_{j=i+1}^{N}\frac{C_c}{\widehat{\mathsf{q}}_i - \widehat{\mathsf{q}}_j}.
\end{aligned}
\tag{A.1}
$$

In coordinate space, $\mathsf{q}_1 > \mathsf{q}_2 > \cdots > \mathsf{q}_{N-1} > \mathsf{q}_N$ because of the strong Coulomb repulsion. We now define a CM and relative coordinates and momenta,

$$
\begin{aligned}
\widehat{Q} &= \frac{1}{N}\sum_{i=1}^{N}\widehat{\mathsf{q}}_i, \qquad \widehat{P} = \sum_{i=1}^{N}\widehat{\mathsf{p}}_i, \\
\widehat{r}_i &= \frac{\widehat{\mathsf{q}}_i - \widehat{\mathsf{q}}_{i+1}}{N}, \qquad \widehat{p}_i = \widehat{\mathsf{p}}_i - \widehat{\mathsf{p}}_{i+1}, \\
i &= 1, 2, \ldots, N-1,
\end{aligned}
\tag{A.2}
$$

corresponding to the inverse transformation

$$\widehat{\mathsf{q}}_i = \widehat{Q} + \sum_{j=1}^{N-i} j\widehat{r}_{N-j} - \sum_{k=1}^{i-1} k\widehat{r}_k,$$

$$\widehat{\mathsf{p}}_i = \widehat{P} + \frac{1}{N}\sum_{j=1}^{N-i} j\widehat{p}_{N-j} - \frac{1}{N}\sum_{k=1}^{i-1} k\widehat{p}_k. \tag{A.3}$$

The Hamiltonian in the new coordinates is

$$\begin{aligned}
\widehat{H} &= \frac{\widehat{P}^2}{2M} + \frac{1}{2}M\omega^2(\widehat{Q} - Q_0)^2 \\
&+ \frac{1}{2NM}\sum_{i=1}^{N}\left[\left(\sum_{j=1}^{N-i} j\widehat{p}_{N-j}\right)^2 + \left(\sum_{k=1}^{i-1} k\widehat{p}_k\right)^2 - 2\sum_{j=1}^{N-i}\sum_{k=1}^{i-1} jk\widehat{p}_{N-j}\widehat{p}_k\right] \\
&+ \frac{1}{2N}M\omega^2\sum_{i=1}^{N}\left[\left(\sum_{j=1}^{N-i} j\widehat{r}_{N-j}\right)^2 + \left(\sum_{k=1}^{i-1} k\widehat{r}_k\right)^2 - 2\sum_{j=1}^{N-i}\sum_{k=1}^{i-1} jk\widehat{r}_{N-j}\widehat{r}_k\right] \\
&+ \frac{C_c}{N}\left(\sum_{i=1}^{N-1}\frac{1}{\widehat{r}_i} + \sum_{i=1}^{N-2}\sum_{j=i+1}^{N-1}\frac{1}{\sum_{k=i}^{j}\widehat{r}_k}\right), \tag{A.4}
\end{aligned}$$

where $M = Nm$. As for two ions, the Hamiltonian can be written as the sum of two terms $\widehat{H} = \widehat{H}_{cm}(\widehat{Q}, \widehat{P}) + \widehat{H}_r(\{\widehat{r}_i, \widehat{p}_i\})$, where $\widehat{H}_{cm}$ has the same form as that of a single particle driven in a harmonic trap, and $\widehat{H}_r$ depends only on $N-1$ relative coordinates and their corresponding momenta. It does not depend on the trap trajectory $Q_0(t)$, so this system can be transported without final excitations by following any shortcut-to-adiabaticity trap trajectory for a particle of mass $M$.

# Appendix B

# Generalization for an arbitrary force ratio

### B.0.1  Equal-mass ions

In the main text we have studied state-dependent forces which are equal and opposite to each other for up and down spins, $F_i = \sigma_i^z F(t)$. However, depending on laser beam polarization and specific atomic structure, different proportionalities among the two forces will arise. Let us consider a general force ratio $F_i(\uparrow) = -c\tilde{F}(t)$ and $F_i(\downarrow) = -\tilde{F}(t)$, where $c$ is a constant. Then, for equal-mass ions, instead of Eq. (3.49) (corresponding to $c = -1$), we find, see Eq. (3.48),

$$
\begin{aligned}
f_+(\uparrow\uparrow) &= f_+(\downarrow\downarrow) = 0, \\
f_-(\uparrow\uparrow) &= cf_-(\downarrow\downarrow) = \frac{2\tilde{F}c}{\sqrt{2m}}, \\
f_+(\uparrow\downarrow) &= -f_+(\downarrow\uparrow) = -\frac{1-c}{\sqrt{2m}}\tilde{F}, \\
f_-(\uparrow\downarrow) &= f_-(\downarrow\uparrow) = \frac{1+c}{\sqrt{2m}}\tilde{F}.
\end{aligned}
\tag{B.1}
$$

To inverse engineer the forces we start choosing the same ansatz for $\alpha_+(\downarrow\uparrow)$ as in Eq. (3.53). $a_0$ through $a_2$ are also fixed in the same manner to satisfy the boundary conditions. Using Eq. (3.20) this gives $f_+(\downarrow\uparrow; t)$ as a function of $a_3$, $a_4$,

and in fact all other $f_\pm$ by scaling them according to the Eq. (B.1). As in the main text, the same $a_3$ in Eq. (3.55) guarantees that $\dot{\alpha}_\pm(t_b) = 0$ for all spin configurations. Now, using Eq. (3.47) we can write down the phase produced by each spin configuration. Individually, they depend on $c$ but, adding them all in $\Delta\phi = \phi(\uparrow\downarrow) + \phi(\downarrow\uparrow) - \phi(\uparrow\uparrow) - \phi(\downarrow\downarrow)$, the dependence on $c$ is cancelled, as can be seen from Eq. (C.1) or Eq. (3.20) and Eq. (B.1). Following the method described in the main text, imposing $\Delta\phi = \gamma$ fixes the remaining parameter $a_4$, so that the same expression in Eq. (3.59) is found. Using Eqs. (3.49) and (B.1), the generic control function $\tilde{F}$ is simply proportional to that for $c = -1$ (see Eq. (3.60)),

$$\tilde{F} = \frac{2}{1-c}F. \tag{B.2}$$

## B.0.2   Different masses

Similarly, for different-mass ions in the generic case both ions could have different proportionality factors for the spin-dependent forces:

$$\begin{aligned} F_1(\uparrow) &= -c_1\tilde{F}_a, \quad F_1(\downarrow) = -\tilde{F}_a, \\ F_2(\uparrow) &= -c_2\tilde{F}_b, \quad F_2(\downarrow) = -\tilde{F}_b. \end{aligned} \tag{B.3}$$

Instead of Eq. (3.62), the normal-mode forces are now, see Eq. (3.14),

$$\begin{aligned} f_\pm(\uparrow\uparrow) &= \pm\frac{b_\mp}{\sqrt{m}}c_1\tilde{F}_a \mp \frac{a_\mp}{\sqrt{\mu m}}c_2\tilde{F}_b, \\ f_\pm(\uparrow\downarrow) &= \pm\frac{b_\mp}{\sqrt{m}}c_1\tilde{F}_a \mp \frac{a_\mp}{\sqrt{\mu m}}\tilde{F}_b, \\ f_\pm(\downarrow\uparrow) &= \pm\frac{b_\mp}{\sqrt{m}}\tilde{F}_a \mp \frac{a_\mp}{\sqrt{\mu m}}c_2\tilde{F}_b, \\ f_\pm(\downarrow\downarrow) &= \pm\frac{b_\mp}{\sqrt{m}}\tilde{F}_a \mp \frac{a_\mp}{\sqrt{\mu m}}\tilde{F}_b. \end{aligned} \tag{B.4}$$

This implies that the $\alpha_\pm$ are in general all different and the inverse scheme in Eq. (3.65) is replaced by

$$\alpha_\pm(\uparrow\downarrow) \dashrightarrow f_\pm(\uparrow\downarrow) \dashrightarrow \tilde{F}_a, \tilde{F}_b \dashrightarrow \underbrace{\left\{ \begin{array}{ccc} f_\pm(\uparrow\uparrow) & \dashrightarrow & \alpha_\pm(\uparrow\uparrow) \\ f_\pm(\downarrow\uparrow) & \dashrightarrow & \alpha_\pm(\downarrow\uparrow) \\ f_\pm(\downarrow\downarrow) & \dashrightarrow & \alpha_\pm(\downarrow\downarrow). \end{array} \right.}_{\text{functions of } c_1, c_2} \tag{B.5}$$

Using Eq. (3.10) and Eq. (B.4) we may rewrite the control functions $\tilde{F}_a$ and $\tilde{F}_b$ as

$$\begin{aligned} \tilde{F}_a &= \sqrt{m}[a_- f_-(\uparrow\downarrow) + a_+ f_+(\uparrow\downarrow)]/c_1, \\ \tilde{F}_b &= \sqrt{\mu m}[b_- f_-(\uparrow\downarrow) + b_+ f_+(\uparrow\downarrow)]. \end{aligned} \tag{B.6}$$

As in the special case $c_1 = c_2 = -1$ of the main text, we use the ansatzes in Eq. (3.66) for $\alpha_\pm(\uparrow\downarrow)$, and the parameters in Eq. (3.67). In particular $\alpha_-(\uparrow\downarrow) = 0$ and $f_-(\uparrow\downarrow) = 0$, so $\tilde{F}_a$ and $\tilde{F}_b$ are proportional to each other, see Eq. (B.6), and thus all the $f_\pm$ are proportional to $f_+(\uparrow\downarrow)$ according to Eq. (B.4). Thus, from Newton's equations, all (nonzero) solutions $\alpha_+(t)$ are proportional to each other, and similarly all (nonzero) $\alpha_-(t)$ are proportional to each other. The parameter choice in Eq. (3.67) assures that $\alpha_+(t_b) = \dot{\alpha}_+(t_b) = 0$ for all configurations. Fixing, for example $\alpha_-(\uparrow\uparrow)(t_b) = 0$, $a_3$ may be fixed as in Eq. (3.68), so that $\dot{\alpha}_-(t_b) = 0$, and therefore $\alpha_-(t_b) = \dot{\alpha}_-(t_b) = 0$ as well for all configurations. Using Eq. (3.47) to calculate the phases, and imposing $\Delta\phi = \gamma$, the remaining parameter ($a_4$) is fixed as

$$a_4 = C a_4^0, \tag{B.7}$$

where $a_4^0 \equiv a_4(c_1 = c_2 = -1)$ is given in Eq. (3.70) and

$$C = 2\sqrt{\frac{-c_1}{(c_1 - 1)(c_2 - 1)}}. \tag{B.8}$$

All coefficients in $\alpha_+(\uparrow\downarrow)$ are proportional to $a_4$, so $\alpha_+(\uparrow\downarrow)$ is just scaled by the factor C with respect to the ones for $c_1 = c_2 = -1$ in the main text, and $f_+(\uparrow\downarrow)$

is also scaled by the same factor according to Eq. (3.20). Comparing Eqs. (B.6) and (3.64), and using $f_-(\uparrow\downarrow) = 0$, we find that

$$
\begin{aligned}
\tilde{F}_a &= -\frac{C}{c_1}F_a, \\
\tilde{F}_b &= CF_b,
\end{aligned}
\tag{B.9}
$$

in terms of the forces $F_a$, $F_b$ given in Eq. (3.73) for $c_1 = c_2 = -1$. All these functions have odd symmetry with respect to the middle time $t_f/2$ so that there is no contribution to the phase from the time integral of $\tilde{f}$, see Eq. (3.14).

Finally let us analyze the limit of equal masses where $c_1 = c_2 = c$ and $\mu = 1$. In the main text, this implies $c_1 = c_2 = c = -1$ and $F_a(\mu \to 1) = F_b(\mu \to 1) = F$, in agreement with the physical constraint of using the same laser for both ions. However, when $c \neq 1$, $\tilde{F}_a(\mu \to 1) \neq \tilde{F}_b(\mu \to 1)$, see Eq. (B.9). Physically this implies the use of two different lasers which is not possible in practice, so equal masses with $c \neq 1$ have to be treated separately, as specified in Sec. B.0.1.

# Appendix C

# Integral expression for the phase

For $\alpha_\pm(0) = \dot{\alpha}_\pm(0) = 0$, Eq. (3.20) may be solved as $\alpha_\pm(t) = \frac{1}{\Omega_\pm} \int_0^t dt' f_\pm(t') \sin[\Omega_\pm(t-t')]$, see Eq. (3.37). Thus the phase (3.47) can be also expressed by double integrals of the form

$$
\begin{aligned}
\phi(t_f) &= \sum_{\mu=\pm} \int_0^{t_f} dt' \int_0^{t'} dt'' f_\mu(t') f_\mu(t'') \frac{\sin[\Omega_\mu(t'-t'')]}{2\hbar\Omega_\mu} \\
&= \sum_{\mu=\pm} \int_0^{t_f}\!\!\int_0^{t_f} dt' dt'' f_\mu(t') f_\mu(t'') \frac{\sin(\Omega_\mu|t'-t''|)}{4\hbar\Omega_\mu}.
\end{aligned}
$$

(C.1)

# Appendix D

# Worst case fidelity

To simplify notation, let us denote the internal state configurations by a generic index $s = \uparrow\uparrow, \uparrow\downarrow, \downarrow\uparrow, \downarrow\downarrow$. Assume an initial state $|\psi_m\rangle(\sum_s c_s|s\rangle)$, where $\sum |c_s|^2 = 1$ and the "m" here stands for "motional". The ideal output state, up to a global phase factor, is

$$|\psi_{id}\rangle = \left( \sum_s c_s e^{i\phi(s)}|s\rangle \right) |\psi_m\rangle, \tag{D.1}$$

where

$$\phi(\uparrow\downarrow) + \phi(\downarrow\uparrow) - \phi(\uparrow\uparrow) - \phi(\downarrow\downarrow) = \pm\pi. \tag{D.2}$$

The actual output state is generally entangled,

$$|\psi_{ac}\rangle = \sum_s c_s e^{i\phi'(s)}|s\rangle|\psi_{ms}\rangle, \tag{D.3}$$

with a different motional state $|\psi_{ms}\rangle$ for each spin configuration, and actual phases $\phi'(s)$. First we can compute the total overlap

$$\langle\psi_{id}|\psi_{ac}\rangle = \sum_s |c_s|^2 e^{i[\phi'(s)-\phi(s)]}\langle\psi_m|\psi_{ms}\rangle. \tag{D.4}$$

Moreover, writing each motional overlap in the form $\langle\psi_m|\psi_{ms}\rangle = |\langle\psi_m|\psi_{ms}\rangle|e^{i\phi_{ms}} = \epsilon_s e^{i\phi_{ms}}$, we have

$$\langle\psi_{id}|\psi_{ac}\rangle \;\; = \;\; \sum_s |c_s|^2 \epsilon_s e^{i\delta_s} = \Re + i\Im, \tag{D.5}$$

where $\delta_s \equiv \phi'(s) - \phi(s) + \phi_{ms}$, and

$$\Re \;\; = \;\; \sum_s |c_s|^2 \epsilon_s \cos\delta_s,$$
$$\Im \;\; = \;\; \sum_s |c_s|^2 \epsilon_s \sin\delta_s. \tag{D.6}$$

The fidelity is

$$\mathcal{F} \;\; = \;\; |\Re + i\Im|^2 = \Re^2 + \Im^2 \geq \Re^2$$
$$= \;\; \Big(\sum_s |c_s|^2 \epsilon_s \cos\delta_s\Big)^2. \tag{D.7}$$

Assuming a "good gate", such that $|\delta_s| \ll 1$ for all $s$, then the fidelity is bounded from below by the worst possible case,

$$\mathcal{F} \geq \mathrm{Min}[(\epsilon_s \cos\delta_s)^2]. \tag{D.8}$$

# Appendix E

# Spread of the position of one ion in the ground state of the two ions

An approximate analytical wave function for the ground state of the two ions subjected to the Hamiltonian (3.5), is given by multiplying the ground states of the two normal modes, see Eq. (3.24),

$$\psi_{NM} = \left( \frac{\Omega_+ \Omega_-}{\pi^2 \hbar^2} \right)^{1/4} e^{-\frac{1}{2\hbar}(\Omega_+ \mathsf{x}_+^2 + \Omega_- \mathsf{x}_-^2)}. \tag{E.1}$$

In laboratory coordinates, and for the specific case of equal mass ions, the normalized ground state is

$$\psi(x_1, x_2) = \left( \frac{m\sqrt{3}\omega^2}{\pi^2 \hbar^2} \right)^{1/4} e^{-\frac{m\omega}{4\hbar} \left[ (1+\sqrt{3})(x_1+\frac{x_0}{2})^2 + (1+\sqrt{3})(x_2-\frac{x_0}{2})^2 + 2(1-\sqrt{3})(x_1+\frac{x_0}{2})(x_2-\frac{x_0}{2}) \right]}. \tag{E.2}$$

The expectation values of $x_1$ and $x_1^2$ are calculated as

$$
\begin{aligned}
\langle x_1 \rangle &= \int_{-\infty}^{\infty} \int_{-\infty}^{\infty} dx_1 dx_2 x_1 \psi^2(x_1, x_2) = -\frac{x_0}{2}, \\
\langle x_1^2 \rangle &= \int_{-\infty}^{\infty} \int_{-\infty}^{\infty} dx_1 dx_2 x_1^2 \psi^2(x_1, x_2) = \frac{x_0^2}{4} + \frac{(3 + \sqrt{3})\hbar}{12 m \omega},
\end{aligned}
\tag{E.3}
$$

so that the wave packet width for ion 1 is

$$
\Delta x_1 = \sqrt{\langle x_1^2 \rangle - \langle x_1 \rangle^2} = \frac{1}{2} \sqrt{1 + \frac{1}{\sqrt{3}}} \sqrt{\frac{\hbar}{m\omega}}.
\tag{E.4}
$$

# Appendix F

# Alternative inversion protocols

An approximate analytical wave function for the ground state of the two ions subjected to the Hamiltonian (3.5), is given by multiplying the ground states of the two normal modes, see Eq. (3.24),

$$\psi_{NM} = \left(\frac{\Omega_+\Omega_-}{\pi^2\hbar^2}\right)^{1/4} e^{-\frac{1}{2\hbar}(\Omega_+\mathsf{x}_+^2 + \Omega_-\mathsf{x}_-^2)}. \tag{F.1}$$

In laboratory coordinates, and for the specific case of equal mass ions, the normalized ground state is

$$\psi(x_1, x_2) = \left(\frac{m\sqrt{3}\omega^2}{\pi^2\hbar^2}\right)^{1/4} e^{-\frac{m\omega}{4\hbar}\left[(1+\sqrt{3})(x_1+\frac{x_0}{2})^2 + (1+\sqrt{3})(x_2-\frac{x_0}{2})^2 + 2(1-\sqrt{3})(x_1+\frac{x_0}{2})(x_2-\frac{x_0}{2})\right]}. \tag{F.2}$$

The expectation values of $x_1$ and $x_1^2$ are calculated as

$$\langle x_1 \rangle = \int_{-\infty}^{\infty} \int_{-\infty}^{\infty} dx_1 dx_2 x_1 \psi^2(x_1, x_2) = -\frac{x_0}{2},$$

$$\langle x_1^2 \rangle = \int_{-\infty}^{\infty} \int_{-\infty}^{\infty} dx_1 dx_2 x_1^2 \psi^2(x_1, x_2) = \frac{x_0^2}{4} + \frac{(3+\sqrt{3})\hbar}{12m\omega}, \tag{F.3}$$

so that the wave packet width for ion 1 is

$$\Delta x_1 = \sqrt{\langle x_1^2 \rangle - \langle x_1 \rangle^2} = \frac{1}{2}\sqrt{1 + \frac{1}{\sqrt{3}}}\sqrt{\frac{\hbar}{m\omega}}. \tag{F.4}$$

# Appendix G

# Ansatz for $\rho_+$

The ansatz for $\rho_+$ that satisfies the BC $\rho_+(0) = 1$, $\rho_+(t_f) = \gamma_+$, $\dot{\rho}_+(t_b) = \ddot{\rho}_+(t_b) = \dddot{\rho}_+(t_b) = \ddddot{\rho}_+(t_b) = 0$ with two free parameters takes the form

$$
\begin{aligned}
\rho_+ \;=\; & 1 - (126 - 126\gamma_+ + a_{10} + 5a_{11})s^5 \\
& + (420 - 420\gamma_+ + 5a_{10} + 24a_{11})s^6 \\
& - (540 - 540\gamma_+ + 10a_{10} + 45a_{11})s^7 \\
& + (315 - 315\gamma_+ + 10a_{10} + 40a_{11})s^8 \\
& - (70 - 70\gamma_+ + 5a_{10} + 15a_{11})s^9 \\
& + a_{10}s^{10} + a_{11}s^{11}.
\end{aligned}
\tag{G.1}
$$

To minimize the perturbation energy in Eq. (5.28), three free parameters are introduced,

$$
\begin{aligned}
\rho_+ \;=\; & 1 - (126 - 126\gamma_+ + c_{10} + 5c_{11} + 15c_{12})s^5 \\
& + (420 - 420\gamma_+ + 5c_{10} + 24c_{11} + 70c_{12})s^6 \\
& - (540 - 540\gamma_+ + 10c_{10} + 45c_{11} + 126c_{12})s^7 \\
& + (315 - 315\gamma_+ + 10c_{10} + 40c_{11} + 105c_{12})s^8 \\
& - (70 - 70\gamma_+ + 5c_{10} + 15c_{11} + 35c_{12})s^9 \\
& + c_{10}s^{10} + c_{11}s^{11} + c_{12}s^{12}.
\end{aligned}
\tag{G.2}
$$

# Appendix H

# Wave functions

The time-dependent wave functions evolving with the Hamiltonian (6.8) take the form [32, 33, 76]

$$\langle s|\psi(t)\rangle = \sum_n c_n e^{i\alpha_n(t)} \langle s|\phi_n(t)\rangle \tag{H.1}$$

where the $c_n$ are constant,

$$\alpha_n(t) = -\frac{1}{\hbar} \int_0^t dt' \frac{(n+1/2)\hbar\omega_0}{\rho^2} = -\omega_0(n+1/2) \int_0^t dt' \frac{1}{\rho^2}, \tag{H.2}$$

$$\langle s|\phi_n(t)\rangle = e^{\frac{im}{\hbar}\dot{\rho}q^2/(2\rho)} \frac{1}{\rho^{1/2}} \Phi_n\left(\frac{s}{\rho}\right), \tag{H.3}$$

and $\Phi_n(x)$ is the Hermite polynomial solution of the harmonic oscillator with angular frequency $\omega_0$ and with energy eigenvalue $(n+1/2)\hbar\omega_0$, that is, $\Phi_n(x) = \frac{1}{\sqrt{2^n n!}}(\frac{m\omega_0}{\pi\hbar})^{1/4} e^{\frac{-m\omega_0 x^2}{2\hbar}} H_n(\sqrt{\frac{m\omega_0}{\hbar}}x)$. Note that $\frac{1}{\rho^{1/2}}\Phi_n(s/\rho)$ is just a scaled state that corresponds to the $n$th eigenstate of a trap with angular frequency $\omega_0/\rho^2$.

# Bibliography

[1] N. F. Ramsey, "*Experiments with separated oscillatory fields and hydrogen masers*", Reviews of Modern Physics **62**, 541–552 (1990).

[2] H. Dehmelt, "*Experiments with an isolated subatomic particle at rest*", Reviews of Modern Physics **62**, 525–530 (1990).

[3] W. Paul, "*Electromagnetic traps for charged and neutral particles*", Reviews of Modern Physics **62**, 531–540 (1990).

[4] S. Chu, "*Nobel Lecture: The manipulation of neutral particles*", Reviews of Modern Physics **70**, 685–706 (1998).

[5] C. N. Cohen-Tannoudji, "*Nobel Lecture: Manipulating atoms with photons*", Reviews of Modern Physics **70**, 707–719 (1998).

[6] W. D. Phillips, "*Nobel Lecture: Laser cooling and trapping of neutral atoms*", Reviews of Modern Physics **70**, 721–741 (1998).

[7] W. Ketterle, "*Nobel lecture: When atoms behave as waves: Bose-Einstein condensation and the atom laser*", Reviews of Modern Physics **74**, 1131–1151 (2002).

[8] E. A. Cornell and C. E. Wieman, "*Nobel Lecture: Bose-Einstein condensation in a dilute gas, the first 70 years and some recent experiments*", Reviews of Modern Physics **74**, 875–893 (2002).

[9] R. J. Glauber, "*Nobel Lecture: One hundred years of light quanta*", Reviews of Modern Physics **78**, 1267–1278 (2006).

[10] J. L. Hall, "*Nobel Lecture: Defining and measuring optical frequencies*", Reviews of Modern Physics **78**, 1279–1295 (2006).

[11] T. W. Hänsch, "*Nobel Lecture: Passion for precision*", Reviews of Modern Physics **78**, 1297–1309 (2006).

[12] S. Haroche, "*Nobel Lecture: Controlling photons in a box and exploring the quantum to classical boundary*", Reviews of Modern Physics **85**, 1083–1102 (2013).

[13] D. J. Wineland, "*Nobel Lecture: Superposition, entanglement, and raising Schrödinger's cat*", Reviews of Modern Physics **85**, 1103–1114 (2013).

[14] D. Deutsch, "*Quantum Theory, the Church-Turing Principle and the Universal Quantum Computer*", Proceedings of the Royal Society of London A: Mathematical, Physical and Engineering Sciences **400**, 97–117 (1985), `http://rspa.royalsocietypublishing.org/content/400/1818/97.full.pdf`.

[15] J. I. Cirac and P. Zoller, "*Quantum Computations with Cold Trapped Ions*", Physical Review Letters **74**, 4091–4094 (1995).

[16] T. P. Harty, D. T. C. Allcock, C. J. Ballance, L. Guidoni, H. A. Janacek, N. M. Linke, D. N. Stacey, and D. M. Lucas, "*High-Fidelity Preparation, Gates, Memory, and Readout of a Trapped-Ion Quantum Bit*", Physical Review Letters **113**, 220501 (2014).

[17] C. J. Ballance, T. P. Harty, N. M. Linke, M. A. Sepiol, and D. M. Lucas, "*High-Fidelity Quantum Logic Gates Using Trapped-Ion Hyperfine Qubits*", Physical Review Letters **117**, 060504 (2016).

[18] J. P. Gaebler, T. R. Tan, Y. Lin, Y. Wan, R. Bowler, A. C. Keith, S. Glancy, K. Coakley, E. Knill, D. Leibfried, and D. J. Wineland, "*High-Fidelity Universal Gate Set for $^9$Be$^+$ Ion Qubits*", Physical Review Letters **117**, 060505 (2016).

[19] R. Blatt and D. Wineland, *"Entangled states of trapped atomic ions."*, Nature **453**, 1008–15 (2008).

[20] R. Blatt and C. F. Roos, *"Quantum simulations with trapped ions"*, Nature Physics **8**, 277–284 (2012).

[21] S. Korenblit, D. Kafri, W. C. Campbell, R. Islam, E. E. Edwards, Z.-X. Gong, G.-D. Lin, L.-M. Duan, J. Kim, K. Kim, and C. Monroe, *"Quantum simulation of spin models on an arbitrary lattice with trapped ions"*, New Journal of Physics **14**, 095024 (2012).

[22] D. J. Wineland, C. Monroe, W. M. Itano, D. Leibfried, B. E. King, and D. M. Meekhof, *"Experimental issues in coherent quantum-state manipulation of trapped atomic ions"*, Journal of Research of the National Institute of Standards and Technology **103**, (1998), `arXiv:9710025 [quant-ph]`.

[23] D. Kielpinski, C. Monroe, and D. J. Wineland, *"Architecture for a large-scale ion-trap quantum computer."*, Nature **417**, 709–11 (2002).

[24] J. I. Cirac and P. Zoller, *"A scalable quantum computer with ions in an array of microtraps"*, Nature **404**, 579-581 (2000).

[25] C. Monroe, R. Raussendorf, A. Ruthven, K. R. Brown, P. Maunz, L.-M. Duan, and J. Kim, *"Large-scale modular quantum-computer architecture with atomic memory and photonic interconnects"*, Physical Review A **89**, 022317 (2014).

[26] D. J. Rowe, M. A.; Ben-Kish, A.; DeMarco, B.; Leibfried, D.; Meyer, V.; Beall, J.; Britton, J.; Hughes, J.; Itano, W. M.; Jelenkovic, B.; Langer, C.; Rosenband, T.; and Wineland, *"Transport of quantum states and separation of ions in a dual rf ion trap"*, Quantum Inf. Comput. **2**, 257 (2002).

[27] R. Reichle, D. Leibfried, R. Blakestad, J. Britton, J. Jost, E. Knill, C. Langer, R. Ozeri, S. Seidelin, and D. Wineland, *"Transport dynamics of*

*single ions in segmented microstructured Paul trap arrays*", Fortschritte der Physik **54**, 666–685 (2006).

[28] C. Roos, "*Viewpoint: Moving Traps Offer Fast Delivery of Cold Ions*", Physics **5**, (2012).

[29] C. Monroe and J. Kim, "*Scaling the ion trap quantum processor.*", Science (New York, N.Y.) **339**, 1164–9 (2013).

[30] J. P. Home, D. Hanneke, J. D. Jost, J. M. Amini, D. Leibfried, and D. J. Wineland, "*Complete methods set for scalable ion trap quantum information processing.*", Science (New York, N.Y.) **325**, 1227–30 (2009).

[31] E. Torrontegui, S. Ibáñez, S. Martínez-Garaot, M. Modugno, A. del Campo, D. Guéry-Odelin, A. Ruschhaupt, X. Chen, and J. G. Muga, *Shortcuts to Adiabaticity*, volume 62 of *Advances In Atomic, Molecular, and Optical Physics*. Elsevier, 2013.
`http://www.sciencedirect.com/science/article/pii/B9780124080904000025`.

[32] X. Chen, A. Ruschhaupt, S. Schmidt, A. del Campo, D. Guéry-Odelin, and J. G. Muga, "*Fast Optimal Frictionless Atom Cooling in Harmonic Traps: Shortcut to Adiabaticity*", Physical Review Letters **104**, 063002 (2010).

[33] E. Torrontegui, S. Ibáñez, X. Chen, A. Ruschhaupt, D. Guéry-Odelin, and J. G. Muga, "*Fast atomic transport without vibrational heating*", Physical Review A **83**, 013415 (2011).

[34] E. Torrontegui, S. Martínez-Garaot, and J. G. Muga, "*Hamiltonian engineering via invariants and dynamical algebra*", Physical Review A **89**, 043408 (2014).

[35] H.-K. Lau and D. F. V. James, "*Proposal for a scalable universal bosonic simulator using individually trapped ions*", Physical Review A **85**, 062329 (2012).

[36] S. Schulz, U. Poschinger, K. Singer, and F. Schmidt-Kaler, "*Optimization of segmented linear Paul traps and transport of stored particles*", Fortschritte der Physik **54**, 648–665 (2006).

[37] A. Couvert, T. Kawalec, G. Reinaudi, and D. Guéry-Odelin, "*Optimal transport of ultracold atoms in the non-adiabatic regime*", EPL (Europhysics Letters) **83**, 13001 (2008).

[38] M. Murphy, L. Jiang, N. Khaneja, and T. Calarco, "*High-fidelity fast quantum transport with imperfect controls*", Physical Review A **79**, 020301 (2009).

[39] S. Masuda and K. Nakamura, "*Fast-forward of adiabatic dynamics in quantum mechanics*", Proceedings of the Royal Society A: Mathematical, Physical and Engineering Sciences **466**, 1135–1154 (2010).

[40] X. Chen, E. Torrontegui, D. Stefanatos, J.-S. Li, and J. G. Muga, "*Optimal trajectories for efficient atomic transport without final excitation*", Physical Review A **84**, 043415 (2011).

[41] E. Torrontegui, X. Chen, M. Modugno, S. Schmidt, A. Ruschhaupt, and J. G. Muga, "*Fast transport of BoseEinstein condensates*", New Journal of Physics **14**, 013031 (2012).

[42] R. Bowler, J. Gaebler, Y. Lin, T. R. Tan, D. Hanneke, J. D. Jost, J. P. Home, D. Leibfried, and D. J. Wineland, "*Coherent Diabatic Ion Transport and Separation in a Multizone Trap Array*", Physical Review Letters **109**, 080502 (2012).

[43] A. Walther, F. Ziesel, T. Ruster, S. T. Dawkins, K. Ott, M. Hettrich, K. Singer, F. Schmidt-Kaler, and U. Poschinger, "*Controlling Fast Transport of Cold Trapped Ions*", Physical Review Letters **109**, 080501 (2012).

[44] A. Ruschhaupt, X. Chen, D. Alonso, and J. G. Muga, *"Optimally robust shortcuts to population inversion in two-level quantum systems"*, New Journal of Physics **14**, 093040 (2012).

[45] J. P. Home, D. Hanneke, J. D. Jost, D. Leibfried, and D. J. Wineland, *"Normal modes of trapped ions in the presence of anharmonic trap potentials"*, New Journal of Physics **13**, 073026 (2011).

[46] N. W. Evans, *"On Hamiltonian systems in two degrees of freedom with invariants quartic in the momenta of form p21p22"*, Journal of Mathematical Physics **31**, 600 (1990).

[47] M. Karlovini, G. Pucacco, K. Rosquist, and L. Samuelsson, *"A unified treatment of quartic invariants at fixed and arbitrary energy"*, Journal of Mathematical Physics **43**, 4041 (2002).

[48] S. Masuda, *"Acceleration of adiabatic transport of interacting particles and rapid manipulations of a dilute Bose gas in the ground state"*, Physical Review A **86**, 063624 (2012).

[49] E. Torrontegui, S. Martínez-Garaot, A. Ruschhaupt, and J. G. Muga, *"Shortcuts to adiabaticity: Fast-forward approach"*, Physical Review A **86**, 013601 (2012).

[50] W. Klink, *"Quantum Mechanics in Nonintertial Reference Frames"*, Annals of Physics **260**, 27–49 (1997).

[51] E. Torrontegui, X. Chen, M. Modugno, A. Ruschhaupt, D. Guéry-Odelin, and J. G. Muga, *"Fast transitionless expansion of cold atoms in optical Gaussian-beam traps"*, Physical Review A **85**, 033605 (2012).

[52] M. Palmero, E. Torrontegui, D. Guéry-Odelin, and J. G. Muga, *"Fast transport of two ions in an anharmonic trap"*, Physical Review A **88**, 053423 (2013).

[53] J. Pedregosa-Gutierrez, C. Champenois, M. R. Kamsap, and M. Knoop, "*Ion transport in macroscopic RF linear traps*", International Journal of Mass Spectrometry **381-382**, 33–40 (2015).

[54] G. Huber, T. Deuschle, W. Schnitzler, R. Reichle, K. Singer, and F. Schmidt-Kaler, "*Transport of ions in a segmented linear Paul trap in printed-circuit-board technology*", New Journal of Physics **10**, 013004 (2008).

[55] H. A. Fürst, M. H. Goerz, U. G. Poschinger, M. Murphy, S. Montangero, T. Calarco, F. Schmidt-Kaler, K. Singer, and C. P. Koch, "*Controlling the transport of an ion: classical and quantum mechanical solutions*", New Journal of Physics **16**, 075007 (2014).

[56] X.-J. Lu, J. G. Muga, X. Chen, U. G. Poschinger, F. Schmidt-Kaler, and A. Ruschhaupt, "*Fast shuttling of a trapped ion in the presence of noise*", Physical Review A **89**, 063414 (2014).

[57] D. Hanneke, J. P. Home, J. D. Jost, J. M. Amini, D. Leibfried, and D. J. Wineland, "*Realization of a programmable two-qubit quantumprocessor*", Nature Physics **6**, 13–16 (2009).

[58] P. G. L. Lewis, H. Ralph; Leach, "*A direct approach to finding exact invariants for one-dimensional time-dependent classical Hamiltonians*", Journal of Mathematical Physics **23**, 2371 (1982).

[59] G. Morigi and H. Walther, "*Two-species Coulomb chains for quantum information*", The European Physical Journal D **13**, 261–269 (2001).

[60] S. Ibáñez, X. Chen, E. Torrontegui, J. G. Muga, and A. Ruschhaupt, "*Multiple Schrödinger Pictures and Dynamics in Shortcuts to Adiabaticity*", Physical Review Letters **109**, 100403 (2012).

[61] S. Deffner, C. Jarzynski, and A. del Campo, "*Classical and Quantum Shortcuts to Adiabaticity for Scale-Invariant Driving*", Physical Review X **4**, 021013 (2014).

[62] X.-J. Lu, M. Palmero, A. Ruschhaupt, X. Chen, and J. G. Muga, "*Optimal transport of two ions under slow spring-constant drifts*", Physica Scripta **90**, 074038 (2015).

[63] M. Palmero, R. Bowler, J. P. Gaebler, D. Leibfried, and J. G. Muga, "*Fast transport of mixed-species ion chains within a Paul trap*", Physical Review A **90**, 053408 (2014).

[64] A. Sørensen and K. Mølmer, "*Quantum Computation with Ions in Thermal Motion*", Physical Review Letters **82**, 1971–1974 (1999).

[65] E. Solano, R. L. de Matos Filho, and N. Zagury, "*Deterministic Bell states and measurement of the motional state of two trapped ions*", Phys. Rev. A **59**, R2539–R2543 (1999).

[66] G. Milburn, S. Schneider, and D. James, "*Ion Trap Quantum Computing with Warm Ions*", Fortschritte der Physik **48**, 801–810 (2000).

[67] A. Sørensen and K. Mølmer, "*Entanglement and quantum computation with ions in thermal motion*", Physical Review A **62**, 022311 (2000).

[68] C. A. Sackett, D. Kielpinski, B. E. King, C. Langer, V. Meyer, C. J. Myatt, M. Rowe, Q. A. Turchette, W. M. Itano, D. J. Wineland, and C. Monroe, "*Experimental entanglement of four particles*", Nature **404**, 256–259 (2000).

[69] D. Leibfried, B. DeMarco, V. Meyer, D. Lucas, M. Barrett, J. Britton, W. M. Itano, B. Jelenković, C. Langer, T. Rosenband, and D. J. Wineland, "*Experimental demonstration of a robust, high-fidelity geometric two ion-qubit phase gate.*", Nature **422**, 412–5 (2003).

[70] J. J. García-Ripoll, P. Zoller, and J. I. Cirac, "*Speed Optimized Two-Qubit Gates with Laser Coherent Control Techniques for Ion Trap Quantum Computing*", Physical Review Letters **91**, 157901 (2003).

[71] J. J. García-Ripoll, P. Zoller, and J. I. Cirac, "*Coherent control of trapped ions using off-resonant lasers*", Physical Review A **71**, 062309 (2005).

[72] A. M. Steane, G. Imreh, J. P. Home, and D. Leibfried, "*Pulsed force sequences for fast phase-insensitive quantum gates in trapped ions*", New Journal of Physics **16**, 053049 (2014).

[73] C. D. B. Bentley, A. R. R. Carvalho, D. Kielpinski, and J. J. Hope, "*Fast gates for ion traps by splitting laser pulses*", New Journal of Physics **15**, 043006 (2013).

[74] R. L. Taylor, C. D. B. Bentley, J. S. Pedernales, L. Lamata, E. Solano, A. R. R. Carvalho, and J. J. Hope, "*Fast Gates Allow Large-Scale Quantum Simulation with Trapped Ions*", `arXiv:1601.00359`.

[75] L.-M. Duan, "*Scaling Ion Trap Quantum Computation through Fast Quantum Gates*", Phys. Rev. Lett. **93**, 100502 (2004).

[76] H. R. Lewis and W. B. Riesenfeld, "*An Exact Quantum Theory of the Time-Dependent Harmonic Oscillator and of a Charged Particle in a Time-Dependent Electromagnetic Field*", Journal of Mathematical Physics **10**, 1458 (1969).

[77] P. J. Lee, K.-A. Brickman, L. Deslauriers, P. C. Haljan, L.-M. Duan, and C. Monroe, "*Phase control of trapped ion quantum gates*", Journal of Optics B: Quantum and Semiclassical Optics **7**, S371 (2005).

[78] T. R. Tan, J. P. Gaebler, Y. Lin, Y. Wan, R. Bowler, D. Leibfried, and D. J. Wineland, "*Multi-element logic gates for trapped-ion qubits*", Nature **528**, 380–383 (2015).

[79] M. Šašura and A. M. Steane, "*Fast quantum logic by selective displacement of hot trapped ions*", Physical Review A **67**, 062318 (2003).

[80] R. Kosloff, "*Time-dependent quantum-mechanical methods for molecular dynamics*", The Journal of Physical Chemistry **92**, 2087-2100 (1988), `http://dx.doi.org/10.1021/j100319a003`.

[81] R. Kosloff and H. Tal-Ezer, "*A direct relaxation method for calculating eigenfunctions and eigenvalues of the schrödinger equation on a grid*", Chemical Physics Letters **127**, 223–230 (1986).

[82] J. Alonso, F. M. Leupold, B. C. Keitch, and J. P. Home, "*Quantum control of the motional states of trapped ions through fast switching of trapping potentials*", New Journal of Physics **15**, 023001 (2013).

[83] H. Kaufmann, T. Ruster, C. T. Schmiegelow, F. Schmidt-Kaler, and U. G. Poschinger, "*Dynamics and control of fast ion crystal splitting in segmented Paul traps*", New Journal of Physics **16**, 073012 (2014).

[84] T. Ruster, C. Warschburger, H. Kaufmann, C. T. Schmiegelow, A. Walther, M. Hettrich, A. Pfister, V. Kaushal, F. Schmidt-Kaler, and U. G. Poschinger, "*Experimental realization of fast ion separation in segmented Paul traps*", Physical Review A **90**, 033410 (2014).

[85] J. P. Home, *Quantum Science and Metrology with Mixed-Species Ion Chains*, volume 62 of *Advances In Atomic, Molecular, and Optical Physics*. Elsevier, 2013. `http://www.sciencedirect.com/science/article/pii/B9780124080904000049`.

[86] P. O. Schmidt, T. Rosenband, C. Langer, W. M. Itano, J. C. Bergquist, and D. J. Wineland, "*Spectroscopy Using Quantum Logic*", Science **309**, 749–752 (2005).

[87] S. Stenholm, "*The semiclassical theory of laser cooling*", Reviews of Modern Physics **58**, 699–739 (1986).

[88] D. Leibfried, R. Blatt, C. Monroe, and D. Wineland, "*Quantum dynamics of single trapped ions*", Reviews of Modern Physics **75**, 281–324 (2003).

[89] T. Schmiedl, E. Dieterich, P.-S. Dieterich, and U. Seifert, "*Optimal protocols for Hamiltonian and Schrödinger dynamics*", Journal of Statistical Mechanics: Theory and Experiment **2009**, P07013 (2009).

[90] P. Salamon, K. H. Hoffmann, Y. Rezek, and R. Kosloff, "*Maximum work in minimum time from a conservative quantum system*", Phys. Chem. Chem. Phys. **11**, 1027–1032 (2009).

[91] J. G. Muga, X. Chen, A. Ruschhaupt, and D. Guéry-Odelin, "*Frictionless dynamics of BoseEinstein condensates under fast trap variations*", Journal of Physics B: Atomic, Molecular and Optical Physics **42**, 241001 (2009).

[92] A. del Campo and M. G. Boshier, "*Shortcuts to adiabaticity in a time-dependent box.*", Scientific reports **2**, 648 (2012).

[93] J.-F. Schaff, X.-L. Song, P. Vignolo, and G. Labeyrie, "*Fast optimal transition between two equilibrium states*", Physical Review A **82**, 033430 (2010).

[94] J.-F. Schaff, X.-L. Song, P. Capuzzi, P. Vignolo, and G. Labeyrie, "*Shortcut to adiabaticity for an interacting Bose-Einstein condensate*", EPL (Europhysics Letters) **93**, 23001 (2011).

[95] J. C. Lagarias, J. A. Reeds, M. H. Wright, and P. E. Wright, "*Convergence Properties of the Nelder–Mead Simplex Method in Low Dimensions*", SIAM Journal on Optimization **9**, 112–147 (1998).

[96] D. James, "*Quantum dynamics of cold trapped ions with application to quantum computation*", Applied Physics B: Lasers and Optics **66**, 181–190 (1998).

[97] M. Palmero, S. Martínez-Garaot, J. Alonso, J. P. Home, and J. G. Muga, "*Fast expansions and compressions of trapped-ion chains*", Physical Review A **91**, 053411 (2015).

[98] R. Reichle, D. Leibfried, E. Knill, J. Britton, R. B. Blakestad, J. D. Jost, C. Langer, R. Ozeri, S. Seidelin, and D. J. Wineland, "*Experimental purification of two-atom entanglement*", Nature **443**, 838–841 (2006).

[99] J. D. Jost, J. P. Home, J. M. Amini, D. Hanneke, R. Ozeri, C. Langer, J. J. Bollinger, D. Leibfried, and D. J. Wineland, "*Entangled mechanical oscillators.*", Nature **459**, 683–5 (2009).

[100] M. D. Barrett, J. Chiaverini, T. Schaetz, J. Britton, W. M. Itano, J. D. Jost, E. Knill, C. Langer, D. Leibfried, R. Ozeri, and D. J. Wineland, "*Deterministic quantum teleportation of atomic qubits.*", Nature **429**, 737–9 (2004).

[101] J. P. Home and a. M. Steane, "*Electrode Configurations for Fast Separation of Trapped Ions*", Quantum Inf. Comput. **6**, 289 (2006), `arXiv:0411102 [quant-ph]`.

[102] A. H. Nizamani and W. K. Hensinger, "*Optimum electrode configurations for fast ion separation in microfabricated surface ion traps*", Applied Physics B **106**, 327–338 (2012).

[103] W. H. Press, *Numerical Recipes 3rd Edition: The Art of Scientific Computing.* Cambridge University Press, 2007. `https://books.google.com/books?id=1aAOdzK3FegC{&}pgis=1`.

[104] A. C. Wilson, Y. Colombe, K. R. Brown, E. Knill, D. Leibfried, and D. J. Wineland, "*Tunable spin-spin interactions and entanglement of ions in separate potential wells.*", Nature **512**, 57–60 (2014).

[105] X.-J. Lu, X. Chen, A. Ruschhaupt, D. Alonso, S. Guérin, and J. G. Muga, "*Fast and robust population transfer in two-level quantum systems with dephasing noise and/or systematic frequency errors*", Physical Review A **88**, 033406 (2013).

[106] M. Palmero, S. Martínez-Garaot, U. G. Poschinger, A. Ruschhaupt, and J. G. Muga, "*Fast separation of two trapped ions*", New Journal of Physics **17**, 093031 (2015).

[107] W. K. Hensinger, S. Olmschenk, D. Stick, D. Hucul, M. Yeo, M. Acton, L. Deslauriers, C. Monroe, and J. Rabchuk, "*T-junction ion trap array for

*two-dimensional ion shuttling, storage, and manipulation*”, Applied Physics Letters **88**, 034101 (2006).

[108] J. M. Amini, H. Uys, J. H. Wesenberg, S. Seidelin, J. Britton, J. J. Bollinger, D. Leibfried, C. Ospelkaus, A. P. VanDevender, and D. J. Wineland, “*Toward scalable ion traps for quantum information processing*”, New Journal of Physics **12**, 033031 (2010).

[109] R. B. Blakestad, C. Ospelkaus, A. P. VanDevender, J. M. Amini, J. Britton, D. Leibfried, and D. J. Wineland, “*High-Fidelity Transport of Trapped-Ion Qubits through an X-Junction Trap Array*”, Physical Review Letters **102**, 153002 (2009).

[110] F. Splatt, M. Harlander, M. Brownnutt, F. Zähringer, R. Blatt, and W. Hänsel, “*Deterministic reordering of $^{40}Ca^{+}$ ions in a linear segmented Paul trap*”, New Journal of Physics **11**, 103008 (2009).

[111] A. K. Dhara and S. V. Lawande, “*Feynman propagator for time-dependent Lagrangians possessing an invariant quadratic in momentum*”, Journal of Physics A: Mathematical and General **17**, 2423–2431 (1984).

[112] L. S. Pontryagin, *Mathematical theory of optimal processes.* New York: Interscience, 1962.

[113] L. Mandel and E. Wolf, *Optical Coherence and Quantum Optics.* Cambridge University Press, 1995. `http://dx.doi.org/10.1017/CBO9781139644105`. Cambridge Books Online.

[114] S. Masuda and S. A. Rice, “*Rotation of the Orientation of the Wave Function Distribution of a Charged Particle and its Utilization*”,.

[115] M. Palmero, S. Wang, D. Guéry-Odelin, J.-S. Li, and J. G. Muga, “*Shortcuts to adiabaticity for an ion in a rotating radially-tight trap*”, New Journal of Physics **18**, 043014 (2016).

[116] H. Kaufmann, T. Ruster, C. T. Schmiegelow, M. A. Luda, V. Kaushal, J. Schulz, D. von Lindenfels, F. Schmidt-Kaler, and U. G. Poschinger, "*Fast ion swapping for quantum information processing*", arXiv preprint arXiv:1607.03734 (2016).

[117] D. Nigg, M. Müller, E. A. Martinez, P. Schindler, M. Hennrich, T. Monz, M. A. Martin-Delgado, and R. Blatt, "*Quantum computations on a topologically encoded qubit*", Science **345**, 302–305 (2014).

[118] I. Lizuain, M. Palmero, and J. G. Muga, "*Dynamical normal modes for time-dependent Hamiltonians in two dimensions*", `arXiv:1611.05229`.